Oxidized Phospholipids in Mouse and Man

Targeting oxidized phospholipids by AAV-mediated gene therapy in non-alcoholic fatty liver disease

Clint Michael Upchurch

Sherrills Ford, NC

B.S. Chemistry (Biochemistry) - University of North Carolina at Chapel Hill

A Dissertation Presented to the Graduate Faculty of the
University of Virginia in Candidacy for the
Degree of Doctor of Philosophy

Department of Pharmacology

University of Virginia

February 2023

Norbert Leitinger, Ph.D.
Thurl E. Harris, Ph.D.
Irina Bochkis, Ph.D.
Mete Civelek, Ph.D.
Ku-lung Hsu, Ph.D.
Zachary Henry, M.D.

Table of Contents

Figures

Tables

Appendix

Acknowledgements

It goes without saying that the work that follows in the next few pages was not completed in a vacuum and would have been an insurmountable challenge without many people who contributed either directly or indirectly to the work or my experience in Charlottesville.

I would like to start by thanking my parents for their unwavering support for any endeavor I decided to pursue, academic or otherwise. For this reason, I never once felt that I didn't have someone in my corner rooting for my success. Thank you for instilling in me confidence and understanding that no hurdle in life is too big to be cleared with the right preparation. Your guidance over the years has been valued more than you can know, and a few words here would not adequately impart upon the reader what you have meant to me.

Next, I would like to thank my brother, Caleb, for a friendship that has edified my life in so many ways. It's been a joy watching you grow up and develop into who you are today. Thank you for your patience whenever I ask you to explain once again the simplest of engineering concepts and for listening to me ramble about my latest interesting experimental results. I look forward to future weeks on the mountain skiing and hope that they are frequent and numerous.

Next, I would like to thank my PI, Norbert Leitinger. I have thoroughly enjoyed learning how to be a scientist under your tutelage. Thank you for taking a chance on me! Over the years (surely it hasn't been 7 already?), I always appreciated that your door was always open (well except for those times when a global pandemic intervened) for discussion about any and everything and

occasionally science. I appreciate your holistic approach to science and your constant insistence that we should consider the bigger picture. Thank you for pushing me to achieve more than I thought possible, for consistently expecting a little bit more than I was giving at the time, for conversations over coffee, adventures in Düsseldorf, and for insistence that time dedicated to hobbies is an essential component of a successful person and scientist. Maybe one of these days we can finally get that ski trip in assuming your knees hold up.

Next, I would like to thank my Thesis Committee and all my collaborators without whom none of this would have been possible. It has been an absolute pleasure to work with such excellent scientists, and more importantly, people. I could not have hoped for a better experience.

I would especially like to thank all of my colleagues in the lab. I would like to thank Renata for helping me get adjusted to life in the lab. I would also like to thank Subbu and Akshaya for their willingness to help a complete novice and answer my many questions. Next, I would like to thank Vlad for helping me get a foothold in the lab and teaching me everything I know about cellular bioenergetics and lipid mass spectrometry. Your guidance and willingness to teach me the basics in those first few months in the lab were instrumental in my success. I would like to thank Scott and Katie for countless hours spent around the coffee table hashing out experiments, talking about grandiose ideas for hypotheses that were never tested, and for just shooting the breeze. Both of you enriched my experience in the lab and I am better for it. I look forward to seeing what you both will achieve in what will undoubtedly be incredible careers!

Next, I would like to thank all of my friends from Charlottesville that helped shape my experience here. From those that I met in the first week and developed a strong friendship with during the core course to those I met more recently, you all have shaped my life for the better. I will always fondly remember hours spent on the golf course chasing my ball through the woods, plodding up Charlottesville's innumerable hills on bike rides, frustratingly and consistently losing to Adi in squash, chasing and occasionally catching intramural softball and soccer championships, floating down the James, and finally, relaxing at a summer happy hour after a successful week in the lab. Thank you all!

I would like to thank Darcy for her unconditional support through this process, your willingness to listen to me complain even when my problems really are not all that big, and your unshakeable conviction that dinner should always be accompanied by dessert. In a short time, you have drastically changed my life and have made my time in Charlottesville unforgettable.

Lastly, some of my family that provided unwavering support over the years were not able to see the culmination of my academic efforts, but that doesn't mean their support has ended. I know they would be extremely proud of my accomplishments, and I would like to leave the reader with a quote that was one of my Grandma's favorite refrains as long as I can remember and rings especially poignant now:

"Get all the education you can because they can't take that away from you."

-Joy Tate

Mawmaw, I think I finally did!

Abstract

Oxidized phospholipids are a diverse class of molecules that have been implicated in nearly all pathologies involving oxidative stress. Here, we will examine the role of oxidized phospholipids in a murine model of non-alcoholic fatty liver disease as well as investigate the complexity of the oxophospholidome in critically ill patients.

In the first part of this dissertation, we developed an AAV8-mediated gene therapy to express a neutralizing antibody fragment against oxidized phospholipids. We inoculated mice either prophylactically or after the development of hepatic steatosis and were able to neutralize plasma oxidized phosphatidylcholine (OxPC) species, lowering their concentrations, as well as protect mice from developing hepatic steatosis or hepatic fibrosis. In the second part of this dissertation, we identified and quantified OxPC species present in plasma of critically ill patients. We determined concentration ranges of individual OxPC species and discovered that classes of OxPC species associated with unique clinical parameters suggesting specific roles of OxPC species in different pathologies.

In conclusion, we have developed a suite of tools to interrogate the role of OxPCs in vivo directly which will provide novel insight into the function of OxPCs in diverse pathologies.

Chapter 1: Introduction

Phospholipids are a fundamental necessity for life and are evolutionarily conserved across all phyla. They exhibit incredible flexibility in their function ranging from physical barriers separating “us” from “not us” as demonstrated by phospholipid monolayer and bilayer membranes to highly specific signaling molecules like phosphatidyl inositol species. Despite their remarkably diverse functions, phospholipids that are composed of unsaturated fatty acids are subject to environmental conditions that can result in the formation of oxidized phospholipids. The remainder of this introduction will be dedicated to understanding how oxidized phospholipids form, how they are reduced *in vivo*, their role in physiology and pathology, and recent approaches developed to study their effects *in vivo*.

1.1 - What are oxidized phospholipids?

Oxidized phospholipids (OxPLs) are comprised of a glycerol backbone that contains two acyl-chains in the *sn*-1 and *sn*-2 positions and a phosphate head group in the *sn*-3 position (*1*). Typically, the *sn*-2 position contains an unsaturated acyl-chain that is susceptible to oxidation. The *sn-3* position contains a phosphodiester head group that can include phosphatidyl -choline (PC), -ethanolamine (PE), -serine (PS), -inositol (PI), -glycerol (PG), and phosphatidic acid (PA). For the sake of this dissertation, I will primarily focus on PC, PE, and PS species; however, all phospholipids, and further, any lipids, containing an unsaturated acyl chain are susceptible to oxidation independent of head group. Oxidation of phospholipids can occur through free radical-mediated oxidation or

enzyme catalyzed oxidation. Oxidation products that arise from these initial oxidation events can be further functionalized and ultimately decompose via Hock rearrangement to form truncated oxidized phospholipids liberating bioactive, aldehydic compounds like 4-hydroxynonenal (4-HNE) and malondialdehyde (MDA) (*2*).

1.2 - How do they form?

1.2.1 - Free radical-mediated oxidation

Halliwell and Gutteridge defined a free radical as any molecule with an orbital containing an unpaired electron (*3*). By this definition, the life-sustaining molecular oxygen we have evolved to require is a free radical in its ground state. Endogenous free radicals can be generated in many different cellular compartments including by the mitochondrial electron transport chain that converts glucose and fatty acids to ATP, NADH, and metabolites leading to generation of the free radical superoxide (O_2^-). Consequently, biological organisms are constantly bombarded by free radicals and have evolved mechanisms to combat the oxidation process which will be discussed later in this chapter. Free radical oxidation can occur within nearly every class of biomolecules from complex superstructures like DNA, RNA, and protein to simple molecules like lipids and metabolites (*1*).

Here, we will focus exclusively on the free radical oxidation of unsaturated lipid compounds. Free radical oxidation of polyunsaturated fatty acids (PUFAs) is a two-step process that starts with initiation (*3*). This occurs when a free radical molecule like a hydroxyl radical reacts with an α or β hydrogen from the methylene

group in one of the double bonds of a PUFA (*3*). The methylene radical generated by this process is highly reactive and can then react with molecular oxygen resulting in a radical, peroxy lipid completing the initiation phase (*3*). At this point, the peroxy lipid radical can then propagate the chain reaction to other compounds in close proximity. In many cases this includes other PUFA in adjacent phospholipids and proceeds through the mechanism described previously, resulting in a non-radical lipid peroxide species and an acyl chain containing a radical methylene group. Therefore, one might imagine that low concentrations of radicals are sufficient to initiate and further propagate super-stoichiometric lipid oxidation resulting in a "chain reaction."

Upon abstraction of the subsequent hydrogen by a peroxy lipid radical, the non-radical lipid peroxide can give rise to numerous lipid oxidation products that are classified as full-length lipid oxidation products (*1*). Lipid peroxide species are susceptible to further oxidation and may further participate in propagation of the chain reaction resulting in a single lipid with multiple peroxide species present (*4*). Lipid peroxides can be reduced to the alcohol by enzymatic or non-enzymatic mechanisms (*1*). Additionally, through autooxidation lipid peroxides can cyclize and form epoxides, isoprostane-like compounds, and cyclic endoperoxides (*5, 6*). Endoperoxides can further decompose to form the lipid oxidation byproduct MDA (*2*). Phospholipids may be oxidized by other free radical species like reactive nitrogen species, but that is beyond the scope of this introduction and will not be discussed here (*7*).

1.2.2 – Enzymatic Oxidation

In addition to free radical mediated oxidation, phospholipids can be oxidized by direct enzymatic mechanism. Lipoxygenase family enzymes act on 1,4 pentadiene motifs and oxidized lipids to form hydroperoxide containing phospholipids which can decompose through the mechanisms described previously resulting in formation of a chemically diverse set of OxPLs (*8*).

1.2.3 – Hock rearrangement

Formation of truncated oxidized phospholipids occurs through Hock rearrangement, also known as the cumene process (*9*). In this process, organic peroxides react to form a truncated oxidized phospholipid species that are oxidatively modified with either an aldehyde or carboxylic acid. As a byproduct of this reaction both 4-HNE and MDA can be liberated depending on the starting PUFA (*1*).

1.3 – How are OxPLs reduced *in vivo*?

Once synthesized, bioactive OxPLs can regulate numerous cellular and physiological processes (see section 1.4). Mechanisms have evolved to limit rampant oxidation of phospholipids *in vivo*. Compared to the external environment, the internal *milieu* of a cell is shifted to favor reduction. When this balance is shifted toward an oxidizing environment electrophilic compounds like truncated OxPLs are generated and can covalently modify Kelch-like ECH-associating protein 1 (KEAP1), disrupting the inhibitory action of KEAP1 on the transcription factor nuclear factor erythroid 2-related factor 2 (NRF2) and allowing its translocation to the nucleus (*10*). NRF2 regulates expression of a host of genes involved in redox

homeostasis and promotes expression of an antioxidant and reducing gene program (*11*). Electrophilic activation of NRF2, upregulates expression of reductases that use NADPH and NADH to maintain a delicate redox balance (*12*). Additionally, NRF2 activation regulates glutathione production, a tripeptide that is used by the cell as a reducing agent to maintain redox homeostasis (*13*).

Glutathione is a co-factor for the class of enzymes known as glutathione peroxidases (GPx) that were first discovered in 1957 (*14*). Reduction of linolenic acid hydroperoxide by a GPx was the first evidence that the GPx family could reduce a wide variety lipid hydroperoxides using glutathione as a substrate (*15*). Recent work has demonstrated that GPx4 is responsible for reduction of lipid hydroperoxides to their cognate alcohols (*16*). Recently, GPx4 has been implicated as key regulator of the iron-dependent cell death, ferroptosis (*17, 18*). Consequently, GPx4-mediated reduction and subsequent detoxification of oxidized phospholipid is an essential pathway for clearance of potential damaging OxPLs.

In addition to direct enzymatic reduction of OxPLs, phospholipase-mediated cleavage of oxidatively modified phospholipids serves to detoxify damaged phospholipids. Lipoprotein-associated phospholipase A2 (Lp-PLA2 or PAF-AH) has been shown to cleave oxidatively modified fatty acids in the *sn-2* position of oxidized phospholipids, and the ablation of Lp-PLA2 exacerbated CCl_4-induced oxidative damage (*19-21*).

Recently, it has been shown that a single chain variable fragment of the natural IgM mouse antibody, E06 (scFV-E06) is sufficient to protect mice from atherosclerosis, NAFLD, CCl_4-induced hepatic fibrosis, and age-related loss in bone density (*22-25*). It has been demonstrated that E06 can bind OxPC species *in vitro* and evidence suggests that expression of scFv-E06 neutralizes plasma OxPCs as there is a reduced signal when assessed with an E06-based ELISA assay (*22, 24, 26*). The work disclosed in this dissertation will demonstrate direct evidence of a reduction in plasma OxPC species in response to expression of scFv-E06 (*27*).

1.4 – OxPLs in physiology and pathology

Given the large number of possible acyl-chain combinations and the numerous oxidative derivatizations, the possible number of endogenous OxPLs is vast, and consequently, OxPLs have been demonstrated to regulate an array of biological processes (*1*). OxPLs have been described as danger-associated molecular patterns (DAMPs) and been shown to regulate endothelial barrier function, as well as immune cell migration, activation, and metabolism in the context of obesity and atherosclerosis (*28-38*) . As a DAMP, OxPLs have been demonstrated to bind CD14 and CD36 and regulate whole body responses to endotoxemia and septic challenge (*36-41*). Additionally, OxPLs have been implicated in processes as fundamental as cell death, including apoptosis, caspase 11-dependent inflammasome-mediated pyroptosis, and redox-mediated ferroptosis (*42-46*).

In the following sections, I will highlight some of the many pathologies and cellular processes in which OxPLs play a role.

1.4.1 – Atherosclerosis

Oxidized phospholipids were discovered on minimally modified (oxidized) low density lipoproteins (MM-LDL) and shown to be a bioactive component of MM-LDL (*28*). MM-LDL has been shown to be a risk factor in cardiovascular disease and coronary heart disease (*47*). The mechanism through which oxidized LDL (OxLDL) exacerbates CVD and CHD have been explored extensively. Previous work has demonstrated that OxLDL can accumulate in the sub-endothelial space resulting in activation of endothelial cells, smooth muscle cells, and macrophages (*48*). OxLDL accumulation results in increased inflammatory tone and promote monocyte endothelium interactions (*49*). Additionally, OxLDL promotes foam cell macrophage formation by promoting increased expression of CD36, a class B scavenger receptor that binds γ-keto/hydroxy phospholipids (*37, 50*).

Lipoprotein (a) (Lp(a)) has been identified as a carrier of oxidized phospholipids and can contain the apoplipoprotein apoB-100 (*51*). Elevated Lp(a) is a risk factor for atherosclerosis as well as other vascular pathologies including calcific aortic stenosis and coronary artery disease (*51-56*). Nevertheless, the specific role of Lp(a) bound OxPLs in disease progression remains unclear.

1.4.2 – Blood

In addition to its role in atherosclerosis, MM-LDL has been show to activate platelets resulting in platelet aggregation which could not be rescued by antioxidants like α-tocopherol (Vitamin E) and probucol (*57*). Previously, it has

been shown that treatment of platelet activating factor acetylhydrolase (PAF-AH) ablated the effect of MM-LDL suggesting that platelet activating factor or lipid species structurally similar, for which PAF-AH is promiscuous, is the bioactive component promoting platelet aggregation (*20*). PAF-acetylhydrolases are a small family of enzymes that exhibit *sn-2* specific lipase activity (*58*). While the canonical substrate of PAF-AH is the potent prothrombotic platelet activating factor, it has been demonstrated that oxidative modification of *sn-2* acyl chain promotes promiscuous hydrolysis of aldehyde- and carboxylic acid-modified truncated OxPLs resulting in MM-LDL lipid remodeling (*19, 20*). In fact, PONPC was hydrolyzed with nearly identical efficiency compared to PAF by PAF-AH (*19*).

$CD36^{-/-}$ mice on a Western diet exhibited blunted platelet activation suggesting that CD36 is necessary for a complete thrombotic response in the context of hyperlipidemia (*38*). Podrez *et. al.* demonstrated that CD36 ligands like hydroxyoctadecadienoic acid-PC (HODA-PC), but not 1-palmitoyl-2-(5'-oxo-valeroyl)-sn-glycero-3-phosphocholine (POVPC), were sufficient to promote human platelet fibrinogen activation and platelet P-selectin expression *in vitro (36-38).* Irreversible pharmacological inhibition of PAF-AH resulted in an increase in truncated OxPL species including *bona fide* CD36 ligands *in vitro (59)*.

In addition to the role of CD36 ligands to thrombus formation, recent work has demonstrated a role for full-length OxPL species. $ALOX12^{-/-}$ and $ALOX15^{-/-}$ mice exhibited impaired venous coagulation assessed by tail bleed compared to WT controls (*60*). Application of 12-hydroxyeicosatetraenoic acid-PE (12-HETE-PE) liposomes rescued coagulation demonstrating that full-length hydroxy-

modified phospholipids are necessary for a complete thrombotic response (*60*). Additionally, 5-, 12-, and 15-HETE-PE and -PC were all sufficient to induce thrombin formation *in vitro* with PC isomers demonstrating a higher potency (*60*). The mechanism through which these OxPL species promote coagulation is not clear, but it has been proposed that incorporation of these lipid species into the membrane permits Ca^{2+} membrane association and supports phosphatidyl serine dependent activation of clotting factors (*60*). Interestingly, the more potent HETE-PC species refute the previously accepted "Anything But PCs" hypothesis as important lipid mediators in PS-dependent clotting cascade activation (*60, 61*).

Remarkably, these lipid species were also sufficient to restore thrombin formation in plasma from patients with Factor VIII (Hemophilia A), Factor IX (Hemophilia B), or Factor XI deficiency (*62*). 9-, 12-, and 15-HETE-PLs were more effective at enhancing coagulation which suggests some isomeric selectivity (*62*).

These findings demonstrate a critical role of OxPLs in coagulation and further exemplify why it is necessary to elucidate the role of individual OxPL species. Moreover, it confirms that OxPL should not solely be consider "bad" lipids, but rather, their functions should be considered within each biological context.

1.4.3 – Polarization of macrophages

OxPLs can be recognized as DAMPs by toll-like receptor 2 and 4 (TLR2 and TLR4) to regulate macrophage function. Kadl *et. al.* demonstrated that treatment of bone-marrow derived macrophages (BMDMs) with oxidized 1-palmitoyl-2-arachidonoyl-sn-glycero-3-phosphocholine (OxPAPC) polarized BMDMs to a unique M_{ox} phenotype. This phenotype was characterized be

decreased phagocytosis and chemotaxis commiserate with an upregulation of NRF2-dependent gene programs (*32*). They further determined that approximately one third of macrophages present in atherosclerotic lesions from mice resemble this phenotype (*32*).

Further investigation revealed that polarization of BMDMs to an M_{ox} phenotype resulted in a significant increase in reducing potential most likely through metabolic rewiring to promote production of glutathione from glutamate at the expense of ATP production (*34, 63*). Additionally, resident adipose tissue macrophages phenocopy M_{ox} polarized BMDMs suggesting that OxPLs present in healthy adipose tissue promote a homeostatic, redox-regulatory tissue resident macrophage (*64*).

1.4.4 – Bone

Age-related bone loss has been associated with increased lipid peroxidation and oxidative stress. Bone density is regulated by the antagonistic function of osteoblasts and osteoclasts present within the bone. Recent work has also suggested that osteal macrophages which are typically found in close proximity with osteoblasts also regulate bone density (*65*). The number of osteoblasts and osteoclasts present in the bone as well as the osteoblast and osteoclast surface area to bone area are reduced in response to aging (*25*). Likewise bone formation rate to bone surface area (BFR/BS) is significantly decreased in aged mice (*25*). Expression of scFv-E06 and neutralization of oxidized phospholipids resulted in increased in BFR/BS rate in both young and aged mice. This is most likely due to significant decrease in osteoclast number and

surface area in mice expressing scFv-E06 compared to their littermate controls (*25*). Interestingly, ovariectomized mice were not protected from a loss in bone density by expression of scFv-E06, which implies a separate, OxPL-independent regulation of bone density (*25*).

Consequently, this strongly suggests OxPLs play a role in regulating osteoblast and osteoclast differentiation. RNA-seq analysis of vertebrae from scFv-E06 expressing mice showed a significant increase in genes involved in *Wnt* signaling as well as genes involved in osteoblast differentiation and survival, mesenchymal proliferation, bone mineralization, and extracellular matrix organization (*25*). It has been demonstrated that OxPLs can inhibit osteoblast differentiation and survival (*66*). Indeed, previous work has demonstrated that treatment of either osteoblast or osteoclasts with oxidized FFAs like 9-HODE, 12-HETE, 13- HODE, 15-HETE, as well as the lipid oxidation byproduct 4-HNE inhibit osteoblastogenesis and *Wnt* signaling while promoting osteoblast and -clast apoptosis *in vitro* (*66*). Additionally, both OxLDL and OxPLs like POVPC and 1-palmitoyl-2-glutaryl phosphatidylcholine (PGPC) have been shown to be ligands for low-density of lipoprotein receptor related protein 6 (LRP6) which is a co-receptor for *Wnt* signaling. LRP6 cell surface expression in mesenchymal stromal cells (MSCs), progenitors for osteoblast and osteoclasts, significantly impaired MSCs response to osteogenic factors (*67*).

1.4.5 – Eye

Recent work has demonstrated that OxPC species are present in both rat and human aqueous humor (*68*). Truncated OxPC species POBPC, POVPC,

PONPC, PMPC, PGPC, and PazPC were significantly upregulated in a rat model of uveitis (*68*). Human aqueous humor was collected from patients with cataracts with or without concomitant uveitis (*68*). Patients with uveitis exhibited an increase in truncated OxPCs that reflected what was observed in rats (*68*). Additionally, treatment of a retinal pigment epithelial cell line (ARPE-19) revealed that the commercially available truncated OxPC species POVPC, PGPC, PONPC, and PazPC were cytotoxic (*68*).

Similarly, an increase in PGPC and POVPC in retinal pigment epithelial cells in response to *Alu* RNA was reported in a model of geographic atrophy which is a form of age-related macular degeneration (*69*). This increase may exacerbate macular degeneration through numerous possible cytotoxic mechanisms like non-canonical inflammasome activation or ferroptosis (*44, 69*). Additionally, this suggests that OxPLs may serve as critical mediator of eye pathologies and may provide a potential therapeutic target for inflammatory or aged-related ocular pathologies.

1.4.6 – Lung

The lung epithelium must constantly protect itself from a pro-oxidizing environment. In addition to constant exposure to molecular oxygen and ozone, the lung epithelium must also contend with oxidizing environmental pollutants. Pulmonary epithelium and pulmonary vascular endothelium are essential for proper lung function, and loss of barrier function is a hallmark of many lung pathologies including acute lung injury, idiopathic pulmonary fibrosis, pathogen infection, and sepsis (*70-72*)

Oxidized phospholipids both protect and exacerbate loss of lung barrier function depending on the type of OxPL present. Full-length OxPCs have been shown to protect lung barrier function likely through many different mechanisms of action including indirectly inhibiting TLR signaling in the context of a sterile inflammation and non-sterile *S. aureus* infection (*73, 74*) and stabilization of tight junction and adherens junction interactions through a RAC1/CDC42 dependent mechanism (*75-78*).

Conversely, truncated OxPL species have been shown to be detrimental in the context of lung injury. Truncated OxPC species like POVPC and PGPC have been shown to significantly decrease endothelial barrier function assessed by transendothelial electrical resistance by inducing hyperphosphorylation of VE-cadherin at Tyr^{658} and Tyr^{731} *(79)*. Both phosphorylation sites are necessary for VE-cadherin function in formation of adherens junctions (*80*). Interestingly, truncated OxPCs are increased in the lungs of aged mice and predisposes them to a more severe response to LPS induced acute lung injury likely due to increased pulmonary vasculature permeability (*81*).

This poignant dichotomy between full-length and truncated OxPC species effects in the lung should be noted. It is not sufficient to consider OxPCs as simply a group of similarly acting molecules. To fully understand the complex role of OxPC species *in vivo* it is necessary to consider species with different functional groups separately, if not each individual lipid species.

1.4.7 – Liver

Recent work has demonstrated a role for oxidized phospholipids in nonalcoholic fatty liver disease. Expression of a single chain variable fragment of E06 (scFv-E06), a natural IgM antibody that binds oxidized phosphatidylcholines phospholipids, via the ApoE promoter protected $Ldlr^{-/-}$ mice from developing diet-induced hepatic steatosis (*22*). Further work demonstrated that expression of scFv-E06 protected mice from carbon tetrachloride-induced hepatic fibrosis and decreased incidence of liver tumors. Sun et. al. showed that expression of scFv-E06 decreased inflammatory tone resulting in reduced levels of blood cytokines like RANTES, M-CSF, and TNFα, and also demonstrated an increase in Tim4+ Kupffer cells, the liver resident macrophage (*24*). They further demonstrate that aldehyde containing oxidized phospholipids, specifically POVPC, can form an adduct with proteins like manganese superoxide dismutase (MnSOD) and result in impaired mitochondrial membrane potential and function (*24*). This may contribute to and exacerbate genesis and perpetuation of nonalcoholic fatty liver disease (*24*).

1.4.8 – Apoptosis, Pyroptosis, and Ferroptosis

Oxidized phospholipids are enriched in blebs from cells undergoing apoptosis and promote endothelial-monocyte interactions mediate clearance of activated endothelial cell (*82*). PS is externalized in response to loss of flipase activity during apoptosis. Studies have shown that selective oxidation of externalized PS is required for clearance of apoptotic cells by macrophages in a CD36-dependent manner (*42, 43, 83*).

Recent work has demonstrated that exposure to OxPAPC is sufficient to induce caspase-11 mediated activation of the inflammasome resulting in interlukin-1 β release; however, OxPAPC induced inflammasome activation does not result in pyroptosis (*44, 84*).

Lastly, OxPLs have been implicated as a central regulator of an iron-mediated form of cell death, ferroptosis (*17*). Ferroptosis is driven by excess oxidative stress promoting rampant oxidation of plasma membrane phospholipids and culminated in loss of membrane integrity and cell death. Arachidonic acid and adrenic acid PEs are preferentially oxidized during ferroptosis though exact mechanism through which OxPEs facilitate ferroptotic cell death remains an open question (*42, 45*).

1.5 – Conclusion

Oxidized phospholipids are involved in a wide host of biological processes and consequently are fundamental to our full understanding of many pathologies. To date, there have been few tools to effectively study this class of lipids *in vivo* as conventional molecular genetics and pharmacology cannot effectively produce “oxidized lipid knockout models.”

The recent development of the scFv-E06 expressing mouse provided the first tool to directly assess the role of OxPLs in physiology and pathology *in vivo* and resulted in a renaissance of high impact papers demonstrating the role of OxPC species in atherosclerosis and non-alcoholic fatty liver disease.

In this dissertation, we developed a viral vector to express scFv-E06 in a therapeutic capacity and an analytical approach to identify and quantify oxidized

phospholipids present in plasma and tissue. This vector combined with our analytical approach has opened the door to explore the role of individual oxidized phospholipid species in the development and progression of many different pathologies for the first time.

Chapter 2: Targeting oxidized phospholipids by AAV-based gene therapy in mice with hepatic steatosis prevents progression to fibrosis

2.1 – Abstract

Oxidized phosphatidylcholines (OxPC) are implicated in chronic tissue damage. Hyperlipidemic LDL-R-deficient mice transgenic for an OxPC-recognizing IgM fragment (scFv-E06) are protected against non-alcoholic fatty liver disease (NAFLD). To examine the effect of OxPC elimination at different stages of NAFLD progression, we utilized cre-dependent, adeno-associated virus serotype 8-mediated expression of the single chain variable fragment of E06 (AAV8-scFv-E06) in hepatocytes of albumin-cre mice. AAV8-induced expression of scFv-E06 at the start of FPC diet protected mice from developing hepatic steatosis. Independently, expression of scFv-E06 in mice with established steatosis prevented the progression to hepatic fibrosis. Mass-spectrometry-based oxophospholipidomics identified individual OxPC species that were reduced by scFv-E06 expression. *In vitro*, identified OxPC species dysregulated mitochondrial metabolism and gene expression in hepatocytes and hepatic stellate cells. We demonstrate that individual OxPC species independently affect disease initiation and progression from hepatic steatosis to steatohepatitis, and that AAV-mediated expression of scFv-E06 is an effective therapeutic intervention.

2.2 – Introduction

Non-alcoholic fatty liver disease (NAFLD) is a multi-stage disease that affects approximately 30% of the global population (*85, 86*). Hepatic steatosis is

the hallmark of NAFLD, which in a subset of patients will progress into non-alcoholic steatohepatitis (NASH). Steatosis can arise as a result of caloric overload, which dysregulates hepatocyte bioenergetics and metabolism (*87*), increases reactive oxygen species (ROS) (*88*) and hepatic triglyceride accumulation (*89, 90*), resulting in organ damage indicated by elevated plasma alanine aminotransferase (ALT) and aspartate aminotransferase (AST) (*88, 91-95*). The culmination of multiple hepatic insults leads to the development of NASH, which is characterized by inflammation (*96*) and activation of hepatic stellate cells, ultimately leading to irreversible hepatic fibrosis (*96-101*). In the absence of FDA-approved pharmacological interventions and suitable biomarkers for NASH, there is an urgent need for new therapeutic and diagnostic tools (*102*).

Excess radical oxygen species (ROS) generation in steatotic livers leads to the formation of lipid oxidation products, including oxidized phosphatidylcholines (OxPCs) (*32, 36, 39, 103*). Free radical- and enzymatically-driven oxidation of polyunsaturated fatty acids contained in phospholipids forms chemically unique classes of oxidized species whose location and chemical functionalization dictate the regulation of specific cellular responses, including endothelial barrier integrity (*29, 74, 81, 104, 105*); immune cell migration (*31*), activation (*32, 103*), and metabolism (*34*); bone homeostasis (*106*); and regulated cell death (*43, 45*). Consequently, OxPCs are thought to play a central role in acute pathologies such as sepsis (*39*), lung injury (*81, 104, 107*), as well as in chronic diseases including those of the metabolic syndrome (*24, 64*). Moreover, plasma levels of OxPCs, as measured by reactivity with E06, a natural IgM that binds oxidized

phosphorylcholine (*54*), predict severity of human carotid and femoral atherosclerosis (*26*).

Recent work from the Witztum laboratory has demonstrated that constitutive transgenic expression of a single chain variable fragment of E06 (scFv-E06) protects hypercholesterolemic *Ldlr*$^{-/-}$ mice from diet-induced HS and subsequent NASH (*22, 24, 26*). While these studies demonstrated that targeting OxPCs in general is sufficient to improve clinical outcomes in a mouse model of chronic disease, the identity of individual OxPC species that are eliminated by scFv-E06 *in vivo* remains unknown. Furthermore, it is unknown whether OxPC sequestration by scFv-E06 is sufficient to independently halt the progression to NASH and the transition to hepatic fibrosis, and it is necessary to identify the cellular targets and the pathological mechanisms by which OxPCs drive hepatic steatosis and fibrosis.

Here, we show that adeno-associated virus serotype 8-mediated hepatic expression of scFv-E06 (AAV8-E06) eliminates defined plasma OxPC species derived from oxidation of 1-palmitoyl-2-arachidonoyl-*sn*-3-choline (PAPC) and 1-palmitoyl-2-linoleoyl-*sn*-3-choline (PLPC), which protects mice from diet-induced hepatic steatosis. Identified OxPC species regulate hepatocyte gene expression and shift cellular metabolism toward a bioenergetically impaired state, which results in reduced oxygen consumption and increased lipid droplet accumulation. Moreover, intervention with AAV8-scFv-E06 in mice with established hepatic steatosis prevents the progression to NASH and hepatic fibrosis. OxPC species that were reduced during the progression phase regulate hepatic stellate cell

bioenergetics and gene expression. Together, we identify specific pathology-driving OxPC species in plasma that may be used as non-invasive biomarkers to diagnose distinct stages of NAFLD, and we demonstrate efficacy of AAV8-mediated gene transfer of scFv-E06 as an intervention-based therapeutic measure that attenuates the initiation of hepatic steatosis and the progression to fibrotic steatohepatitis in mice.

2.3 – Results

2.3.1 – Development of cre-dependent adeno-associated virus serotype 8 expression of scFv-E06 in a diet-induced murine model of NAFLD

Previous reports demonstrated that constitutive transgenic expression of scFv-E06 *via* the *Apoe* promoter protected *Ldlr*$^{-/-}$ mice fed a high cholesterol diet from hepatic steatosis and ensuing steatohepatitis (*22, 24*). To investigate the effect of scFv-E06 at different stages of disease progression and to establish a therapeutic approach utilizing virus-mediated gene transfer of scFv-E06, we developed an adeno-associated virus serotype 8 construct containing a myc- and 6xHis-tagged scFv-E06 flanked by double-inverse orientation flox sites (AAV8-scFv-E06) for cre-dependent expression (Figure 1A). Speer6-ps1$^{Tg(Alb\text{-}cre)21Mgn}$/J (Alb-cre) mice, which express Cre recombinase specifically in hepatocytes, were injected *via* tail vein with AAV8-scFv-E06 or a control AAV8 expressing green fluorescent protein (AAV8-GFP). Viral transduction resulted in incorporation of the scFv-E06 vector predominantly in the liver, and to some extent in adipose tissue, kidney, and spleen, while it was not detected in the heart or lungs (Figure 1B). Messenger RNA and protein expression of scFv-E06 was restricted to the liver, demonstrating that expression was dependent on cre-recombinase (Figure 1C, 1D). Interestingly, scFv-E06 protein was secreted into the plasma with detectable levels as early as 10 days after AAV administration (Figure 1J).

AAV8-mediated hepatic expression of scFv-E06 had no observable effect on total body weight, and liver, gonadal adipose tissue, heart, kidney, or spleen mass (Figure 2A-F). There were also no differences in levels of ALT (Figure 1E) and AST (Figure 1F) in plasma, or esterified (Figure 1G), free (Figure 1H), and

total cholesterol (Figure 1I) in livers of mice given AAV8-scFv-E06 compared to AAV-GFP controls. Taken together, these data demonstrate that AAV8-mediated hepatic expression of scFv-E06 in mice leads to accumulation of scFv-E06 protein in the liver and plasma without inducing overt physiological changes.

Using a high fructose, palmitate, and cholesterol (FPC) diet supplemented with 4.2% sugar water (55/45% glucose/fructose) we establish a progressive model NAFLD defined by distinct stages of hepatic steatosis and subsequent inflammation and fibrosis (*108*). These stages were evident in histopathological assessment of livers from mice fed FPC-diet compared to chow-fed controls (Figure 2G-J). This allowed us to assess the impact of scFv-E06 expression at different stages of NAFLD progression.

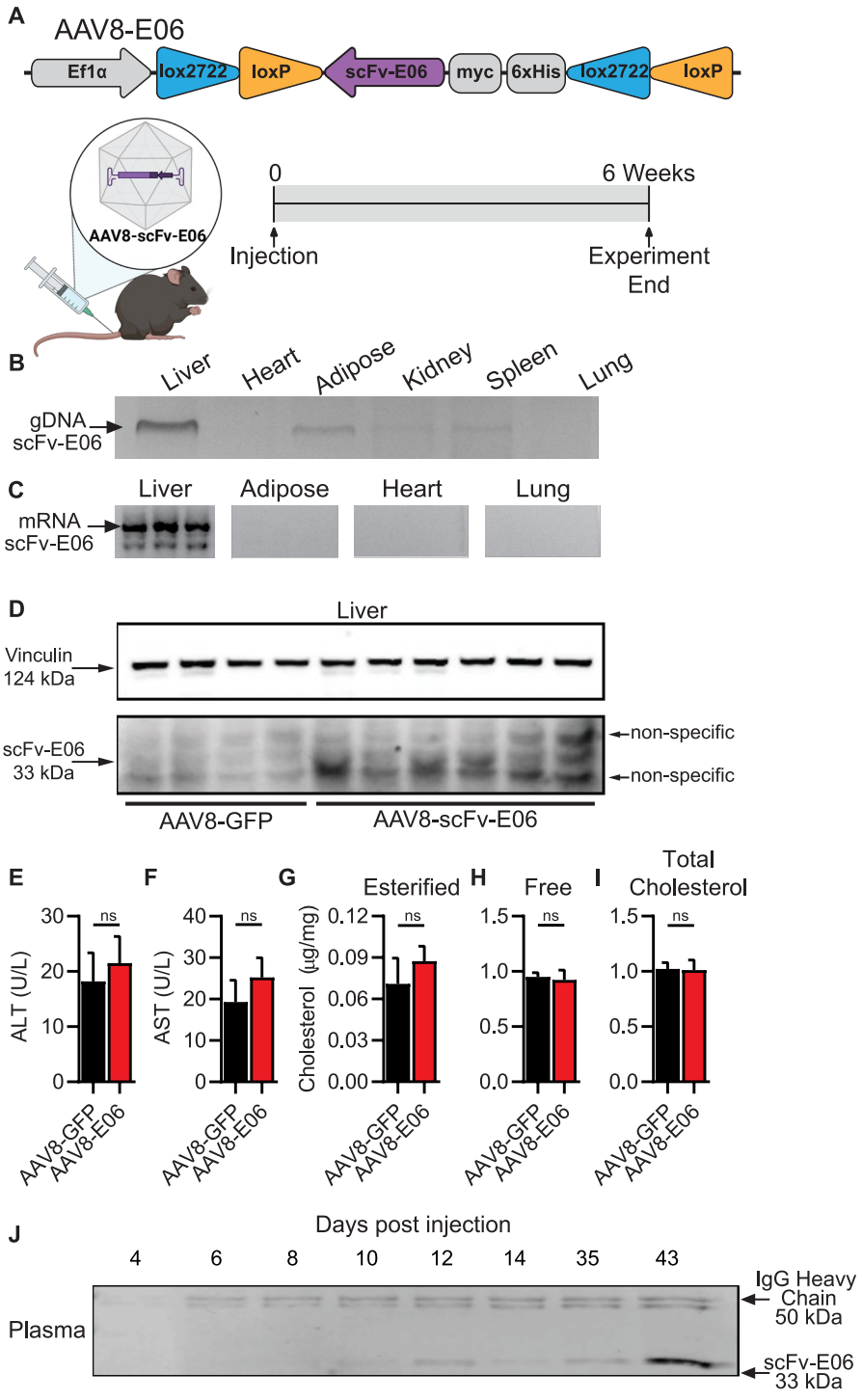

Figure 1. Virus-mediated gene transfer for cre-dependent expression of scFv-E06 in a murine model.

Figure 1. Virus-mediated gene transfer for cre-dependent expression of scFv-E06 in a murine model.

(A) Schematic of experimental design. Mice were injected via tail vein with AAV8-E06 or AAV-GFP and fed chow diet for 6 weeks (Created with BioRender.com). Viral transduction of AAV8-scFv-E06 were assessed by **(B)** PCR of genomic DNA and **(C)** RT-PCR of mRNA. scFv-E06 expression in the **(D)** liver was confirmed via western blotting six weeks post injection. Vinculin was used as a loading control. There were no significant changes in **(E)** ALT, **(F)** AST, **(G)** esterified, **(H)** free, and **(I)** total liver cholesterol between scFv-E06 and GFP expressing mice (AAV8-GFP – n=5; AAV8-E06 – n=6). **(J)** scFv-E06 was detectable in plasma 12 days post-injection and remained elevated after six weeks. Non-specific IgG heavy chain staining was used as a loading control. Statistical significance was determined by Student's T-test (*=$p<0.05$).

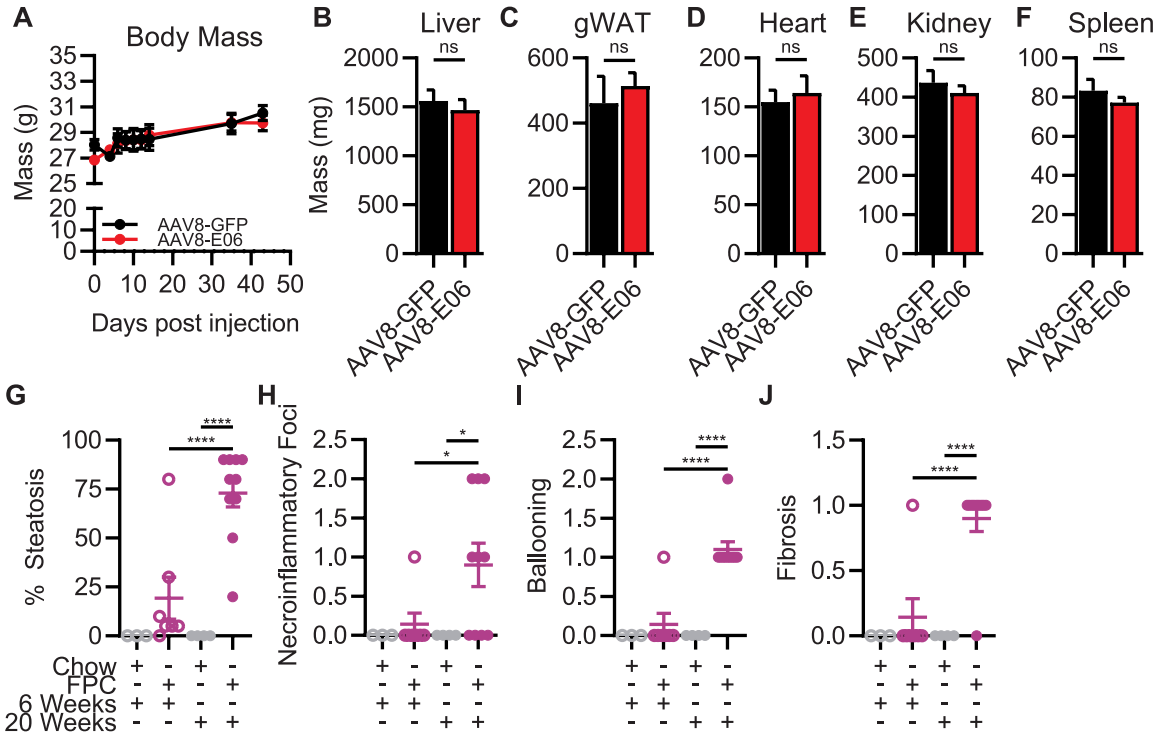

Figure 2. Adeno-associated virus serotype 8 scFv-E06 and FPC diet verification.

Figure 2. Adeno-associated virus serotype 8 scFv-E06 and FPC diet verification.

Mice were injected with either AAV8-GFP or AAV8-E06. There were no differences in **(A)** body mass, or mass of **(B)** liver, **(C)** gonadal white adipose tissue, **(D)** heart, **(E)** kidney, and **(F)** spleen (AAV8-GFP – n=5; AAV8-E06 – n=6). Mice injected with AAV8-GFP were fed chow or FPC diet for 6 or 20 weeks and histopathological assessment of **(G)** percent steatosis, **(H)** necroinflammatory foci, **(I)** hepatocellular ballooning, and **(J)** fibrosis was performed by a clinical pathologist. Statistical significance was determined by 2-way ANOVA (*=$p<0.05$, ****=$p<0.0001$).

2.3.2 - Prevention of hepatic steatosis by expression of scFv-E06

To determine whether induced expression of scFv-E06 could be used as a therapeutic approach to prevent hepatic steatosis in mice, we inoculated Speer6-ps1$^{Tg(Alb\text{-}cre)21Mgn}$/J (Alb-cre) mice *via* tail vein with AAV8-scFv-E06 or AAV8-GFP two weeks before feeding mice FPC diet for six weeks to induce hepatic steatosis (Figure 3A). After 6 weeks, we confirmed expression of myc-tagged scFv-E06 in the liver by Western blot (Figure 3B), and mRNA by qRT-PCR in the liver (Figure 4A) and confirmed detectable titers of scFv-E06 in the plasma by ELISA (Figure 3C). scFv-E06-expressing mice exhibited no difference in weight gain compared to GFP-expressing mice over six weeks (Figure 4B); however, scFv-E06 expression reduced body fat percentage starting at four weeks on FPC diet (Figure 4C). FPC diet feeding increased liver and adipose mass; however, there was no difference in organ mass between GFP and scFv-E06 expressing mice (Figure 4D-I). Histological assessment of liver sections by H&E or Oil red O staining revealed that treatment with AAV8-scFv-E06 reduced hepatic tissue damage and lipid accumulation compared to GFP controls (Figure 3D). Hepatic triglyceride levels were significantly reduced in scFv-E06-expressing mice and negatively correlated with hepatic mRNA expression of scFv-E06 (Figure 3E,F). Moreover, plasma ALT (Figure 3G) and AST (Figure 3H) levels were significantly decreased in mice expressing scFv-E06, while alkaline phosphatase, cholesterol, low-density and high-density lipoprotein cholesterol, plasma triglycerides, albumin, and total protein were unchanged (Figure 4J-R). These data demonstrate that AAV8-

mediated expression of scFv-E06 protects mice from diet-induced hepatic lipid accumulation and liver damage.

Previously published studies have demonstrated that constitutive scFv-E06 expression reduced overall plasma reactivity with IgM E06(*22, 24*), indicative of reduced OxPC levels in plasma. However, the identity of OxPC species that are reduced by scFv-E06 expression, and the degree of reduction remains unknown.

To identify OxPC species that are affected by scFv-E06 in plasma, we used an *in silico* platform, LPPTiger (*109*), to predict structures of possible oxidation products that can be generated from oxidation of 1-palmitoyl-2-arachidonyl-*sn*-glycero-3-phosphocholine (PAPC) and 1-palmitoyl-2-linoleoyl-*sn*-glycero-3-phosphocholine (PLPC). We then validated predicted OxPC species by ESI-LCMS using air- or copper (I) chloride-oxidized PAPC (OxPAPC) and PLPC (OxPLPC) (Figure 5A, B), which resulted in validation of 48 PAPC- and 35 PLPC-derived oxidized individual analytes or groups of isobaric compounds (Figure 3I,J). Next, we assessed the presence of validated compounds in the plasma of GFP- or scFv-E06-expressing mice after six weeks on FPC diet (Figure 5C, D). We identified 23 individual OxPC species and isobaric groups containing OxPCs, and 6 non-oxidized PC and lyso-PC species in mouse plasma. Levels of non-oxidized PCs and lyso-PCs were not different in GFP- and scFv-E06-expressing mice; however, all identified OxPC species, including truncated and full-length OxPCs, were markedly decreased in plasma of mice expressing scFv-E06 (Figure 3K). A similar pattern was observed in the liver; however, the differences in OxPC species were less pronounced between the two groups (Figure 4S).

In the plasma, the truncated and full-length OxPCs that were significantly decreased in scFv-E06-expressing mice included several previously described biologically active compounds containing specific functional groups: among decreased truncated OxPC species were γ-keto/hydroxy OxPCs (*m/z* 650) (*36, 37*), the aldehyde-containing 1-palmitoyl-2-(5′-oxo-valeroyl)-*sn*-glycero-3-phosphocholine (*m/z* 594, POVPC) (*28*), the 4-carbon aldehyde 1-palmitoyl-2-(4'-oxo-butanoyl)-*sn*-glycero-3-phosphocholine (POBPC, *m/z* 580) (*68*), the 8-carbon aldehyde 1-palmitoyl-2-(8'-oxo-octanoyl)-*sn*-glycero-3-phosphocholine (*m/z* 636), the 9-carbon aldehyde 1-palmitoyl-2-(9'-oxo-nonanoyl)-*sn*-glycero-3-phosphocholine (*m/z* 650) (*110, 111*), as well as carboxylic acid-containing 1-palmitoyl-2-azelaoyl-*sn*-glycero-3-phosphocholine (PazPC, *m/z* 666)(*111, 112*) (Figure 3K).

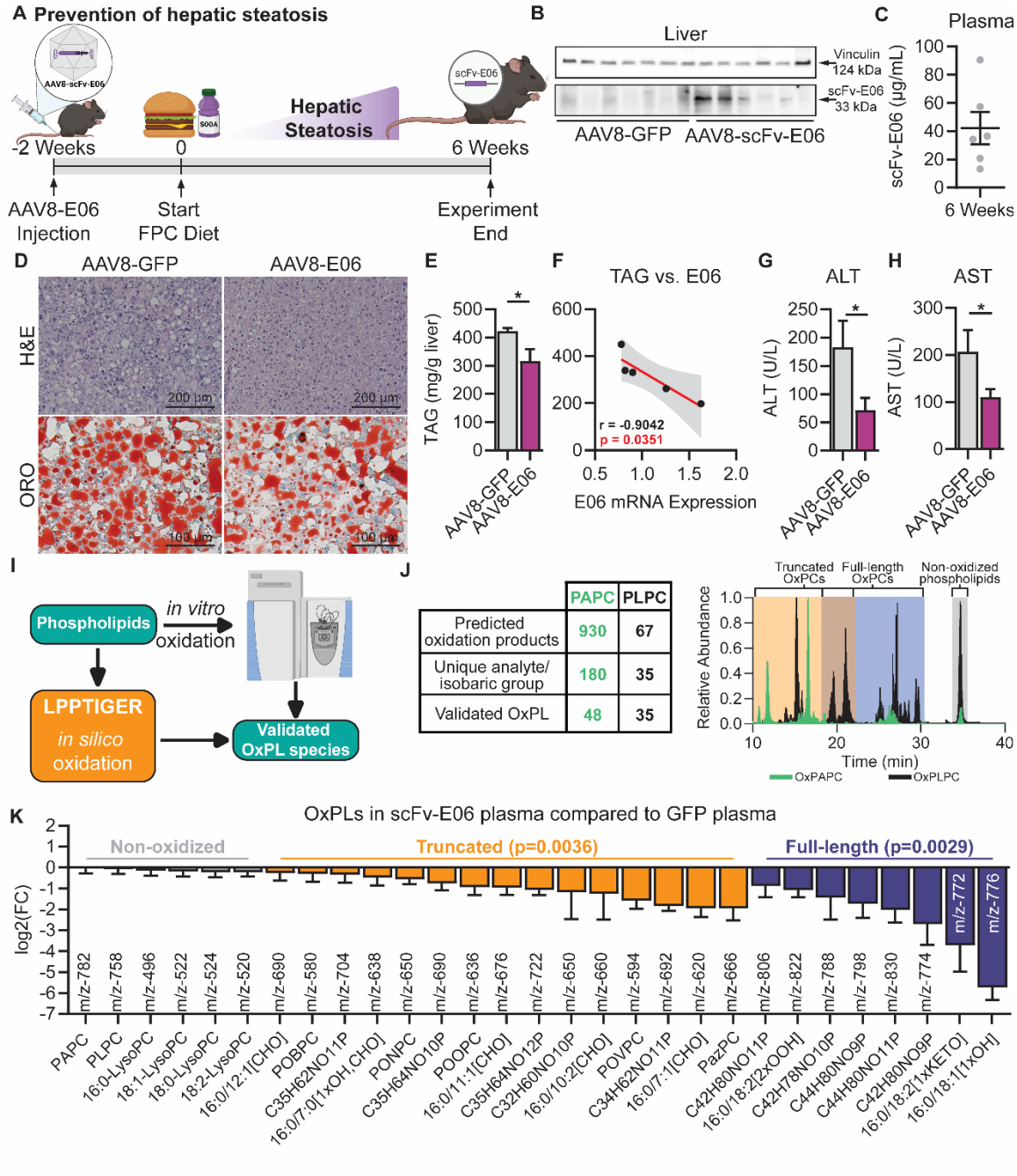

Figure 3. Virus-mediated hepatic expression of scFv-E06 prevented development of diet induced hepatic steatosis.

Figure 3. Virus-mediated hepatic expression of scFv-E06 prevented development of diet induced hepatic steatosis.
(A) Schematic of experimental design. Mice were injected via tail vein with AAV8-E06 or AAV8-GFP 2 weeks prior to the start of 6-week FPC-diet challenge (Created with BioRender.com). **(B)** scFv-E06 protein expression in mouse liver eight weeks after injection. **(C)** scFv-E06 titer concentrations were estimated in plasma by competitive sandwich ELISA. **(D)** Hematoxylin and eosin and Oil Red O staining revealed decreased hepatic lipid burden in mice expressing scFv-E06 and was confirmed by **(E)** quantification of hepatic triglycerides (GFP – n=6, scFv-E06 – n=5). **(F)** Hepatic triglyceride concentrations negatively correlated with hepatic mRNA expression of scFv-E06 (scFv-E06 – n=5). scFv-E06 expression protected mice from diet-induced liver toxicity resulting in significantly lower **(G)** ALT and **(H)** AST (GFP – n=6, scFv-E06 – n=6). **(I)** Schema demonstrating strategy for mass spectrometry method development and validation. **(J)** 48 analytes/isobaric groups from PAPC and 35 analytes/isobaric groups from PLPC were validated. **(K)** Both truncated and full-length OxPC species were significantly reduced in mice expressing scFv-E06 (GFP – n=7, scFv-E06 – n=6). Statistical significance was determined by 2-way ANOVA, Spearman's Rank Correlation, and Student's T-test (*=$p<0.05$).

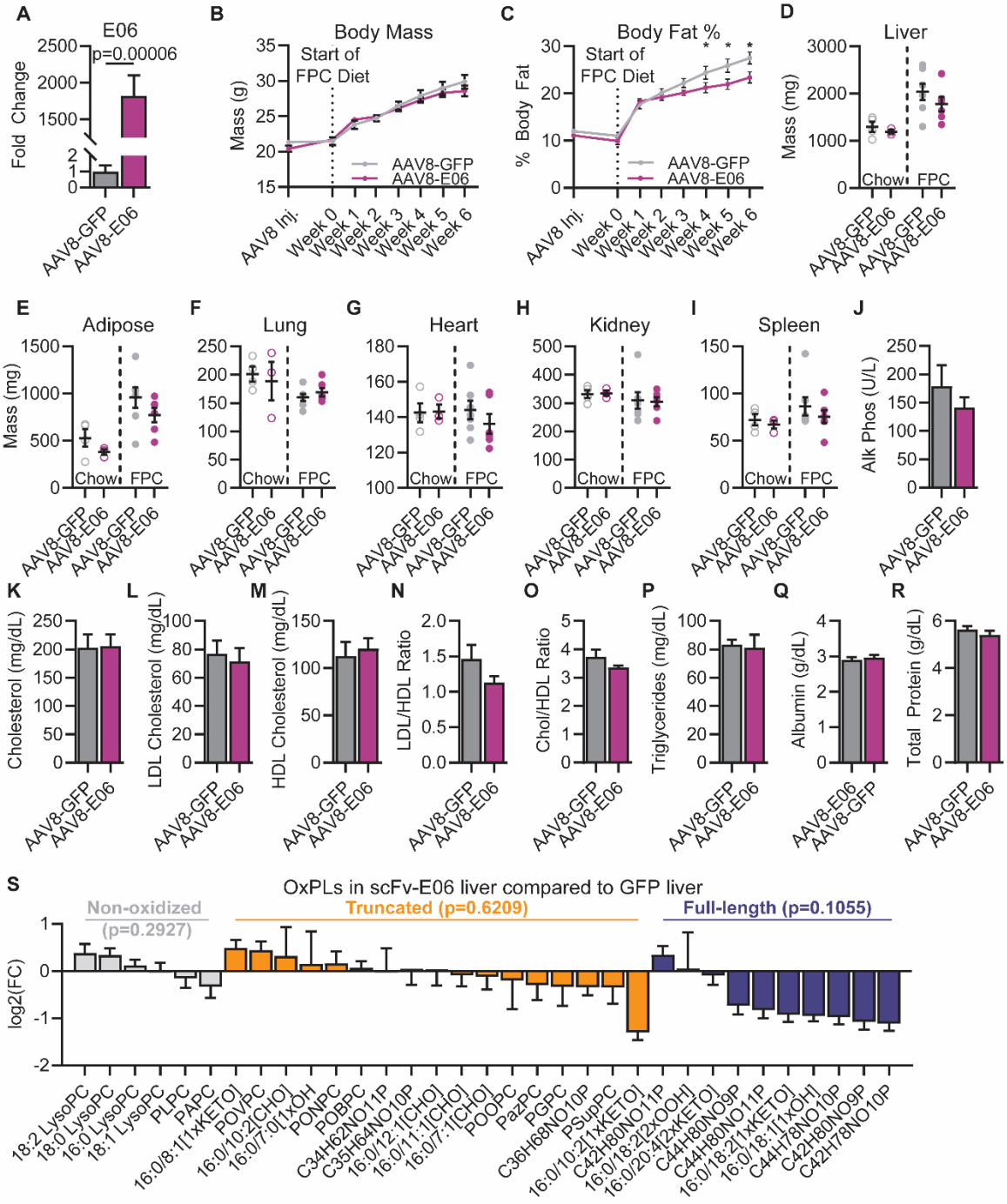

Figure 4. Characterization of mice treated with AAV8-scFv-E06 after six weeks of FPC diet.

Figure 4. Characterization of mice treated with AAV8-scFv-E06 after six weeks of FPC diet.

Speer6-ps1$^{Tg(Alb\text{-}cre)21Mgn}$/J mice were injected with AAV8-GFP or AAV8-scFv-E06. Two weeks after injection, mice were fed FPC diet for six weeks (FPC AAV8-GFP, n=7; FPC AAV8-E06, n=6). **(A)** scFv-E06 mRNA expression was significantly increased in mice injected with AAV8-scFv-E06 (AAV8-GFP – n=6; AAV8-E06 – n=6). **(B)** Body mass (FPC AAV8-GFP, n=7; FPC AAV8-E06, n=6) and **(C)** body fat percentage (FPC AAV8-GFP, n=6; FPC AAV8-E06, n=6) were recorded weekly. While there was no difference in body mass, there was a significant decrease in body fat percentage between FPC diet-fed mice expressing scFv-E06 compared to mice expressing GFP after four weeks on diet. There was significant increase in body fat percentage between chow fed and FPC diet-fed mice after six weeks. After six weeks, mouse plasma was collected, and hepatic function and lipid profile were measured. (**D-I)** There were no significant differences in organ mass between AAV8-GFP and AAV8-scFv-E06 in either chow-fed or FPC-fed mice (FPC AAV8-GFP, n=7; FPC AAV8-E06, n=6). There was no significant difference in **(J)** alkaline phosphatase, **(K)** cholesterol, **(L)** LDL cholesterol, **(M)** HDL cholesterol, **(N)** LDL/HDL ratio, **(O)** cholesterol/HDL ratio, **(P)** triglycerides, **(Q)** albumin, and **(R)** total protein in the plasma of FPC diet-fed mice expressing scFv-E06 compared to GFP-expressing mice (AAV8-GFP – n=6; AAV8-E06 – n=6). **(S)** Truncated and full-length OxPCs extracted from liver tissue demonstrate a similar pattern to that observed in the plasma. Statistical significance was determined by 1-way and 2-way ANOVA and Student’s T-test. Multiple comparisons were corrected by Dunnet or Tukey

multiple comparisons correction (*=p<0.05, **=p<0.01, ***=p<0.001, ****=p<0.0001). Statistical outliers were excluded based on the ROUT test (Q=5%).

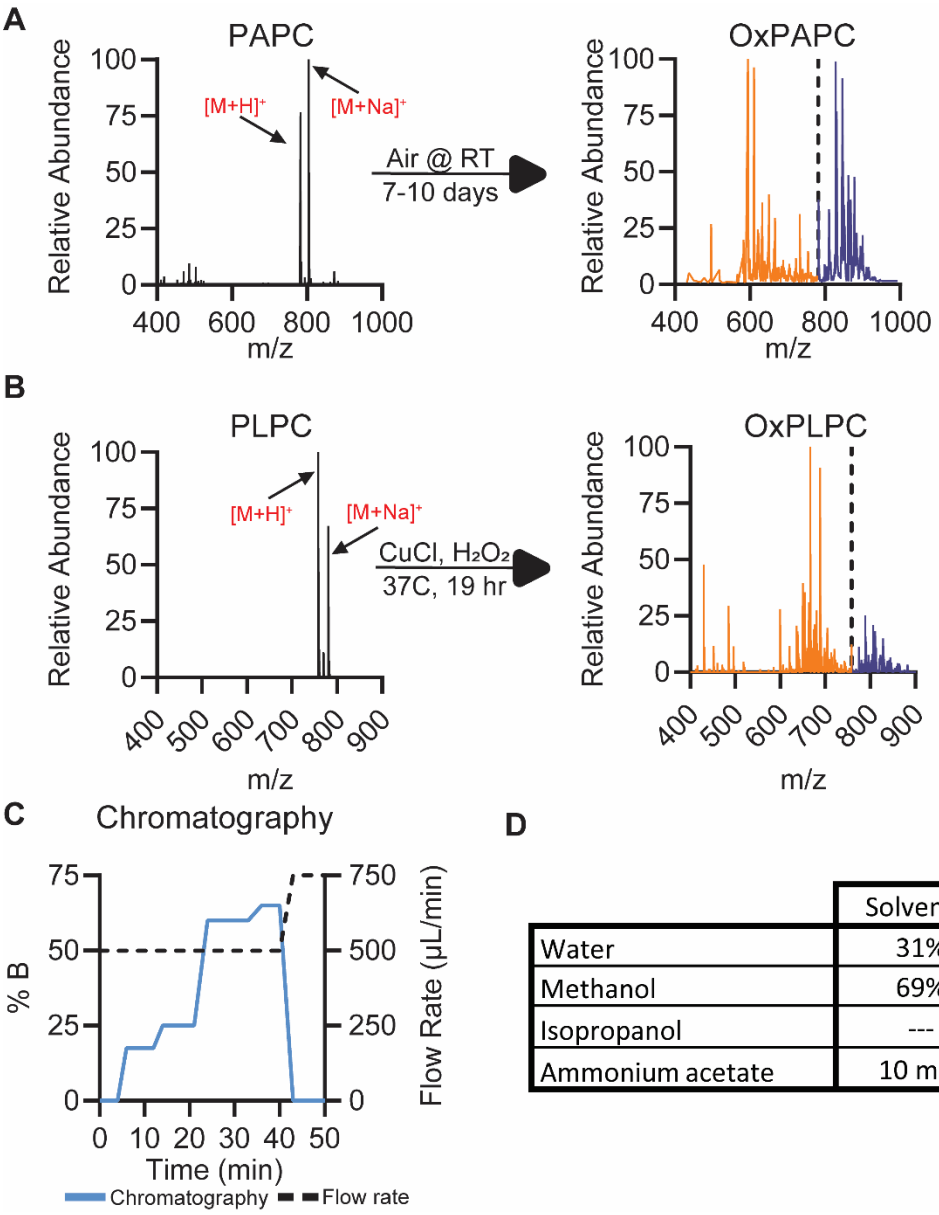

	Solvent A	Solvent B
Water	31%	---
Methanol	69%	50%
Isopropanol	---	50%
Ammonium acetate	10 mM	10 mM

Figure 5. Oxidation and detection of oxidation products of PAPC and PLPC.

Figure 5. Oxidation and detection of oxidation products of PAPC and PLPC. Oxidized phospholipids were prepared for LCMS by *in vitro* oxidation. **(A)** PAPC was oxidized by air for 7-10 days. **(B)** PLPC was oxidized by Fenton-like copper reaction for 18 hours. **(C)** Schematic of chromatography for analysis mass spectrometric analysis of oxidized phospholipids. **(D)** Solvent system for separation of OxPL species by HPLC.

Among the most significantly reduced full-length OxPC were 1-palmitoyl-2-((E)-8'-hydroxyoctadec-12'-enoyl)-*sn*-glycero-3-phosphocholine (HODE-PC, *m/z* 776), an isobaric group with a *m/z* of 798 containing 1-palmitoyl-2-((5E,8E,11E,14E)-4'-hydroxyicosa-5',8',11',14'-tetraenoyl (HETE-PC) (*113*), and an isobaric group with a *m/z* of 830 containing isoprostane-PC (*5, 114*) (Figure 3K). The structures of the identified compounds with the corresponding *m/z* values are represented in table S1.

Together, these data demonstrate that AAV8-dependent hepatic expression of scFv-E06 results in its secretion into the plasma, decreased plasma levels of defined OxPC species, and protection from diet-induced hepatic. Remarkably, scFv-E06 showed specificity towards OxPCs, but not non-oxidized phospholipids, recognizing a variety of oxidation-specific functional groups that are associated with previously reported biological functions (*1, 115*).

2.3.3 – OxPCs regulate hepatocyte gene expression and mitochondrial bioenergetics

These data imply a role of OxPCs in the development of hepatic steatosis; however, it is unknown if hepatocytes recognize and respond to OxPCs. To investigate if OxPCs regulate hepatocyte function, we treated a murine hepatocyte cell line (AML12) with a mixture of full length and truncated OxPCs (OxPAPC) (*28*) for four hours and analyzed changes in gene expression by ribonucleic acid sequencing (RNA-seq). OxPAPC regulated the expression of 1,367 genes in AML12 hepatocytes (fold change > 1.5, FDR < 0.05), of which 782 were upregulated and 585 were downregulated compared to vehicle-treated cells (Figure 6A, table S2). EnrichR (*116, 117*) gene ontology pathway analysis revealed that OxPAPC induced pathways associated with oxidative stress, including the "NRF2-mediated oxidative stress response", the "unfolded protein response", and the "aryl hydrocarbon receptor signaling pathway", as well as the "superpathway of cholesterol biosynthesis" (Figure 7A), suggesting that OxPCs contribute to dysregulating cholesterol metabolism, a hallmark of NAFLD (*118*).

Since our data showed that levels of both truncated and full-length OxPCs were decreased by scFv-E06, we separated OxPAPC into two fractions enriched for either truncated or full-length OxPC species using a strong anionic solid phase exchange chromatography method we previously described (*64*). Treatment of AML12 cells with truncated OxPCs resulted in regulation of 720 genes (427 upregulated, 293 downregulated), while full-length OxPCs regulated expression of 259 (204 upregulated, 55 downregulated) genes (Figure 6B). Of those, truncated

OxPCs uniquely regulated 78 genes (30 up/45 down) while full-length OxPCs uniquely downregulated 2 genes (Figure 6B, table S2). Both truncated and full-length OxPAPC upregulated genes associated with oxidative stress such as *Hmox1*, *Gsta1*, *Txnrd1*, *Hspa1a*, and *Hspa1b*, as well as *Ptgs2* (Cyclooxygenase 2) (table S2). Additionally, RT-qPCR confirmed that full-length OxPCs, truncated OxPCs, and OxPAPC upregulated expression of *Hmox1* (Figure 7D) and *Pgd* (Figure 7E), while only truncated OxPCs upregulated *Acly* (Figure 7F)*, Hmgcoas* (Figure 7G)*,* and *Hmgcoar* (Figure 7H). GO Biological Pathway analysis revealed that like OxPAPC, both truncated OxPCs and full-length OxPCs induced the "NRF2-mediated oxidative stress pathway", however, only truncated OxPCs induced the "superpathway of cholesterol biosynthesis" (Figure 6C-E, Figure 7A). Moreover, truncated OxPAPC downregulated expression of *Cav1* (Caveolin 1), which has been shown to increase hepatic lipid droplet size in NAFLD (*119-121*), and upregulated *Slc25a1*, which has recently been associated with hepatic steatosis and glucose intolerance by dysregulation of hepatocyte metabolism (*122*).

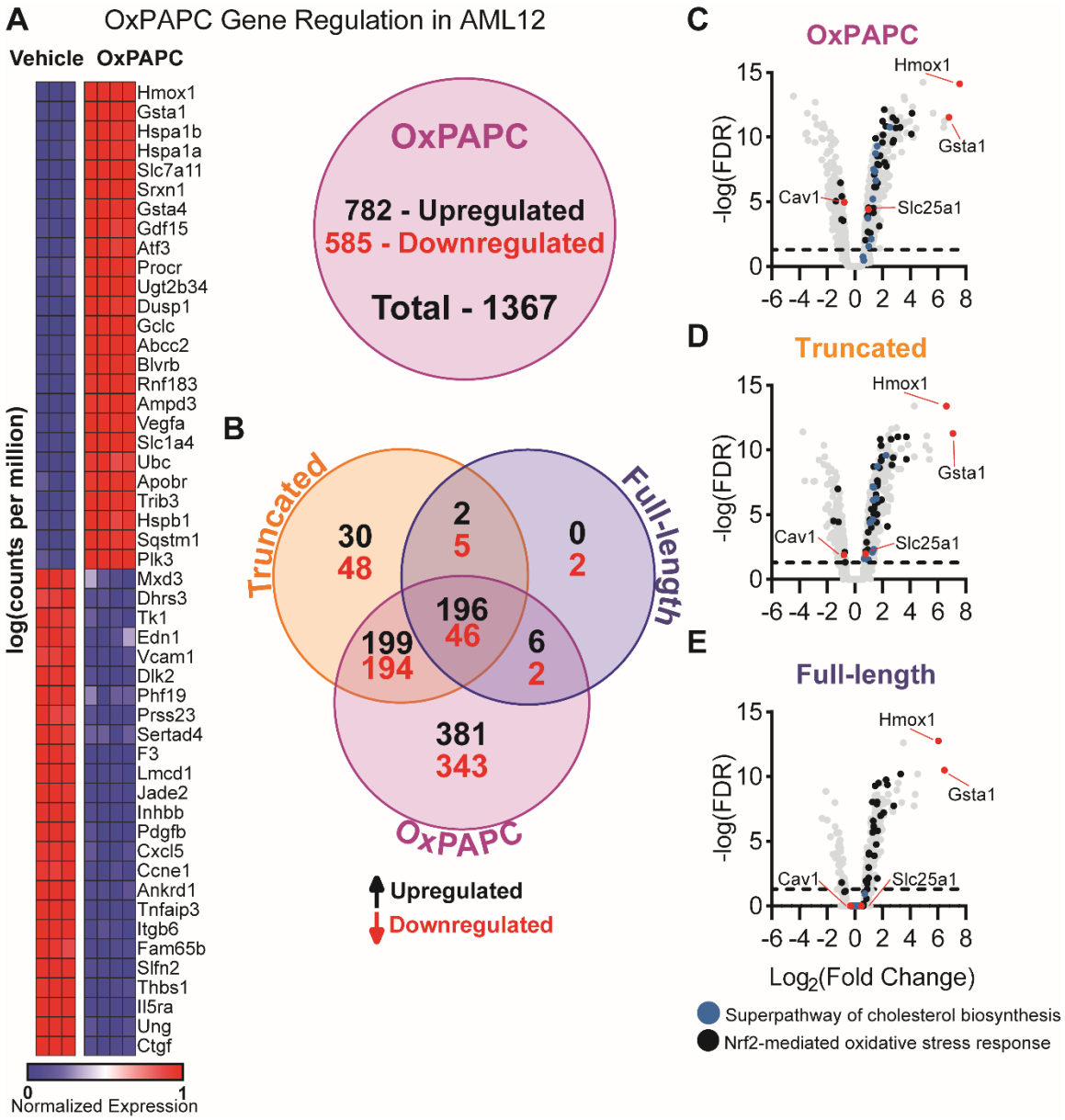

Figure 6. Truncated OxPLs shift AML12 hepatocytes to an anabolic metabolic programming.

Figure 6. Truncated OxPLs shift AML12 hepatocytes to an anabolic metabolic programming.

AML12 hepatocytes were treated with OxPAPC (100 μg/mL) for 4 hours and gene expression was measured via RNA-seq. **(A)** OxPAPC regulated 1367 genes (782 upregulated/585 downregulated – fold change > |1.5| and adjusted p-value < 0.05, vehicle – n=3, OxPAPC – n=4). **(B)** Truncated OxPLs uniquely regulated 78 genes (30 upregulated/48 downregulated) compared to 2 down-regulated genes in full-length OxPL and 724 (381 upregulated/343 down-regulated) in OxPAPC treatment with 242 regulated by all three treatments (196 upregulated/46 downregulated) (fold change > |1.5| and adjusted p-value < 0.05, n=3-4). Volcano plot analysis of **(C)** OxPAPC, **(D)** truncated OxPAPC, and **(E)** full-length OxPAPC revealed *Hmox1* and *Gsta1* were the most highly upregulated genes in all three treatments along with genes associated with the NRF2-mediated oxidative stress response. *Slc25a1* and *Cav1* were regulated in OxPAPC and truncated OxPL treatment, but not in full-length OxPL treatment. The same pattern was observed for genes associated with the superpathway of cholesterol biosynthesis. Statistical significance was determined by 1-way ANOVA and Student's t-test. Multiple comparisons were corrected by False Discovery Rate or Dunnet's multiple comparison correction.

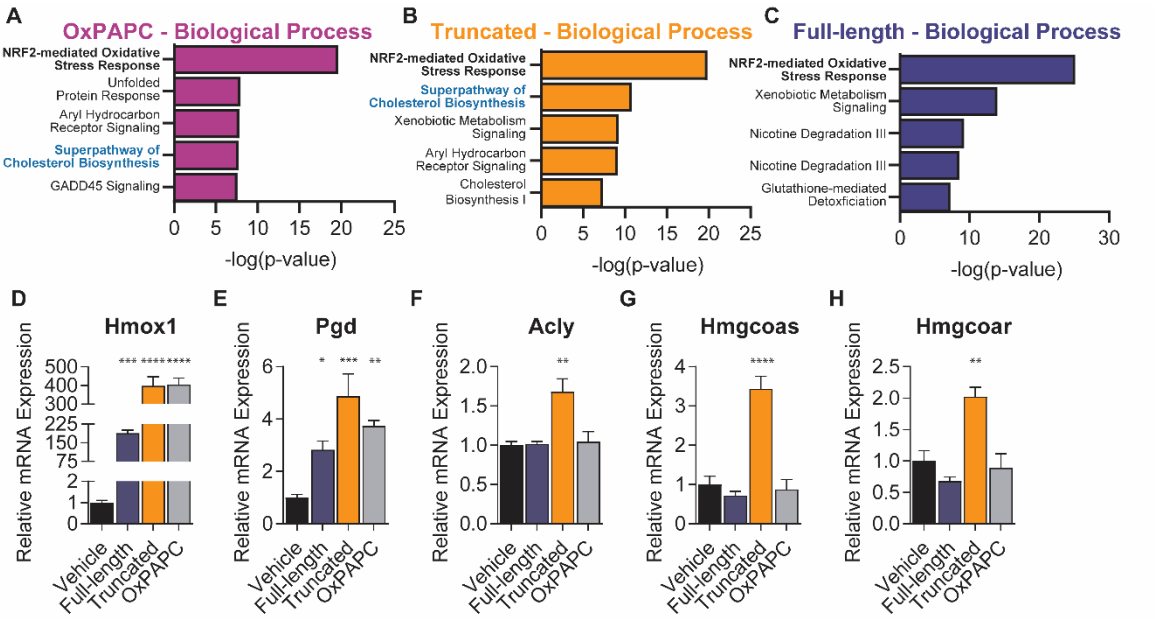

Figure 7. Gene ontology and gene expression of AML12 hepatocytes treated with truncated OxPAPC, full-length OxPAPC, and OxPAPC.

Figure 7. Gene ontology and gene expression of AML12 hepatocytes treated with truncated OxPAPC, full-length OxPAPC, and OxPAPC.
AML12 murine hepatocytes were treated with either OxPAPC, truncated OxPAPC, and full-length OxPAPC (100 μg/mL) for 4 hours and gene expression was measured via RNA-seq. GO Biological processes of upregulated genes (fold change > |1.5| and adjusted p-value < 0.05) identified by EnrichR for **(A)** OxPAPC, **(B)** truncated OxPAPC, and **(C)** full-length OxPAPC. Expression of **(D)** *Hmox1,* **(E)** *Pgd,* **(F)** *Acly,* **(G)** *Hmgcoas,* and **(H)** *Hmgcoar* in AML12 hepatocytes were confirmed by RT-qPCR (n=4). *Hmox1* and *Pgd* were regulated by all three oxidized phospholipid treatments; however, *Acly*, *Hmgcoas*, and *Hmgcoar* were exclusively upregulated by truncated OxPAPC. Statistical significance was determined by 1-way ANOVA. Multiple comparisons were corrected by Dunnet's multiple comparisons correction (*=p<0.05, **=p<0.01, ****=p<0.0001).

To investigate the effect of OxPCs on hepatocyte metabolism, we treated AML12 cells with OxPAPC or the fractions enriched for truncated or full-length OxPCs for four hours and measured oxygen consumption rate *via* extracellular flux analysis. Treatment with OxPAPC significantly decreased maximal oxygen consumption rate (Figure 8A), which was mimicked by truncated OxPCs (Figure 8B). Impaired oxygen consumption in hepatocytes is indicative of mitochondrial dysfunction that precedes the transition from steatosis to NASH (*93, 123*). To investigate whether this metabolic dysregulation would lead to increased lipid accumulation, we treated AML12 hepatocytes with OxPAPC, truncated or full-length OxPCs for 48 hours, and then stained cells with Nile Red to quantify lipid droplet numbers and size(*124*). Consistent with the effects on hepatocyte mitochondrial function, OxPAPC (Figure 8C) and truncated OxPCs (Figure 8D) increased average lipid droplet size in cells compared to vehicle, while full-length OxPCs (Figure 8E) did not alter lipid droplet size (Figure 8F). However, both fractions increased the number of lipid droplets per cell compared to vehicle control (Figure 8G).

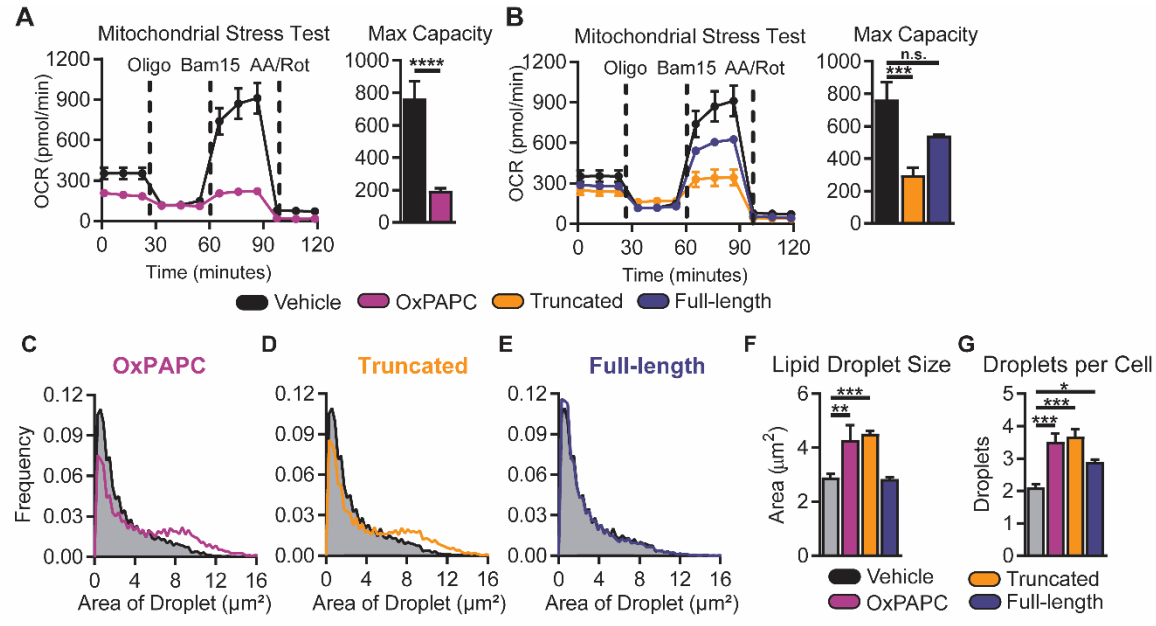

Figure 8. Truncated oxidized phospholipids dysregulate hepatocyte metabolism resulting in lipid droplet accumulation.

Figure 8. Truncated oxidized phospholipids dysregulate hepatocyte metabolism resulting in lipid droplet accumulation.
(A) MST analysis of AML12 murine hepatocytes treated with OxPAPC (100 μg/mL) for four hours significantly inhibited maximum oxygen consumption in hepatocytes (n=5). **(B)** Truncated, but not full-length OxPLs significantly inhibited maximum mitochondrial oxygen consumption rate (n=5). AML12 cells were treated with **(C)** OxPAPC (100 μg/mL), **(D)** truncated OxPAPC, and **(E)** full-length OxPAPC for 48 hours. **(F)** Lipid droplet size and **(G)** number were significantly increased in AML12 cells treated with OxPAPC and truncated OxPLs. Full-length OxPLs increased droplet number per cell (n=4, 3 fields of view per biological replicate). Statistical significance was determined by 1-way ANOVA and Mann Whitney U-Test. Multiple comparisons were corrected by False Discovery Rate or Dunnet's multiple comparison correction (*=$p<0.05$, **=$p<0.01$, ***=$p<0.001$, ****=$p<0.0001$).

Taken together, these data demonstrate that distinct OxPC species differently regulate hepatocyte gene expression and metabolic function *in vitro*. While both truncated and full-length OxPC regulate redox transcriptomic programming, only truncated OxPCs regulate anabolic gene programming, such as the superpathway of cholesterol biosynthesis, and inhibit mitochondrial oxygen consumption resulting in increased lipid droplets.

2.3.4 - Interventional therapy to treat established hepatic fibrosis scFv-E06 intervention after development of hepatic steatosis halts disease progression to fibrosis

To test whether elimination of OxPCs through inducible expression of scFv-E06 during the transition from steatosis to NASH could halt the progression to fibrosis, we first fed age-matched Alb-cre mice an FPC diet for six weeks (Figure 9A), which established hepatic steatosis without signs of fibrosis. Then weight-randomized mice were injected with AAV8-scFv-E06 or AAV8-GFP *via* tail vein. To induce fibrosis, mice were fed FPC diet for an additional 14 weeks (Figure 9A). Sustained scFv-E06 gene expression was confirmed in the liver (Figure 10A) and scFv-E06 protein was detected in the liver by Western blot and in the plasma by ELISA (Figure 9B,C) at the end of the experiment (20 weeks). As expected, FPC diet significantly elevated body mass and body fat percentage compared to chow control (Figure 105B,C); however, there were no differences in body mass (Figure 10B); body fat percentage (Figure 10C); liver, adipose, lung, heart, kidney, and spleen mass (Figure 10D-I); and fasting glucose and insulin tolerance between AAV8-scFv-E06 or AAV8-GFP-treated mice at 20 weeks (Figure 10Q-S).

Strikingly, intervention with AAV8-scFv-E06 protected mice with established hepatic steatosis from further liver injury as evidenced by significantly reduced plasma AST (Figure 9D), ALT (Figure 9E), alkaline phosphatase (ALP) (Figure 9F), LDL:HDL ratio (fig. S5J), and cholesterol:HDL ratio (Figure 10K) indicating significantly improved liver function compared to control mice. Plasma cholesterol (Figure 10L), LDL (Figure 10M), HDL (Figure 10N), triglycerides (Figure 10O), and albumin (Figure 10P) were not changed by expression of scFv-E06. Total hepatic triglyceride levels were not affected by AAV8-E06 (Figure 9G), however, histological analysis by hematoxylin-eosin and oil red O staining revealed a decrease in average lipid droplet size and a concomitant increase in lipid droplet number (Figure 9H,I) in the livers of mice expressing scFv-E06, a pattern of lipid droplet morphology suggestive of improved liver health (*90*) .

To examine if intervention with AAV8-scFv-E06 affects hepatic gene expression in mice with established steatosis during NASH progression, we performed RNA-seq in bulk liver tissue from mice that were treated with either AAV8-scFv-E06 or AAV8-GFP. Strikingly, 701 genes (154 upregulated and 547 downregulated in scFv-E06 expressing mice) were differentially expressed (fold change > 1.5, FDR < 0.05) between AAV8-scFv-E06 or AAV8-GFP-treated mice. EnrichR and GO Pathway Analysis for Biological Processes revealed that the most significantly downregulated GO term in the scFv-E06 expressing group was “Extracellular Matrix Organization” indicating downregulation of genes associated with matrix production and consequently hepatic fibrosis (Figure 9J). Additionally,

“Regulation of Cell Migration”, “PDGFR Signaling Pathway”, “Cell Matrix Adhesion”, and “Regulation of Macrophage Cytokine Production” were all downregulated suggesting a reduced fibrotic and inflammatory tone in the liver of mice expressing scFv-E06. Extracellular matrix protein (ECM) gene regulation was confirmed by RT-qPCR. Overall, expression of a panel of ECM proteins was significantly lower in livers of scFv-E06 expressing mice (Figure 11A). To assess the extent of hepatic fibrosis in mice expressing scFv-E06, we quantified picrosirius red staining in livers after 20 weeks of FPC diet, which revealed a trend toward a decrease in positive staining in mice which received intervention with scFv-E06 (Figure 9K). Liver hydroxyproline concentration was significantly increased in GFP-expressing mice fed FPC diet for 20 weeks compared to chow (Figure 9L) and the FPC-induced increase in hydroxyproline was attenuated by intervention with scFv-E06 after six weeks on diet (Figure 9M). Taken together, these data demonstrate that intervention with scFv-E06 in mice with established steatosis protects mice from further diet-induced liver damage and hepatic fibrosis.

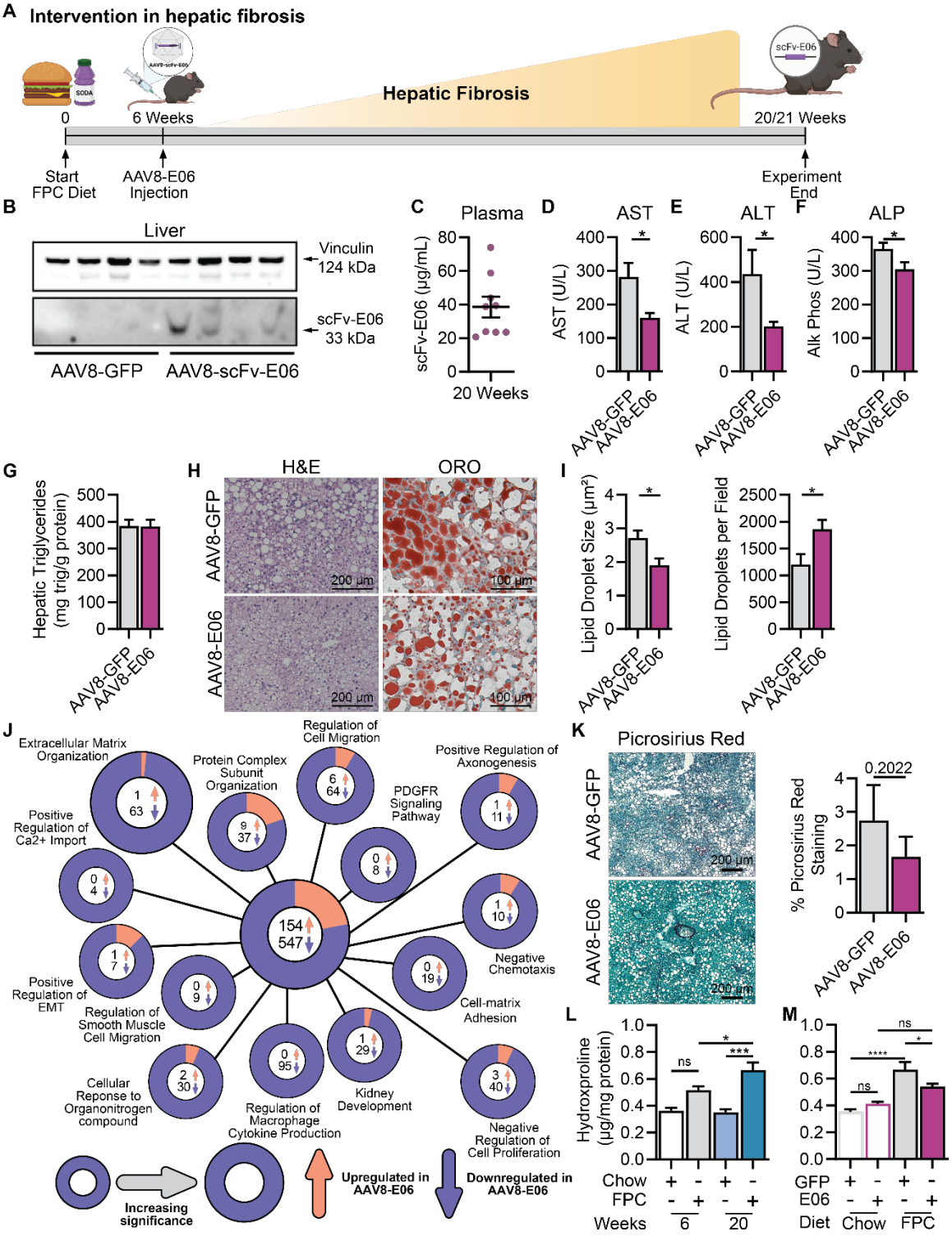

Figure 9. Passive genetic immunization against oxidized phospholipids inhibits liver fibrogenesis.

Figure 9. Passive genetic immunization against oxidized phospholipids inhibits liver fibrogenesis.
(A) Schematic of experimental design. Mice were challenged with FPC diet for six weeks. After six weeks mice were injected with AAV8-GFP or -E06 and fed FPC diet for an additional 14 weeks (total – 20 weeks) (Created with BioRender.com). **(B)** Expression of scFv-E06 in mouse liver14 weeks after injection. **(C)** scFv-E06 titer concentrations were estimated in plasma by competitive sandwich ELISA **(D)** Plasma AST, **(E)** ALT, and **(F)** alkaline phosphatase levels were decreased in mice expressing scFv-E06 (n=6). **(G,H)** Hematoxylin and eosin and oil red o staining revealed no difference in hepatic triglycerides with an **(I)** increased droplet size but reduced number in mice expressing scFv-E06 (GFP – n=6, scFv-E06 – n=6, 15 fields of view per biological replicate). **(J)** Pathway analysis of differential gene expression in bulk liver tissue identified 701 genes (154 upregulated/547 downregulated) that were significantly regulated by scFv-E06 expression (GFP - n=3, scFv-E06 - n=3 - fold change > |1.5| and FDR < 0.05). Extracellular matrix organization was the most significantly downregulated pathway in scFv-E06 expressing mice. **(K)** representative picrosirius red staining of livers from mice expressing GFP or scFv-E06 after 20 weeks of FPC diet. **(L)** Hydroxyproline concentration was measured in liver tissue from mice fed chow or FPC diet for 6 or 20 weeks. **(M)** Liver hydroxyproline concentration was decreased in mice expressing scFv-E06 after 20 weeks on FPC diet compared to GFP-expressing controls. Quantification of picrosirius red confirmed reduced staining in scFv-E06 mice (n = 4). Statistical significance was determined by 1-way ANOVA, 2-way ANOVA, Spearman’s

Correlation, and Student's T-test with Dunnet's multiple comparisons correction (*=p<0.05). Statistical outliers were excluded using ROUT test with a Q=2%.

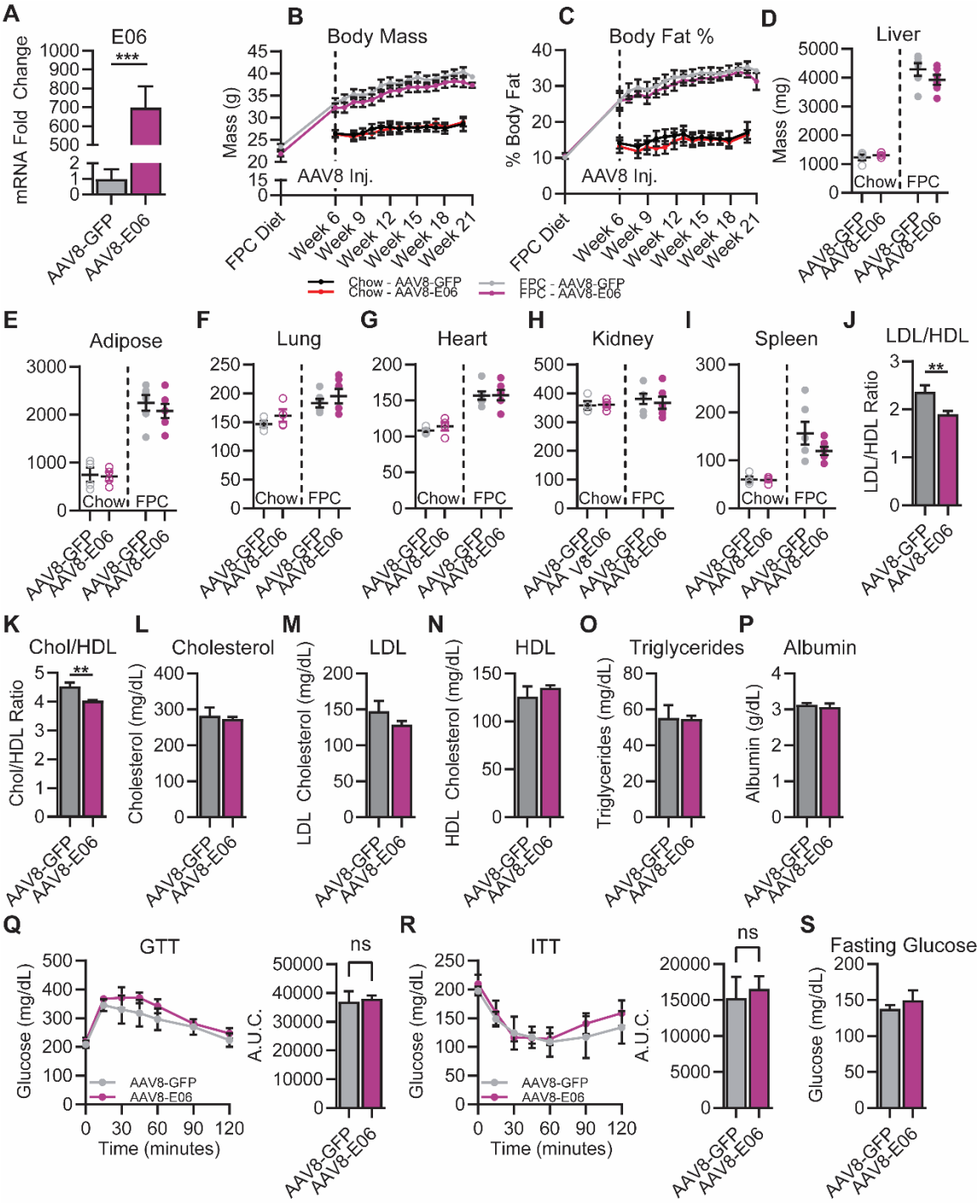

Figure 10. Characterization of mice treated with AAV8-scFv-E06 after 20 weeks on FPC diet.

Figure 10. Characterization of mice treated with AAV8-scFv-E06 after 20 weeks on FPC diet.

Speer6-ps1$^{Tg(Alb\text{-}cre)21Mgn}$/J mice were fed FPC or chow diet for six weeks. After six weeks mice were injected with either AAV8-GFP or AAV8-scFv-E06. Mice continued diet for a total of 20/21 weeks. **(A)** scFv-E06 gene expression was significantly increased in mice injected with AAV8-scFv-E06 ((FPC AAV8-GFP, n=5; FPC AAV8-E06, n=6). There were no significant differences in **(B)** body mass or **(C)** body fat percentage between GFP and scFv-E06 expressing mice on FPC or chow diet; however, there were a significant increase in both body mass and body fat percentage between diet groups (n=10). At the end of the experiment, plasma was collected, and hepatic function and lipid profile were measured. **(D-I)** There were no differences in organ mass between scFv-E06- and GFP-expressing mice fed chow or FPC diet (n=6). Ratios of **(J)** LDL/HDL and **(K)** Cholesterol/HDL in plasma were significantly reduced in mice expressing scFv-E06 compared to GFP after FPC diet feeding (n=6). **(L)** Cholesterol, **(M)** LDL, **(N)** HDL, **(O)** triglycerides, and **(P)** albumin levels in plasma were not significantly changed between scFv-E06 and GFP-expressing mice fed FPC diet (n=6). There were no differences in **(Q)** 6-hour fasted glucose and **(R)** insulin tolerance and **(S)** 18-hour fasting glucose in mice expressing GFP or scFv-E06 after 20 weeks FPC diet feeding (FPC AAV8-GFP, n=3; FPC AAV8-E06, n=4). Statistical significance was determined by 1-way and 2-way ANOVA and Student's T-test. Multiple comparisons were corrected by Dunnet or Tukey multiple comparisons correction (*=$p<0.05$, **=$p<0.01$, ****=$p<0.0001$).

2.3.5 - Biologically active oxidized phospholipids are reduced by interventional expression of scFv-E06 during the progression to hepatic fibrosis

To identify OxPC species that are affected by intervention with AAV8-scFv-E06 in the plasma of mice during the progression to fibrosis, we performed LCMS as described above, using the in silico-predicted and in vitro-validated compound list (Figure 3I,J). We identified 29 OxPC analytes or groups of isobaric compounds and 6 non-oxidized PCs in the plasma of mice with hepatic fibrosis (Figure 12A). A similar but less pronounced reduction in OxPCs was observed in the liver of scFv-E06 mice compared to GFP controls (Figure 11B). Additionally, there was a slight, but statistically significant decrease in non-oxidized PCs in the scFv-E06 liver (Figure 11B).

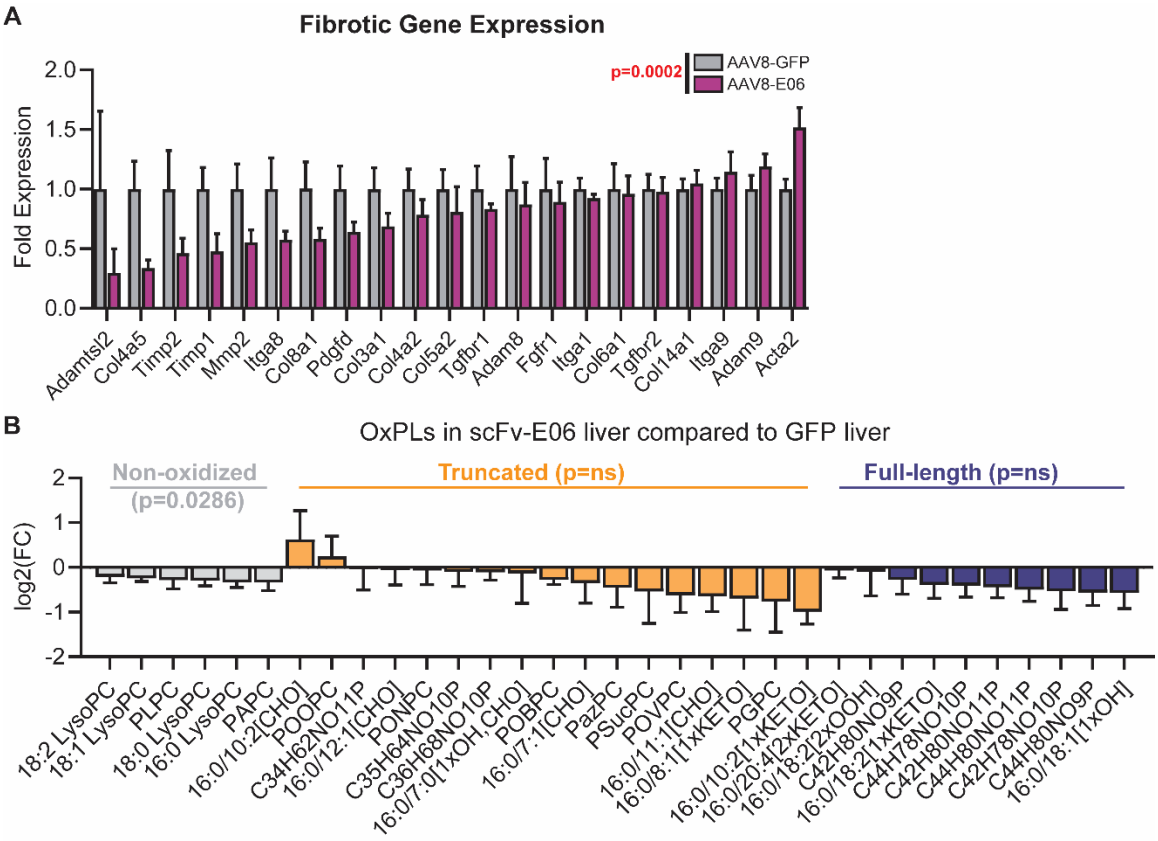

Figure 11. Fibrotic gene expression in mice treated with AAV8-scFv-E06.

Figure 11. Fibrotic gene expression in mice treated with AAV8-scFv-E06. **(A)** Hepatic gene expression of fibrogenic genes were confirmed by RT-qPCR (GFP – n=6, scFv – n=6). **(B)** Truncated and full-length OxPCs extracted from liver tissue demonstrate a similar pattern to that observed in the plasma, while non-oxidized phospholipids were significantly decreased. Statistical significance was determined by 2-way ANOVA with Dunnet's multiple comparisons correction. Statistical outliers were excluded with the ROUT test (Q=5%)

In the plasma, the majority of both truncated and full-length OxPCs were significantly decreased in scFv-E06-expressing mice and included several previously described biologically active compounds containing specific functional groups. Among decreased truncated OxPC species were the carboxylic acid-containing 1-palmitoyl-2-glutaryl-*sn*-glycero-3-phosphocholine (PGPC, *m/z* 610) as well as 1-palmitoyl-2-azelaoyl-*sn*-glycero-3-phosphocholine (PazPC, *m/z* 666) (*111, 112*), a group of γ-keto/hydroxy OxPCs (C32H60NO10P (isobaric group containing HOOA-PC), *m/z* 650); HODA-PC (1-palmitoyl-2-(9-hydroxy-12-oxo-10E-dodecenoyl)-*sn*-glycero-3-phosphocholine), *m/z* 706); KOOA-PC, *m/z* 648; C32H60NO11P (isobaric group containing HOdiA-PC), *m/z* 666) (*36, 37*), the aldehyde-containing 1-palmitoyl-2-(5′-oxo-valeroyl)-*sn*-glycero-3-phosphocholine (POVPC, *m/z* 594) (*28*), the 4-carbon aldehyde 1-palmitoyl-2-(4'-oxo-butanoyl)-*sn*-glycero-3-phosphocholine (POBPC, *m/z* 580) (*68*), and the 8-carbon aldehyde 1-palmitoyl-2-(8'-oxo-octanoyl)-*sn*-glycero-3-phosphocholine (*m/z* 636) (*110, 111*) (Figure 11A). Among the most significantly reduced full-length OxPCs were 1-palmitoyl-2-((E)-8'-hydroxyoctadec-12'-enoyl)-*sn*-glycero-3-phosphocholine (HOME-PC, *m/z* 776), and three isobaric species containing 1-palmitoyl-2-(9E,12E)-8-hydroxyoctadeca-9,12-dienoic acid-*sn*-glycero-3-phosphocholine (HODE-PC, *m/z* 774), an isobaric group with a *m/z* of 798, containing 1-palmitoyl-2-((5E,8E,11E,14E)-4'-hydroxyicosa-5',8',11',14'-tetraenoyl (HETE-PC) (*125*), and an isobaric group with a *m/z* of 830, containing isoprostane-PC (*5, 114*) (Figure 11A). The predicted structures of the identified compounds with corresponding *m/z* values are shown in table S3.

Selectivity of scFv-E06 for oxidized PCs was further illustrated by the fact that expression of scFv-E06 specifically decreased levels of truncated and full-length OxPC species, while none of the other lipid classes were significantly affected, as demonstrated by comparison of the overall plasma lipidome between scFv-E06 and GFP expressing mice after either 6 (steatosis) or 20 (fibrosis) weeks of FPC feeding (Figure 13A). Comparing the OxPC profiles at the different stages of disease progression not only demonstrated that individual OxPC species are differentially affected by scFv-E06, but also indicated that levels of OxPCs may be selectively affected during disease progression.

To study the changes in the levels of the different OxPC classes during the progression from hepatic steatosis to fibrosis, we compared OxPC levels in control mice (expressing AAV8-GFP) that had been fed FPC diet for 6 weeks and 20 weeks to their chow-fed counterparts. Of the non-oxidized species, PAPC and 16:0 LysoPC were decreased after 6, but not 20, weeks on diet, while PLPC, 18:0, 18:1, and 18:2 LysoPC were increased after both 6 weeks and 20 weeks on FPC diet (Figure 14A). Of the truncated OxPC species, levels of a subset of aldehyde-containing OxPCs, including POVPC, were lower at both 6 and 20 weeks, while carboxylic acid-containing and other aldehyde-containing OxPCs, including POBPC, were increased in response to FPC diet (Figure 14A).

Full-length OxPC species were differentially regulated at different time points. At 6 weeks, levels of 16:0/18:1[1xOH] trended to be lower compared to chow but higher at 20 weeks. 16:0/18:2[1xKETO] was higher at 6 weeks compared to chow and lower at 20 weeks. Isobaric groups C44H80NO10P and

C42H80NO9P, which contain HETE-PCs and HODE-PCs, were significantly higher at 20 weeks. Together, these data show for the first time that levels of plasma non-oxidized and individual OxPC species are differently regulated at defined stages of NAFLD progression.

Comparison of OxPCs that were affected by AAV8-scFv-E06 in the plasma of mice at the initiation of hepatic steatosis (Figure 3K) and during the progression to hepatic fibrosis (Figure 11A) revealed 28 OxPC species that were decreased in both settings, while 1 OxPC was uniquely identified in hepatic steatosis and 7 OxPC species were uniquely detected in mice with hepatic fibrosis (Figure 13B). Of the seven unique species identified in hepatic fibrosis, 4 were decreased by more than 50 percent by scFv-E06. These four species include two previously identified biologically active OxPCs: KOOA-PC and the isobaric group C32H60NO11P containing HOdiA-PC (*37*).

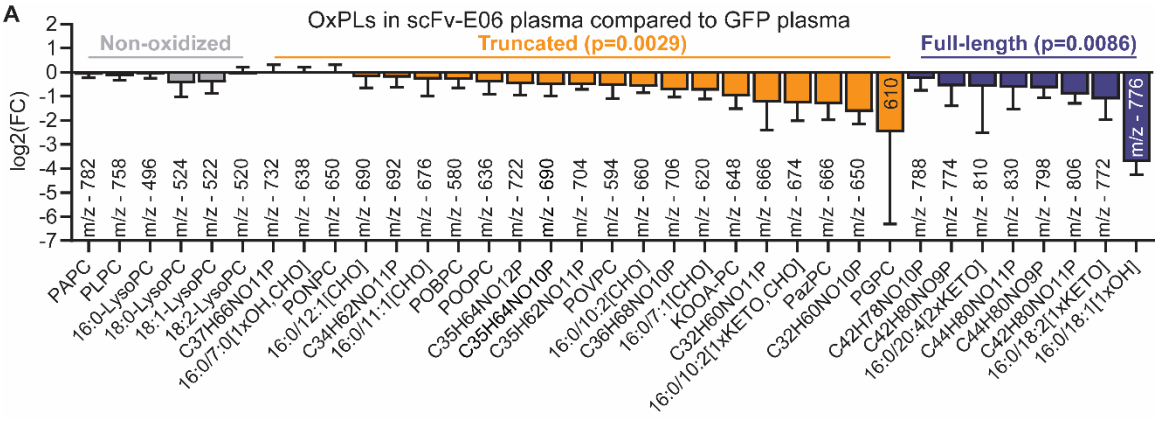

Figure 12. scFv-E06 expression decreases plasma OxPL levels in mice with hepatic fibrosis.

Figure 12. scFv-E06 expression decreases plasma OxPL levels in mice with hepatic fibrosis.

OxPL levels were measured in the plasma by LCMS. **(A)** Both truncated and full-length OxPLs were significantly reduced by scFv-E06 expression. Non-oxidized phospholipids were unaffected by scFv-E06 expression. Statistical significance was determined by 2-way ANOVA. Multiple comparisons were corrected by False Discovery Rate.

To elucidate at which stage of disease progression these identified OxPC species may exert pathologic activity, we took a closer look at the timeline of scFv-E06-mediated reduction of their plasma levels. The aldehyde-containing species POVPC, POOPC, and 16:0/7:1[CHO] were preferentially reduced by scFv-E06 after six weeks on FPC diet (Figure 14B), implying a role in the initiation of hepatic steatosis. To test whether aldehyde-containing OxPCs affect hepatocyte lipid storage, we treated AML12 hepatocytes with POVPC for 48 hours and assessed lipid droplet size and number per cell. POVPC significantly increased the number and size of lipid droplets (Figure 14C). On the other hand, carboxylic acid-containing OxPC species (PazPC and C35H62NO11P) were affected by scFv-E06 predominantly after 20 weeks of FPC diet (Figure 14D), implying a role for these compounds in NAFLD progression to NASH Treatment of AML12 cells with PGPC (a carboxylic acid-containing OxPC) significantly decreased maximum oxygen consumption rate (Figure 14E) and increased lipid droplet size and number in a concentration-dependent manner (Figure 15A,B). Of the γ-keto/hydroxy OxPC species, the levels of KOOA-PC and isobaric group C32H60NO10P (containing HOOA-PC) were reduced by scFv-E06 specifically at 20 weeks of FPC diet (Figure 14F). Treatment of AML12 hepatocytes for four hours with KOdiA-PC, a representative γ-keto/hydroxy OxPC, significantly decreased maximum oxygen consumption rate of hepatocytes in a concentration-dependent manner (Figure 14G). These data show that identified truncated OxPC species that are reduced by scFv-E06 promote a hepatocyte phenotype *in vitro* that is observed in hepatic steatosis and steatohepatitis.

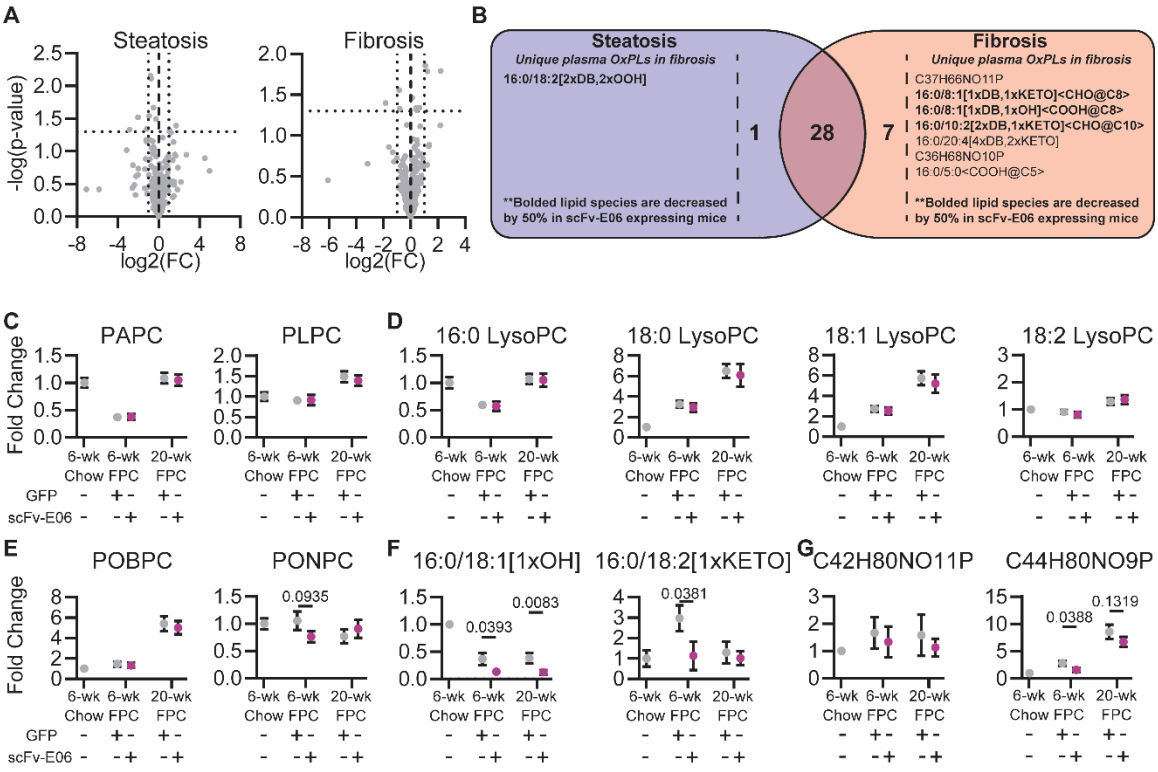

Figure 13. Untargeted and targeted lipid analysis reveal a changing oxo-phospholipidome but no change in the overall lipidome.

Figure 13. Untargeted and targeted lipid analysis reveal a changing oxo-phospholipidome but no change in the overall lipidome.
The plasma lipidome of mice after **(A)** six (GFP – n=7, scFv-E06 – n=6) and twenty weeks (GFP – n=10, scFv-E06 – n=10) of FPC diet were unaffected by expression of scFv-E06. **(B)** Comparison of oxidized phospholipids species detected in steatosis and fibrosis revealed 1 unique plasma oxidized phospholipid in steatotic mice and 7 unique oxidized phospholipids in mice with hepatic fibrosis. **(C)** Non-oxidized phospholipids PAPC and PLPC were unaffected by expression of scFv-E06; though their levels were altered by FPC diet duration (6-wk Chow GFP – n=3, 6-wk FPC GFP – n=7, 6-wk FPC scFv-E06 – n=6, 20-wk FPC GFP – n=10, 20-wk FPC scFv-E06 – n=10). **(D)** 16:0 LysoPC (6-wk Chow GFP – n=3, 6-wk FPC GFP – n=7, 6-wk FPC scFv-E06 – n=6, 20-wk FPC GFP – n=10, 20-wk FPC scFv-E06 – n=10) decreased after 6-weeks of FPC diet feeding while 18:0, 18:1 (6-wk Chow GFP – n=3, 6-wk FPC GFP – n=7, 6-wk FPC scFv-E06 – n=6, 20-wk FPC GFP – n=7/6, 20-wk FPC scFv-E06 – n=7), and 18:2 LysoPC (6-wk Chow GFP – n=2, 6-wk FPC GFP – n=7, 6-wk FPC scFv-E06 – n=6, 20-wk FPC GFP – n=6, 20-wk FPC scFv-E06 – n=7) increased after 6 and 20 weeks on FPC diet compared to 6-week, chow-fed controls. **(E)** POBPC (6-wk Chow GFP – n=3, 6-wk FPC GFP – n=7, 6-wk FPC scFv-E06 – n=6, 20-wk FPC GFP – n=10, 20-wk FPC scFv-E06 – n=10) increased with longer duration FPC-feeding but was unaffected by scFv-E06, while PONPC (6-wk Chow GFP – n=3, 6-wk FPC GFP – n=7, 6-wk FPC scFv-E06 – n=6, 20-wk FPC GFP – n=10, 20-wk FPC scFv-E06 – n=10) was unaffected by feeding and scFv-E06 expression. **(F)** 16:0/18:1[1xOH] (6-wk Chow GFP – n=1, 6-wk FPC

GFP – n=5, 6-wk FPC scFv-E06 – n=6, 20-wk FPC GFP – n=9, 20-wk FPC scFv-E06 – n=10) was decreased by expression of scFv-E06 at both 6-weeks and 20-weeks of FPC-diet feeding, while 16:0/18:2[1xKETO] was only decreased by scFv-E06 after six weeks of feeding (6-wk Chow GFP – n=3, 6-wk FPC GFP – n=7, 6-wk FPC scFv-E06 – n=6, 20-wk FPC GFP – n=10, 20-wk FPC scFv-E06 – n=8). **(G)** The isobaric group C42H80NO11P (6-wk Chow GFP – n=3, 6-wk FPC GFP – n=7, 6-wk FPC scFv-E06 – n=6, 20-wk FPC GFP – n=10, 20-wk FPC scFv-E06 – n=10) was unaffected by diet and scFv-E06 expression while C44H80NO9P was increased after six and 20 weeks of FPC diet. scFv-E06 expression decreased levels of C44H80NO9P after 20 weeks of FPC diet (6-wk Chow GFP – n=3, 6-wk FPC GFP – n=7, 6-wk FPC scFv-E06 – n=6, 20-wk FPC GFP – n=10, 20-wk FPC scFv-E06 – n=10). Statistical significance was determined by 2-way ANOVA with Tukey multiple comparison correction or Student’s t-test.

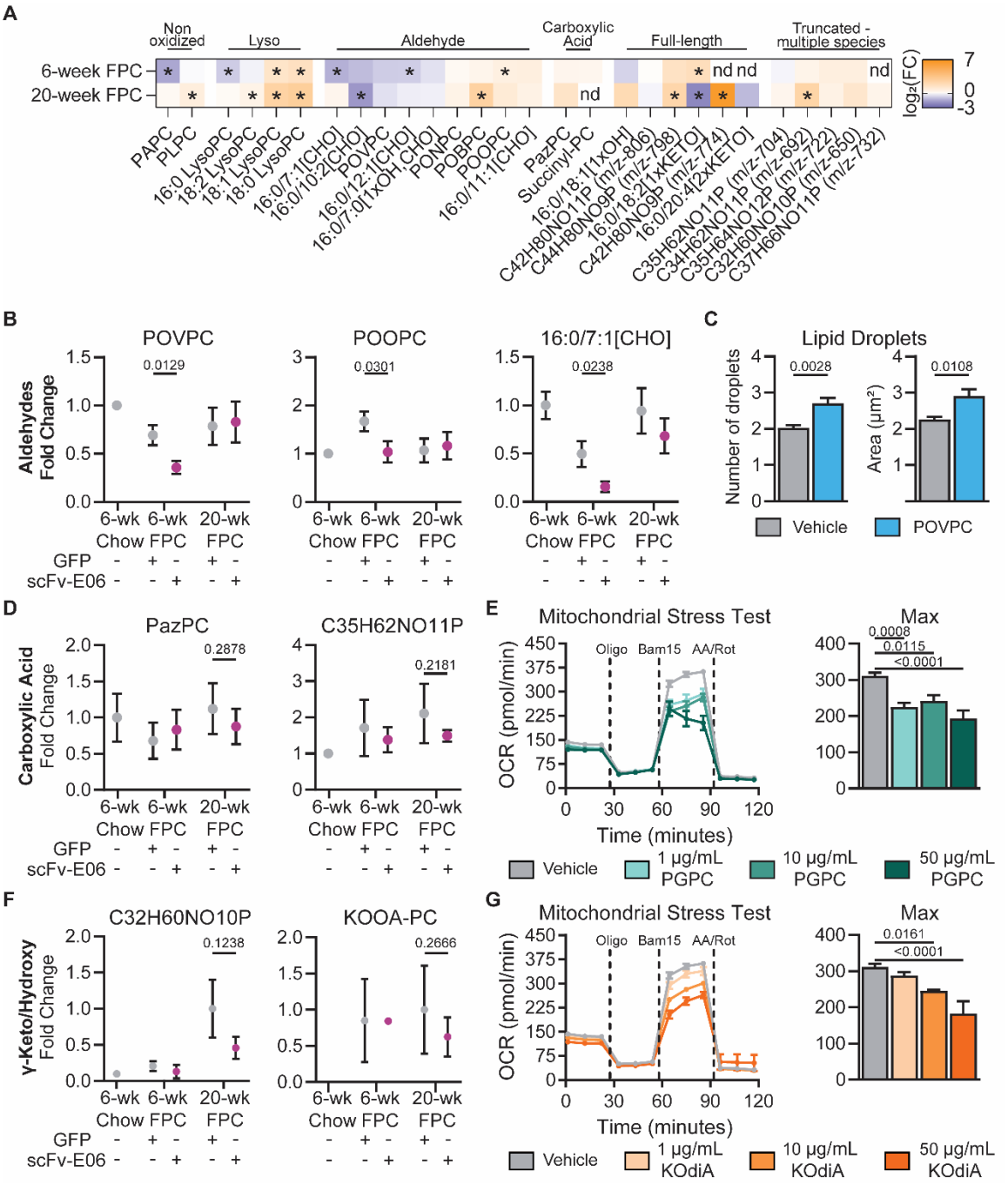

Figure 14. Bioactive oxidized phospholipids are differentially regulated during hepatic steatosis and fibrosis.

Figure 14. Bioactive oxidized phospholipids are differentially regulated during hepatic steatosis and fibrosis.
(A) Semi-quantitative analysis of OxPL species normalized to their chow counterparts demonstrate a complex, pathology-specific pattern. **(B)** Aldehyde-containing OxPLs, POVPC (6-wk Chow GFP – n=3, 6-wk FPC GFP – n=7, 6-wk FPC scFv-E06 – n=6, 20-wk FPC GFP – n=10, 20-wk FPC scFv-E06 – n=10), POOPC (6-wk Chow GFP – n=3, 6-wk FPC GFP – n=7, 6-wk FPC scFv-E06 – n=6, 20-wk FPC GFP – n=10, 20-wk FPC scFv-E06 – n=10), and 16:0/7:1[CHO] (6-wk Chow GFP – n=3, 6-wk FPC GFP – n=5, 6-wk FPC scFv-E06 – n=5, 20-wk FPC GFP – n=7, 20-wk FPC scFv-E06 – n=8), were decreased by scFv-E06 expression at six weeks. **(C)** POVPC, a representative of the aldehyde class, increased lipid droplet size and number after 48 hours in AML12 hepatocytes (n=4). **(D)** Carboxylic acid containing OxPLs were decreased by scFv-E06 after 20 weeks on diet (6-wk Chow GFP – n=3/1, 6-wk FPC GFP – n=7/4, 6-wk FPC scFv-E06 – n=5/2, 20-wk FPC GFP – n=9/5, 20-wk FPC scFv-E06 – n=9/6). **(E)** PGPC, a representative of the carboxylic acid class, decreased maximum oxygen consumption of AML12 hepatocytes after four hours (n=8, 50 μg/mL – n=6). **(F)** γ-keto/hydroxy-containing OxPLs were decreased after 20 weeks on diet (6-wk Chow GFP – n=1/0, 6-wk FPC GFP – n=5/2, 6-wk FPC scFv-E06 – n=2/1, 20-wk FPC GFP – n=9/2, 20-wk FPC scFv-E06 – n=8/4), and **(G)** KOdiA-PC, a class representative, decreased maximum oxygen consumption in AML12 hepatocytes in a dose-dependent manner (n=8). Statistical significance was determined by Student's t-test.

Hepatic stellate cells are the primary cell niche in the liver that produce fibrotic matrix in response to liver injury (*126, 127*). To determine if individual OxPC species that were targeted by scFv-E06 could activate hepatic stellate cells, we challenged LX-2 human hepatic stellate cells with OxPAPC, full-length OxPCs, truncated OxPCs, POVPC or KOdiA-PC. Treatment of LX-2 hepatic stellate cells for four hours with KOdiA-PC, OxPAPC or POVPC significantly decreased maximum oxygen consumption rate of hepatic stellate cells (Figure 15C).

Previously, *Hmox1* has been implicated in fibrotic activation of hepatic stellate cells (*128*). We found that truncated OxPCs and OxPAPC increased expression of the NRF2-dependent genes, *Hmox1* and *Gclm* in LX-2 human hepatic stellate cells (Figure 15D).

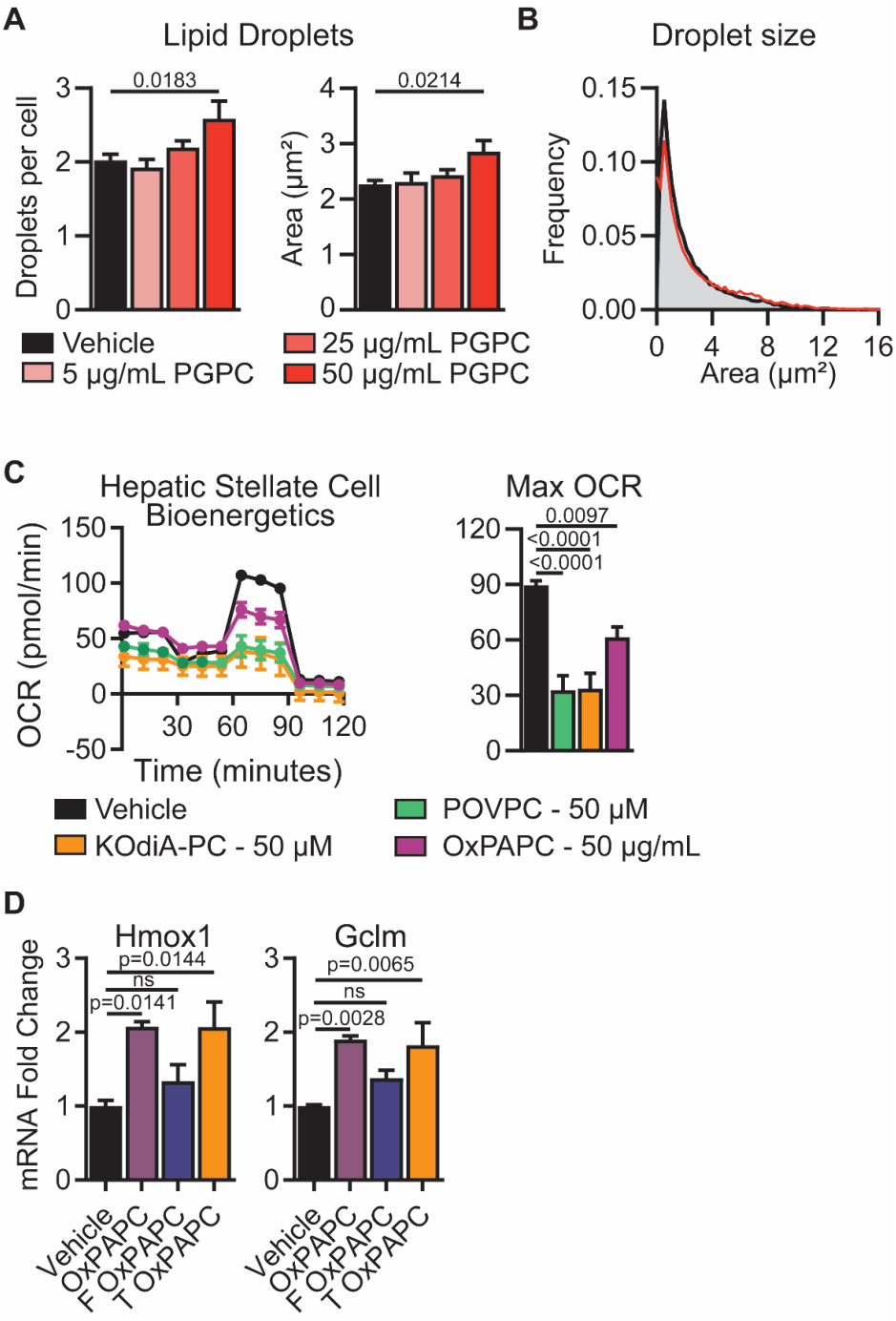

Figure 15. Pathology-driving OxPCs regulate hepatocyte and hepatic stellate cell function in vitro.

Figure 15. Pathology-driving OxPCs regulate hepatocyte and hepatic stellate cell function *in vitro*.

AML12 hepatocytes treated with an increasing concentration of PGPC exhibited increased **(A)** lipid droplet number per cell and size resulting in a shift toward **(B)** a higher frequency of larger lipid droplets (n=4). **(C)** LX-2 hepatic stellate cell oxygen consumption rate was significantly decreased by POVPC, KOdiA-PC, and OxPAPC after 4 hours (Vehicle, n=6; POVPC, n=5; KOdiA-PC, n=5; OxPAPC, n=6), while **(D)** OxPAPC and truncated OxPAPC increased expression of *Hmox1* and *Gclm* after 4 hours (n=4). Statistical significance was determined by 1-way ANOVA with Dunnet's Multiple Comparison Correction or Student's t-test.

Taken together, these data demonstrate that expression of scFv-E06 decreases levels of individual OxPCs in plasma. FPC diet results in multivariate changes in the OxPC lipidome which suggest complex regulation of OxPC species in pathology. Identified OxPC species that were decreased by scFv-E06, including aldehyde-, carboxylic acid-, and γ-keto/hydroxy-containing OxPCs, regulate metabolism and gene expression in hepatocytes and hepatic stellate cells, suggesting that they are actively involved in the initiation and progression of hepatic steatosis and fibrosis (Figure 16A).

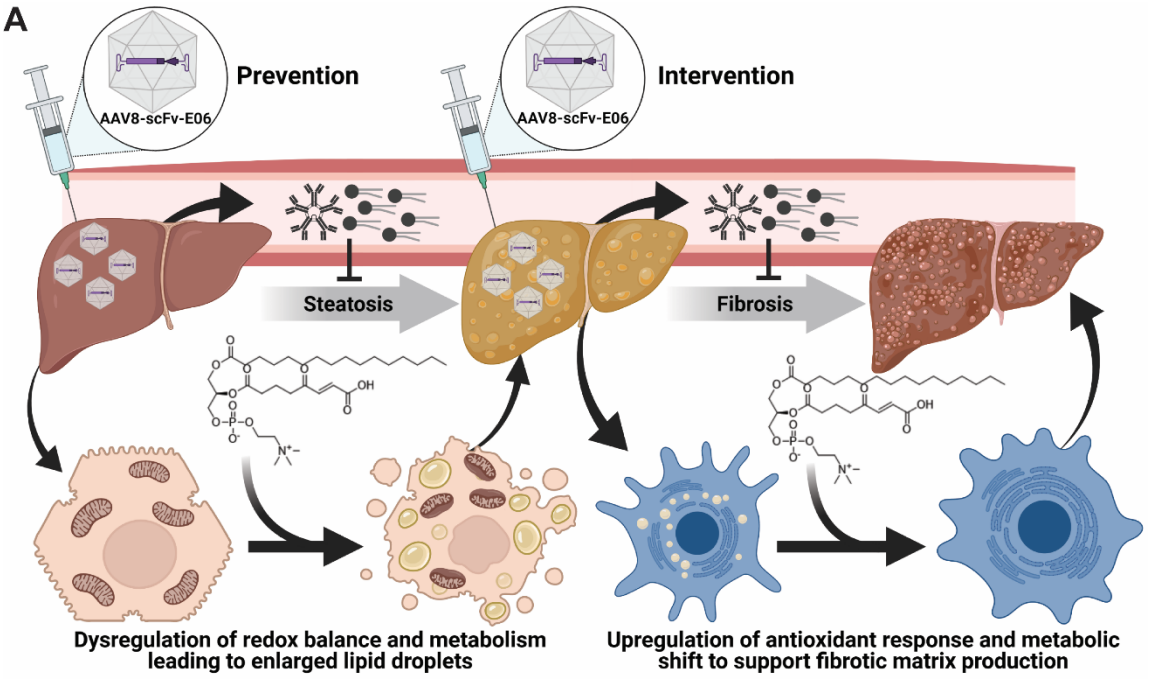

Figure 16. scFv-E06 expression protects mice from hepatic steatosis and intervention with viral expression of scFv-E06 halts disease progression. (Created with BioRender.com)

2.4 - Discussion and Conclusion

Here we examined a potential therapeutic application of adeno-associated virus-mediated hepatic expression of the oxidized phospholipid-binding antibody fragment scFv-E06 for the prevention of the initiation of NAFLD and independently, of progression to NASH and hepatic fibrosis. We show that AAV8-mediated gene transfer of scFv-E06 is sufficient to express scFv-E06 in a Cre-dependent manner in the liver, which by itself leads to secretion of scFv-E06 protein into the plasma. Expression of scFv-E06 in mice fed a chow diet did not alter normal mouse physiology, which provided an excellent tool to interrogate the effect of OxPCs on diet-induced NAFLD initiation and disease progression, without secondary effects on mouse physiology or development, while providing a way to regulate dosing and timing of expression. We demonstrated that hepatic expression of scFv-E06 prior to the start of FPC diet feeding resulted in a marked reduction in individual OxPC species in plasma, which was sufficient to protect mice from diet-induced hepatic steatosis. Given the efficacy of this model in eliminating plasma OxPCs and subsequent protection from diet-induced hepatic steatosis, we leveraged the flexibility of virus-mediated gene transfer to intervene therapeutically with scFv-E06 expression after the establishment of diet-induced hepatic steatosis. We showed for the first time that in a clinically relevant intervention model, scFv-E06 expression prevented further diet-induced liver damage and hepatic fibrosis independent of obesity and insulin resistance. Separately, scFv-E06 expression was sufficient to reduce a variety of OxPC species in plasma. At present, it is unclear whether reduction of OxPCs is protective in NASH pathogenesis or simply

a biomarker of the therapeutic effect of scFv-E06. Using mass spectrometry, we identified individual OxPC species that are decreased by expression of scFv-E06 in mice. Identified OxPC species induced gene expression and metabolic changes in hepatocytes and stellate cells *in vitro*. These data suggest that plasma OxPCs regulate liver function uniquely at different stages of disease progression. For instance, expression of scFv-E06 prior to the start of FPC-diet protected mice from hepatic steatosis while intervention with scFv-E06 after established steatosis did not reduce lipid burden in the liver. Interestingly, despite no overall decrease in lipid burden, scFv-E06-expressing mice had smaller hepatic lipid droplets. This may suggest that OxPCs are involved in dysregulation of cellular lipid storage vital to initiation of hepatic steatosis but not maintenance of steatosis. Taken together, this suggests that lowering the concentration of identified plasma OxPC species is necessary for preventing hepatic steatosis and progression to fibrosis in a normolipidemic mouse model of diet-induced NAFLD without genetic lipodystrophy. Most importantly, using this approach we provide the first evidence that therapeutic intervention after the development of diet induced steatosis with virus-induced scFv-E06 expression halts progression to hepatic fibrosis in a clinically relevant model of NAFLD.

The natural IgM E06 has been shown to recognize oxidized products of PAPC *in vitro* and has been used clinically to assess total plasma OxPC levels (*54, 129*). However, individual OxPC species that are eliminated by E06 *in vivo* had not been identified. Our findings demonstrate that scFv-E06 recognizes a variety of OxPC species irrespective of the type of oxidative modification or *sn*-1 position

acyl-chain length, while not affecting plasma levels of non-oxidized lipids *in vivo*. Further research is necessary to investigate binding affinities and specificity of scFv-E06 amongst OxPC species, and to demonstrate the potency of scFv-E06 as a potential therapeutic in the context of NAFLD and other oxidative stress-induced diseases.

Oxidized phospholipids have previously been shown to regulate numerous cellular functions and biological processes (*22-24, 34, 39, 41, 44, 64, 67, 74, 103*) . We show for the first time that individual OxPCs that are targeted by scFv-E06 activate hepatocytes resulting in upregulation of the evolutionarily conserved NRF2-dependent antioxidant program and metabolic dysregulation. While both truncated and full-length OxPCs upregulated genes related to oxidative stress, only truncated OxPCs upregulated pro-steatotic anabolic pathways including cholesterol biosynthesis. Induction of *de novo* cholesterol synthesis leading to cholesterol accumulation has been shown to promote transition from hepatic steatosis to NASH (*130*) and may be one mechanism through which OxPCs promote disease progression. Furthermore, identified OxPCs inhibited mitochondrial oxygen consumption in hepatocytes, consistent with a switch to an anabolic cellular phenotype, and resulted in increased lipid droplet formation, a hallmark of hepatic steatosis (*90*). Taken together, our findings demonstrate that hepatocytes recognize and respond to OxPCs, and treatment of hepatocytes *in vitro* with truncated OxPCs phenocopies pathological alterations in mitochondrial bioenergetics and lipid droplet regulation seen during the development of hepatic steatosis. Differences in regulation of the transcriptome in mice expressing scFv-

E06 compared to GFP during development of diet-induced hepatic steatosis, may give key insights into the mechanisms by which OxPCs drive early metabolic changes in hepatocytes that promote disease initiation.

Levels of truncated OxPCs containing a γ-keto/hydroxy functional group were also reduced by scFv-E06 *in vivo*. Several biological functions have been described for these lipids (*37, 50*); however, it is unknown if γ-keto/hydroxy-containing OxPCs play a role in NASH and hepatic fibrosis. Here we show that KOdiA-PC inhibits mitochondrial oxygen consumption and extracellular acidification rate in hepatic stellate cells. Additionally, truncated OxPCs induced expression of the NRF2-dependent genes *Hmox1* and *Gclm* in hepatic stellate cells. These data demonstrate that individual truncated OxPCs that are targeted by scFv-E06 regulate hepatic stellate cell bioenergetics and gene expression and may polarize the cells toward a redox-regulatory state.

Plasma levels of both truncated and full-length OxPC species were significantly reduced by scFv-E06 either at the initiation of hepatic steatosis or during the progression to hepatic fibrosis. These data demonstrate for the first time that scFv-E06 specifically recognizes individual oxidized phosphorylcholine phospholipids *in vivo*, without affecting levels of non-oxidized phosphatidylcholines or lyso-PCs, which builds on previous studies that have demonstrated similar specificity of E06 *in vitro* (*26, 131*). We identified one unique OxPC species in the setting of hepatic steatosis and seven unique OxPC species in the setting of hepatic fibrosis that are targeted by scFv-E06. Identification of specific OxPC species that are eliminated by scFv-E06 during the different stages of disease

progression suggests that plasma OxPCs could serve as non-invasive biomarkers of NAFLD severity. In human plasma, oxidized phospholipids are carried on low-density lipoproteins and previous work has shown that the ratio of OxPCs to apoB-100 or apo(a) correlates with cardiovascular disease, calcific aortic valve disease, and aortic valve stenosis (*56, 132*). These risk factors are assessed from lipoprotein bound OxPCs. Our method assesses free or “unconjugated” OxPCs. Considering the pathologic role of OxPCs in NAFLD and the dearth of viable non-invasive biomarkers for NASH, analysis of individual “unconjugated” OxPC species may provide an additional diagnostic metric and possible alternative to more invasive techniques like liver biopsy.

In this study, we limited our analysis to validated oxidized phosphatidylcholine species predicted by LPPTiger (*109*) and identified in air- and copper-oxidized PAPC and PLPC. Combining an *in silico*-based approach with *in vitro* validation allowed us to assess 83 validated analytes (individual lipid species as well as isobaric groups); however, this accounts for only a fraction of the possible oxidation species present *in vivo*. Given the numerous possible oxidative modifications that can arise as products of oxidation, many oxidized phospholipid species are isobaric requiring additional metrics to accurately distinguish individual species. In this study, we leverage both mass and chromatographic retention time to distinguish between OxPC species. Consequently, isobaric species with similar retention times were not uniquely identified. Future studies are necessary to identify unique fragmentation patterns for isobaric species that overlap chromatographically to confidently identify each species. Additionally, expanding

the OxPL panel to include not only other oxidized phosphatidylcholine species, but also phospholipids with other head groups, which have been shown to play critical roles in diverse biological processes ranging from thrombus formation (*62*), to ferroptosis (*45*), and apoptosis (*42*), is essential to understand how OxPLs regulate complex pathologies. Currently, our method is limited to semi-quantitation of OxPL species due to lack of deuterated and non-deuterated OxPL standards. Synthesis of OxPL standards is necessary to directly quantify the concentration of pathology-driving OxPLs in the plasma. Additionally, our method measures OxPCs that can be isolated by liquid-liquid organic extraction, which likely reflects the free OxPC lipidome as it is likely that some electrophilic lipid species bind covalently with proteins. For example, POVPC has previously been shown to bind manganese superoxide dismutase (*24*).

We demonstrate that scFv-E06 expression lowers levels of OxPCs in the plasma, which are necessary for pathogenesis of both hepatic steatosis and fibrosis. Furthermore, though OxPC levels are lowered by scFv-E06 expression as measured by mass spectrometry, the mechanism through which this occurs remains unclear. We propose two possible mechanisms which will require further study: (1) elimination from the biological system by enzymatic activity or excretion or (2) masking of OxPC inhibiting their biological effects. Distinguishing whether it is necessary to lower both plasma and liver OxPC species to inhibit disease progression as well as understanding the mechanism through which OxPC species are lowered by scFv-E06 expression will provide a deeper understanding of the

role of OxPC species in NAFLD pathology and guide future therapeutic approaches.

In conclusion, our study establishes the translational potential of plasma OxPC elimination using AAV8-mediated gene transfer of scFv-E06 in a clinically relevant NAFLD model. This novel approach to target plasma OxPCs provides multi-modal control over oxidized lipid-driven pathologies. Temporal and spatial regulation of scFv-E06 expression will allow for exploration of previously inaccessible OxPC-mediated biology and pathology. Finally, assessment of plasma levels of individually identified, pathology-driving OxPC species during NAFLD initiation and progression may lead to the discovery of urgently needed non-invasive biomarkers.

2.5 - Acknowledgments

AAV8-scFv-E06 was synthesized by the Penn Vector Core. RNA-seq analysis was supported by the UVA Genome Analysis and Technology Core. We thank M. Bevard (UVA CVRC Histology Core) for her expertise and preparation of histological samples. RNA sequencing of in vitro OxPAPC-treated hepatocytes was performed in the Genome Analysis and Technology Core at UVA. We thank J. Gatesman (UVA Center for Comparative Medicine) for technical assistance with viral injections.

Chapter 3: Oxidized phospholipidome as an indicator of comorbidities in critically ill patients

3.1 – Abstract

Critical illness is hallmarked by increased oxidative stress; however, antioxidant therapies developed to combat elevated oxidative stress have yielded mixed results. Therefore, understanding the composition of prooxidant species present during settings of critical illness is essential for efficacious treatment of disease. To identify and quantify oxidized phospholipids species produced during critical illness, we developed a liquid-chromatography mass spectrometry-based method to assess the composition and quantity of oxidized phosphatidyl choline (OxPC) species present in a cohort of critically ill patients admitted to the medical intensive care unit at the University of Virginia. We identified and quantified 19 OxPC species present in at least 20 patients (out of 91). Additionally, we determined that grouping OxPC species by chemical and structural similarity resulting in associations with various clinical parameters. Thus, indicating a potential novel relationship between OxPCs and novel organ pathologies.

3.2 - Introduction

Critically ill patients frequently present with complex medical histories and multi-organ pathologies that necessitate admission to the intensive care unit (ICU). One underlying commonality amongst ICU all-comers is increased oxidative stress. Numerous clinical trials have sought to reduce oxidative stress in ICU patients using antioxidant therapies with mixed success (*133*). Antioxidants are a broad class of molecules that can act at multiple levels to reduce pro-oxidizing

environments (*134*). For instance, primary antioxidants like α-tocopherol (Vitamin E) act as free-radical scavengers and break radical chain propagation (*135*). Other antioxidants like deferoxamine inhibit a pro-oxidizing environment through chelation of iron ions, which is considered a secondary means (*136, 137*). Other secondary means include direct reduction of oxidized molecules and activation of NRF2-dependent gene expression (*136*). At best, antioxidant therapies likely affect numerous pathways and consequently provide a challenging pharmacological problem when assessing their efficacy. Nevertheless, their success, however limited, touted “health benefits,” and seemingly simple solution to restore redox balance has perpetuated their study in many different pathologies.

While the “silver bullet” antioxidant therapy has not yet been discovered, it is well established that critically ill patients have increased oxidative stress largely independent of reason for ICU admission. It has previously been established that critically ill patients have elevated thiobarbituric acid reactive substances like 4-hydroxynonenal (4-HNE) (*138*). A more recent study demonstrated that ICU all-comers exhibited positive correlation between markers of oxidative stress, lipid hydroperoxides and carbonylated proteins, and their sequential organ failure assessment (*139*). This could be partially rescued with timely intervention using antioxidant vitamins; however, only carbonylated proteins were reduced, not lipid hydroperoxides (*139*). Additionally, the lipid oxidation byproduct 4-HNE was upregulated in the serum of patients with community acquired pneumonia on ICU admission compared to healthy controls (*140*). This provides strong evidence that oxidative stress, and more specifically oxidized lipids and their oxidation

byproducts, may play a direct role in disease or could be used as a prognostic biomarker to predict clinical outcome and inform treatment regimens.

Evidence strongly supports the hypothesis that oxidized lipid species may potentiate disease progression in critically ill patients (*134, 138-140*). To further understand the role of oxidized lipid species in critically ill patients, it is necessary to better understand the complexity of the oxophospholipidome present during illness. Here, we developed an approach to identify and quantify oxidized phosphatidyl choline (OxPC) species present in plasma collected from a cohort of 91 critically ill patients admitted to the medical intensive care unit (MICU) at the University of Virginia. We quantified 19 oxidized phospholipids species that were detected in at least 20 (of 91) patient samples. Multivariate analysis of variance revealed close associations between OxPC species grouped based on functional group or hierarchical clustering and clinical parameters. These findings not only suggest that the oxophospholipidome may be a useful metric to stratify patients for medical care, but also elucidate novel pathologies in which OxPCs may play a role.

3.3 - Results

3.3.1 – Development and optimization of an LCMS method for extraction, detection, and quantification of the oxophospholipidome in human plasma

To detect and quantify the oxophospholipidome in human plasma we further developed a liquid-chromatography mass spectrometry approach based on work presented in Chapter 2 (*27*). In brief, we predicted the possible oxidation products of 1-palmitoyl-2-linoleoyl-sn-glycero-3-phosphocholine (PLPC) and 1-palmitoyl-2-arachidonoyl-sn-glycero-3-phosphocholine (PAPC) *in silico (109)*. These species

were chosen because they contain the most abundant plasma saturated fatty acid, palmitic acid, in the *sn-1* position and the two most abundant plasma unsaturated fatty acids, linoleic acid and arachidonic acid, in the *sn-2* position (*141*). The resulting oxidized lipid species were combined into isobaric groups for each parent lipid (PLPC or PAPC). PLPC and PAPC were oxidized *in vitro* and the resulting oxidized PLPC (OxPLPC) and oxidized PAPC (OxPAPC) were used as standards to identify retention times for each OxPL species predicted *in silico*. Species identified with a mass accuracy of less than 5 parts per million were considered validated. This list was further shortened by repeating the same process using extracted pooled human plasma and mouse plasma. Sixty-four OxPC species/isobaric groups were detected in either the pooled human or mouse plasma. With a target list of 64 OxPC species, we optimized ionization temperature and voltage for different OxPC species. Full-length OxPC species were represented by 1-palmitoyl-2-hydroperoxyeicostetraenoyl-sn-glycero-3-phosphocholine (HPETE-PC) (Figure 17A). Truncated OxPC species were represented by the deuterated OxPL standard 1-palmitoyl-2-glutaryl-sn-3-glycero-pshophocholine-d6 (PGPC-d6) (Figure 17A). Lysophospholipids and non-oxidized phospholipids were represented by 1-palmitoyl-2-hydroxy-sn-glycero-3-phosphocholine (16:0 LysoPC) and PAPC, respectively (Figure 17A). Capillary temperature and ionization voltage were increased in a stepwise manner and the area under the curve was recorded for each lipid species. From this analysis it was determined that an ionization voltage of 3.0 kV and a capillary temperature of 275

°C was optimal for maximum detection amongst all lipid species, with a bias toward full-length species.

To quantify OxPC species present in human plasma, extraction efficiency and matrix suppression were analyzed. Internal standards, PGPC-d6, 1,2-dinonanoyl-sn-glycero-3-phosphocholine (DNPC), and 1-oleic-2-hydroxy-sn-glycero-3-phosphocholine-d7 (18:1 LysoPC-d7) were spiked into human plasma or methanol and extracted according to the previously reported method (*27*). Additionally, these lipids were also spiked into human plasma after extraction (matrix effect). Analysis by the established LCMS method revealed that recovery of all three standards was significantly blunted by addition to human plasma prior to extraction (Figure 17B). However, this was not observed if spiked into extracted plasma (Figure 17B). This suggests that there is little to no matrix effect affecting signal intensity and that any loss of signal could be attributed to incomplete extraction. Consequently, using two lipid standards, one oxidized (PGPC-d6) and one non-oxidized (DNPC), we could control for differences in extraction efficiency between samples. Lastly, we established standard curves using commercially available lipid standards for absolute quantification (Figure 17C). Interestingly, log-log transformation of the standard curves revealed that there was minimal difference between the curves corresponding to different lipid species (Figure 17C). Due to the remarkable similarity, we assumed that the average curve could be used to closely estimate the concentration of OxPC species that were present in human plasma, but not commercially available.

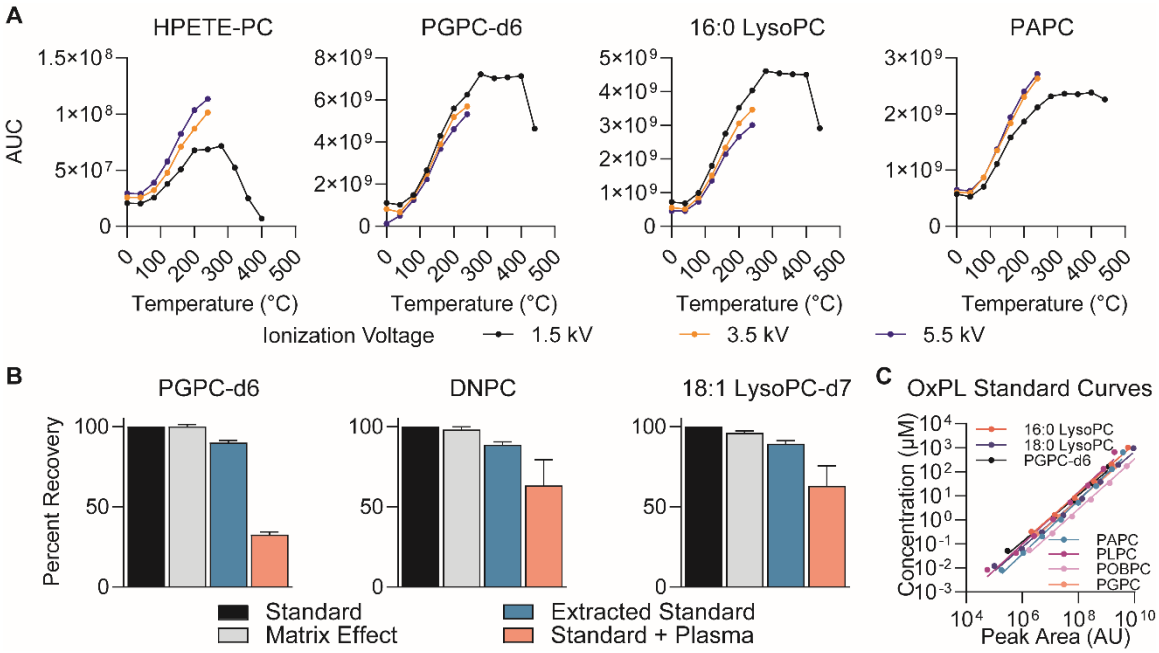

Figure 17. Optimization of mass spectroscopy for detection of OxPLs in human plasma.

Figure 17. Optimization of mass spectroscopy for detection of OxPLs in human plasma.
(A) Nebulization temperature and ionization voltage were optimized for maximum detection of full-length (HPETE-PC), truncated and deuterated OxPL standard (PGPC-d6), lysophospholipids (16:0 LysoPC), and non-oxidized phospholipids (PAPC). **(B)** There was no suppression of signal strength for phospholipid standards PGPC-d6, DNPC, and 18:1 LysoPC-d7; however, signal strength was reduced when extracted in combination with human plasma and could serve as surrogate for sample extraction efficiency. **(C)** Standard curves were generated for 7 commercially available phospholipids.

3.3.2 – Quantification of OxPC species in plasma from critically ill patients

Plasma from critically ill all-comers admitted to the MICU at UVA was collected upon admission and processed using sodium citrate tubes to prevent coagulation. After collection each sample was stored with 50 μM butylated-hydroxytoluene (BHT), which acts as a radical trapping antioxidant preventing further oxidation *ex vivo*. The MICU cohort included slightly more male patients and was predominantly white with an average age of 58.17 years ranging from 18 to 88 (Table 1 & 2). On average, each clinical parameter was elevated outside the normal range (Table 2) as expected in a cohort of critically ill patients.

OxPCs from plasma samples were extracted using the method described previously (*27*). Samples were analyzed over a three-month period. To control for inter-assay variability, lipid standards were prepared at the start of each analysis which allowed for correction of change in signal intensity. The identified OxPC species were quantified using the standard curves and the strategy discussed previously (Figure 17C). The resulting OxPCs and their average correlations are reported in Table 3. OxPC species varied from low nanomolar to low micromolar concentrations depending on the lipid species. The non-oxidized and lyso phospholipid concentration range is corroborated by the literature (*142*).

Race	Female	Male	Total
African American	2.2%	16.7%	18.9%
American Indian and Alaska Native	1.1%	---	1.1%
White or Caucasian	38.9%	40%	78.9%
Other	1.1%	---	1.1%
All	43.3	56.7%	

Table 1. Demographics of 90 patients from MICU cohort.

Variable	Average	Standard Deviation	Range
Age on Admission (Years)	58.17	18.29	18.42-88.84
Length of MICU Stay (Days)	12.76	14.91	1.23-101.01
Mass (kg)	89.25	33.98	39.85-269.4
BMI (kg/m^2)	30.10	9.47	14.62-82.83
Highest Lactate (mmol/L)	3.45	3.19	0.6-18.5
Highest Creatinine (mg/dL)	2.32	2.68	0.6-20
Highest ALT (U/L)	251.59	1157.41	6-7880
Highest AST (U/L)	313.17	1312.30	11-9198
Admission BUN (mg/dL)	30.00	22.46	5-111
Admission Creatinine (mg/dL)	1.86	2.48	0.4-20

Table 2. Clinical parameters of 90 patients from MICU Cohort.

Average of clinical parameters from the MICU cohort. Body mass index (BMI), alanine aminotransferase (ALT), aspartate aminotransferase (AST), blood urea nitrogen (BUN).

Phospholipid species	Number of Patients	Average Concentration (μM)	Standard Deviation of Concentration (μM)	Max Concentration (μM)	Range (μM)	OxPL Group
16:0/7:1[CHO]	84/91	0.12	0.094	0.61	0.014-0.61	Aldehyde
POBPC	89/91	0.20	0.12	0.65	0.011-0.65	Aldehyde
16:0/11:1[CHO]	89/91	0.23	0.17	1.1	0.015-1.1	Aldehyde
16:0/8:0[CHO]	89/91	0.24	0.18	1.2	0.021-1.2	Aldehyde
POVPC	91/91	0.76	0.44	3.2	0.082-3.2	Aldehyde
PONPC	91/91	2.3	1.2	6.2	0.41-6.2	Aldehyde
16:0/8:1[CHO]	22/91	0.089	0.079	0.28	0.013-0.28	Keto/Hydroxy
16:0/11:1[OH,CHO]	39/91	0.13	0.44	2.7	0.011-2.7	Keto/Hydroxy
16:0/14:3[KETO,CHO]	91/91	0.31	0.16	0.84	0.011-0.84	Keto/Hydroxy
PGPC	18/91	0.14	0.43	1.9	0.0069-1.9	Carboxylic Acid
PazPC	86/91	0.20	0.84	7.8	0.007-7.8	Carboxylic Acid
C42H80NO11P	15/91	0.036	0.053	0.22	0.01-0.22	Full-length
16:0/18:2[KETO,OOH]	7/91	0.041	0.032	0.093	0.018-0.093	Full-length
C44H80NO10P	8/91	0.052	0.055	0.18	0.019-0.18	Full-length
C42H80NO10P	54/91	0.13	0.24	1.6	0.014-1.6	Full-length
16:0/18:2[KETO]	41/91	0.13	0.18	0.9	0.016-0.9	Full-length
C42H82NO9P	82/91	0.26	1.6	15	0.011-15	Full-length
C44H80NO9P	88/91	0.28	0.18	0.95	0.024-0.95	Full-length
C42H80NO9P	48/91	0.59	3.5	25	0.013-25	Full-length
18:1 LysoPC	91/91	10	7.2	37	0.37-37	Lyso
18:2 LysoPC	91/91	11	9.2	52	0.75-52	Lyso
18:0 LysoPC	90/91	12	8.0	37	0.027-37	Lyso
16:0 LysoPC	91/91	80	56	290	5.5-290	Lyso
PAPC	91/91	109	40.8	278	19.2-278	Non-oxidized
PLPC	91/91	212	71.4	488	61.6-488	Non-oxidized

Table 3. Concentration of OxPC species in human plasma from MICU cohort.

Table 3. Concentration of OxPC species in human plasma from MICU cohort. Oxidized phospholipid plasma concentrations were quantified by LCMS. Species were reported if above the limit of detection otherwise they were considered “Not detected.” The reported range includes only patients where the OxPC species was detected.

3.3.3 – Hierarchical clustering of OxPC species reveals coregulation amongst species based on functional groups

Identification and quantification of OxPC species present in human plasma provided insight into the complexity of the oxophohospholipidome during critical illness. As previously described, the MICU cohort was not limited to any defined medical history. Consequently, the patient population represented a wide range of pathologies and pre-existing conditions. Given this limitation, we sought to identify OxPCs that correlate with one or many different clinical parameters or pathologies.

Previous literature indicated that biological activity of OxPCs could be attributed to the chemical structure of individual lipids (*27, 35*). Additionally, we hypothesized that formation of OxPCs containing similar functional groups may be regulated in a manner that results in their coevolution. To test this hypothesis, we used a hierarchical clustering analysis to group OxPC species quantified in the critically ill patient population based on how well they correlated amongst each other (*143*). After clustering, we discovered four groups that were correlated with each other (Figure 18A). While Group 1 was a mixture of OxPC species containing different functional groups, Groups 2, 3, and 4 contained OxPCs with similar functional groups, respectively (Figure 18A). For instance, Group 2 contained lysophospholipids while Group 4 contained truncated and primarily aldehyde containing OxPCs (Figure 18A). Coevolution of structurally similar OxPC species under oxidizing conditions implies that OxPC species generated from other parent lipids similar to PLPC and PAPC are likely present. These undetected species could contribute to the overall oxidative burden during critical illness.

Using these identified groups as well as groups based on chemical similarity we evaluated whether there was associations between the described groups of OxPCs and clinical parameters or diagnoses. We tested for associations using multivariate analysis of variance (MANOVA) and discovered a unique fingerprint of association between OxPC concentration and many clinical parameters (Figure 18B). We discovered that the complete group of OxPL associated with many clinical parameters across many organ systems including creatinine, ALT, and AST plasma concentration as well as body weight and BMI (Figure 18B). Groups 1 through 4 which were determined agnostically as described previously also associated with many clinical parameters. Strikingly, Group 1 and Group 4 closely resembled truncated OxPCs in its associations (Figure 18B). This is likely due to the overlap in lipid species between either Group 1 or Group 4 and the truncated OxPC group (Figure 18B). Of these associations, these three groups all associate with kidney related parameters like creatinine, chronic kidney disease, and blood urea nitrogen. Interestingly, full-length OxPC species overlap with many of the associations of truncated OxPCs; however, has unique associations with BMI and body weight (Figure 18B). Aldehyde, carboxylic acids, and γ-keto/hydroxy OxPCs are subsets of the truncated OxPC group and consequently strongly resemble the fingerprint established by the truncated OxPC group (Figure 18B). Yet, each group has some differences which may point to specific pathological roles for each group. Moreover, it should be noted that non-oxidized phospholipids and lysophospholipids do not strongly associate with the same clinical parameters as OxPCs.

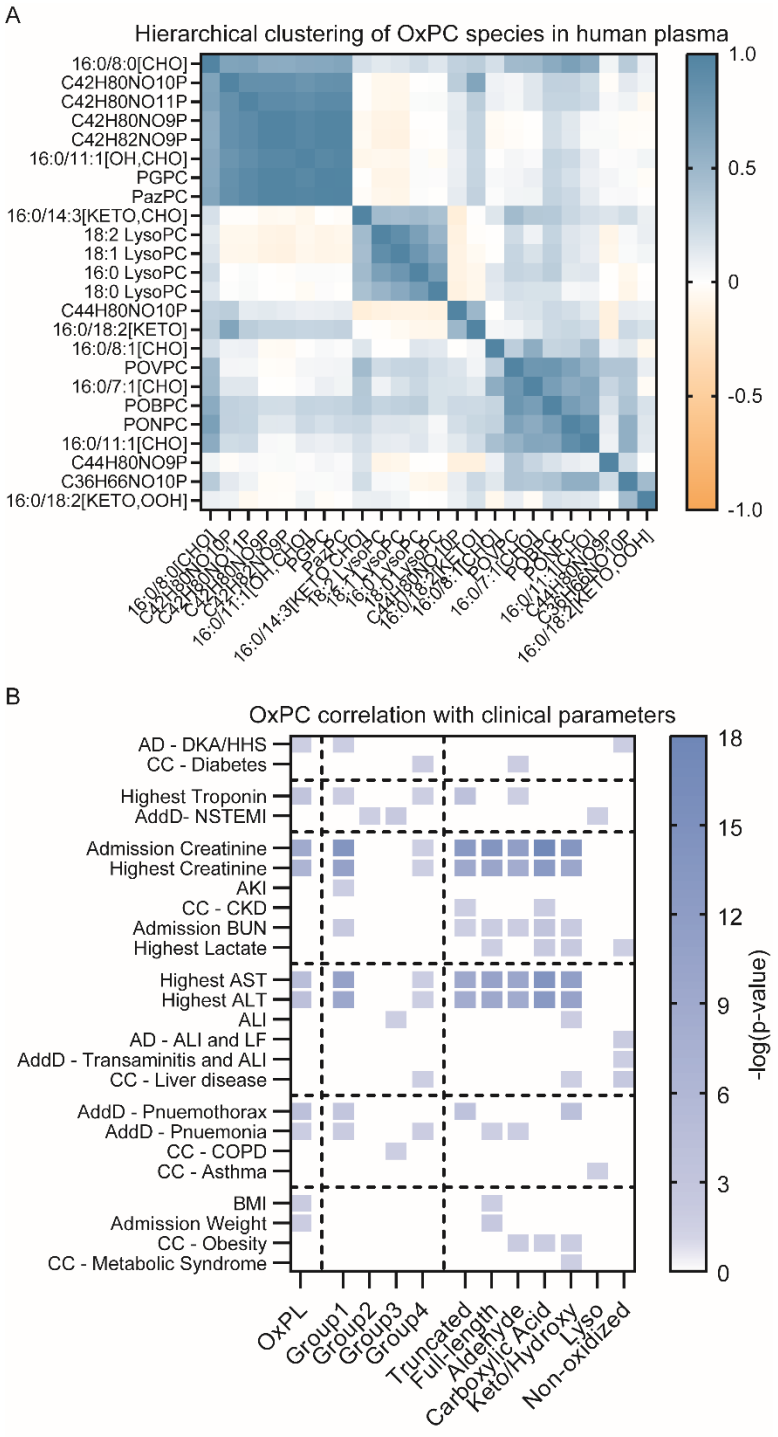

Figure 18. Functionally similar OxPCs are coregulated and correlate with specific clinical parameters.

Figure 18. Functionally similar OxPCs are coregulated and correlate with specific clinical parameters.

OxPC species quantified in plasma of 91 MICU patients were hierarchically clustered. (A) Clustering revealed four distinct groups that closely correlated with each other: Group 1 – 16:0/8:0[CHO] through PazPC; Group 2 – 16:0/14:3[KETO,CHO] through 18:0 LysoPC; Group 3 – C44H80NO10P and 16:0/18:2[KETO]; Group 4 – POVPC through 16:0/11:1[CHO]. OxPCs were grouped according to hierarchical clustering or according to chemical structure and association with clinical parameters was evaluated by MANOVA. (B) Group 1 and Group 4 were associated with similar clinical parameters and largely recapitulated the pattern observed in the truncated OxPC group. Unique association patterns arose for each lipid group. AD – Admission diagnosis, CC – comorbidity, AddD – Additional diagnosis in the hospital, DKA/HHS – diabetic ketoacidosis/hyperosmolar hyperglycemic state, NSTEMI – non-ST elevation myocardial infarction, AKI – acute kidney injury, BUN – blood urea nitrogen, AST – aspartate aminotransferase, ALT – alanine aminotransferase, ALI – acute liver injury, LF – liver failure, COPD – chronic obstructive pulmonary disease, BMI – body mass index.

3.4 - Discussion

Here, we developed an LCMS-based approach to detect, identify, and quantify OxPC species in human plasma and can be applied to other biological matrices. We consistently detected 19 of 64 OxPC species in a study of 91 critically ill patients admitted to the UVA MICU. We empirically determined plasma concentrations of 19 OxPC species that ranged from low nanomolar to low micromolar concentrations. Additionally, we discovered that different groups of structurally similar OxPC species associate with different sets of clinical parameters resulting in unique fingerprints associated with each group of OxPCs.

It has been established that oxidative stress is a major component of critical illness (*138-140*). Often these studies relied on 4-HNE and MDA, which are liberated during lipid oxidation, as an indicator of oxidative stress; however, assessment of OxPLs present during critical illness was overlooked. Given the overwhelming evidence that OxPLs play a role in an impressively wide array of pathologies ranging from chronic diseases like atherosclerosis, obesity, and non-alcoholic fatty liver disease as well as acute pathologies like sepsis and acute lung injury it is not surprising that OxPLs are present in critical illness (*22, 24, 27, 28, 30, 35, 39, 40, 74, 103, 144*). Due to their diverse chemical structures, OxPLs likely play a role in many different organ systems during critical illness and understanding what species are present is the first step towards developing interventional therapy.

The concentration of some individual OxPLs reached micromolar levels in plasma which far exceed physiological concentrations of known lipid mediators like

prostaglandins and resolvins which have previously been reported in the nanomolar range (*145, 146*). Therefore, it is likely that OxPLs are biologically active at the concentrations reported above. One limitation of our approach is that it was limited to OxPC species that we specifically targeted. It is likely that there are many additional OxPC species with equally high abundance present in the plasma but unaccounted for in this study. Furthermore, one must also consider OxPL species with different phospholipid head groups such as phosphatidylethanolamine and phosphatidylserine which have been shown to play an essential role in ferroptosis and apoptosis, respectively (*42, 45*) and were not considered in this study.

The diverse representation of many different pathologies within the patient cohort provided the ideal population to interrogate the relationship between concentrations of OxPC species in the plasma and a wide range of pathologies. Identification of associations with ALT and AST are strongly supported by previous literature that has demonstrated a role for OxPCs in non-alcoholic fatty liver disease (*24, 27*). However, novel associations like that with creatinine may point toward a role for OxPC in pathologies related to the kidney such as acute kidney injury or chronic kidney disease.

Previous literature has established a speculative role for OxPCs in many pathologies. However, recent development of a transgenic mouse model and virus expressing scFv-E06, a single chain variable fragment of the natural IgM, E06 which as previously been shown to bind OxPCs has established a causal role

for OxPCs in atherosclerosis, age-induced loss of bone density, and non-alcoholic fatty liver disease for the first time (*22, 24, 27, 106*). These models now allow for direct interrogation of the role of OxPCs in disease and disease progression. Using the associations between OxPCs and novel pathologies discovered in the MICU cohort as a guide, we can begin to explore the pathological role of OxPCs in these settings.

3.5 – Acknowledgements

We would like to thank all patients who were enrolled in this study.

Chapter 4: Conclusions and Future Directions

In this dissertation, we worked to better understand the complexity of the plasma and liver oxophospholipidome, and how individual OxPC species promote non-alcoholic fatty liver disease pathology.

To this end, we developed a novel AAV8 viral vector to express scFv-E06, an antibody fragment that binds and neutralizes OxPC species. In combination with a targeted LCMS-based analytical approach we were able to determine that expression of scFv-E06 is sufficient to lower plasma concentrations of OxPC species in a diet-induced NAFLD model. Moreover, we concluded that scFv-E06 exhibits exquisite specificity to OxPCs and does not neutralize non-oxidized or lysophospholipids.

This strongly supports the original *in vitro* discovery that the complete IgM E06 antibody has specificity for OxPCs (*26*). We were unable to determine whether scFv-E06 exhibited preference for a particular OxPC species or chemical derivatization in this study, but further optimization of this antibody fragment may yield a suite of fragments targeted to specific OxPC species or OxPC groups.

Nevertheless, the pan-OxPC recognizing scFv-E06 AAV8 vector provided an excellent initial tool to investigate the role of OxPCs in driving hepatic steatosis to NASH and fibrosis. After the development of hepatic steatosis, we inoculated mice with scFv-E06 AAV8. scFv-E06 expression after development of hepatic steatosis was sufficient to neutralize OxPCs, lowering their concentration in the plasma, and protect mice from developing hepatic fibrosis and NASH. This finding

established a direct role for OxPCs in the development of hepatic fibrosis, independent from pre-existing hepatic steatosis. It also demonstrated the therapeutic efficacy of scFv-E06 as an interventional therapy in NAFLD.

While our scFv-E06 AAV8 vector represents a promising advancement in the field of oxidized phospholipid research. There is still much to be explored and optimized. The vector used in this dissertation is a double-inverse orientation vector that is dependent on cre for scFv-E06 expression. This limits its usefulness to mouse models expressing cre. However, we have since developed a similar construct that is not cre-dependent and that should mitigate this limitation. Expression of scFv-E06 in disease models where OxPCs were previously speculated to be causal agents of pathology will provide clarifying insight on the role of OxPCs in disease pathology.

While scFv-E06 exhibited promiscuous neutralization of all OxPC species *in vivo*, we identified unique roles for truncated and full-length OxPAPC *in vitro*. Using AML12 hepatocytes, we established that truncated OxPAPC promoted a switch in hepatocyte metabolism, resulting in a downregulation of oxidative phosphorylation and a commensurate increase in lipid droplet size and number. The decrease in bioenergetics and increase in lipid droplet size was unique to the truncated OxPAPC species.

Building off work from Serbulea *et. al.* and Spinelli *et. al.*, one could speculate that similar to BMDMs, hepatocytes upregulate a redox regulatory program to combat the electrophilic truncated OxPAPC species they encounter

(*34, 63*). Indeed, RNA-seq analysis of AML12 hepatocytes revealed an upregulation of NRF2-dependent genes and genes in the pentose phosphate pathway (PPP). NADPH, a key cofactor for fatty acid synthase (FASN), the rate limiting step of lipogenesis, is produced by the PPP. In addition to downregulation of oxidative phosphorylation, which uses fatty acids as a substrate, this may contribute to accumulation of more and larger lipid droplets.

While this work was largely focused on the effect of OxPCs directly on hepatocytes, I would be remiss not address other cell types present in the liver that could contribute to OxPC-mediated NAFLD pathology. Hepatic stellate cells are a myofibroblast like cell that canonically stores retinoic acid as retinoic esters. Upon activation these cells polarize to a myofibroblast-like state and are thought to be the major driver of extracellular matrix remodeling during homeostatic injuries. During chronic inflammation, like that observed in NASH, HSCs can become chronically activated resulting hepatic fibrosis (*99, 147*).

Kupffer cells are the resident tissue macrophage of the liver and likely play role in activation of HSCs and promoting an increase inflammatory tone in the liver in response to injury. Currently, it is unknown whether OxPCs could potentiate activation of HSCs or Kupffer cells, but it is an important question to address to more fully understand the role of OxPCs in NAFLD.

The versatility of an LCMS-based approach to identify and quantify OxPC species in plasma provided us with the opportunity to quantify OxPC species present in human plasma from critically ill patients. This study provided first

insights into oxophospholipidome complexity in critically ill patients. We were also able to directly quantify many OxPC species providing a concentration range for OxPCs *in vivo* and establishing their relevancy for human disease. More interestingly, we were able to identify unique association patterns between different classes of OxPCs and various clinical parameters. From this data, we were able to identify promising new pathologies in which we can investigate whether OxPCs play a causal role.

Our analysis was limited to OxPCs derived from PAPC and PLPC. Further expansion of our OxPL panel to include other PC species as well as PE and PS species will undoubtedly reveal a more complex oxophospholipidome and likely shed more light on the role of oxidized phospholipids in disease pathology.

In conclusion, we have developed novel tools to directly assess the function of OxPLs *in vivo*. With new tools in hand, we will now be able to push the boundary or our understanding of the diverse and complex OxPL biology, and for the first time begin to delineate what OxPL species are causal agents of pathology.

Chapter 5: Methods

5.1 - Mice

B6.Cg-Speer6-ps1$^{Tg(Alb\text{-}cre)21Mgn}$/J (Jackson Laboratories 003574) (Alb-cre) were obtained from Jackson Laboratories (Bar Harbor, ME) and housed in the Pinn vivarium at the University of Virginia Center for Comparative Medicine. Unless otherwise stated, animals were maintained in pathogen-free housing with a 12-hour light/dark cycle with *ad libitum* access to food and water. All animal experiments were approved by the University of Virginia's Animal Care and Use Committee (Protocol #3444). To assess the impact of scFv-E06 on hepatic steatosis 6-week-old mice were injected with either AAV8-GFP (UNC Vector Core) or AAV8-scFv-E06 (10^{11} genome copies/100 µL sterile PBS). Mice, 8 weeks of age, were fed a high fructose, palmitate, and cholesterol diet (FPC diet, Teklad TD.190142) supplemented with 4.2% glucose (Fisher D12-500)/fructose (Fisher L95-500) water (55%/45% w/w) for six weeks. At the end of the experiment, mice were euthanized via CO_2 inhalation and cardiac puncture. To assess the impact of scFv-E06 expression on fibrosis and whether expression of scFv-E06 after the onset of hepatic steatosis could mitigate progression to hepatic fibrosis, mice, 6 weeks of age, were fed FPC diet for six weeks. After six weeks of feeding, mice were injected via tail vein with AAV8-GFP or AAV8-scFv-E06. Mice continued FPC diet for an additional 14 weeks at which point they were euthanized via CO_2 inhalation. Control mice were fed chow diet (Teklad 7912).

5.2 - Histology

PBS-perfused liver tissue was either fixed in 10% formalin (w/v) for 24 hours and transferred to 200 proof ethanol or cryopreserved in NEG-50™ (Richard Allan

Scientific, 6502) and stored at -80°C. Tissue samples were processed for histology at the Robert M. Berne Cardiovascular Research Center Histology Facility at the University of Virginia. In brief, samples were embedded in paraffin, and 10-micron serial sections were stained with hematoxylin and eosin, picrosirius red, or Oil red O. Images were collected using an Olympus BX51 or Leica Thunder with TIRF microscope operating in brightfield. Picrosirius Red counter-stained with Fast Green was quantified using ImageJ(*148*) to assess stained area in 3 sections from liver tissue each mouse. Positive staining was determined by thresholding while blinded after exclusion of perivascular collagen: threshold settings were kept constant for all samples assessed.

5.3 - Triglyceride assay

Hepatic triglyceride concentration was quantified using triglyceride colorimetric assay (Pointe Scientific T7532500). Liver tissue (20-30 mg) was lysed in 400 µL of 0.6% NaCl using Qiagen Tissue Lyser II (30 Hz for 15 minutes). Samples were diluted 1:4 in 0.6% NaCl and mixed with 4.4 parts chloroform (EMD UN1888/Fisher Scientific C607-1) and 2.2 parts methanol (Sigma-Aldrich 646377-1L). Samples were vortexed vigorously and centrifuged for 10 minutes at 3000*g* to accelerate phase separation. The organic phase (500 µL) of each sample was transferred to a new tube and dried under N_2 purge. The dried organic phase was resuspended in 200 µL of 95% ethanol (200 µL) (Fisher Scientific 04-0355-223). Samples from mice on FPC diet were diluted 1:5 in 95% ethanol. Assay was conducted in triplicate according to manufacturer's recommendations.

5.4 - Plasma liver biomarkers

Whole blood was collected from mice after euthanasia via cardiac puncture and dispensed into heparin-coated plasma collection tubes (Becton Dickinson 365985) and stored on ice. Plasma separated via centrifugation at 2000*g* for 15 minutes at 4°C. Plasma was stored at -80°C. Plasma was diluted 1:1 in sterile 0.9% saline and liver biomarkers were analyzed by UVA Clinical Laboratories.

5.5 - Cell culture

AML12 murine hepatocytes (ATCC CRL-2254) were cultured in DMEM:F12 supplemented with 10% FBS (R&D Systems S12450/Atlanta Biologicals S11150) and 1% Anti-Anti (Gibco 15240-062) and grown at 37°C with 5% CO_2. Cells were passaged when they reached 90% confluency using 0.5% Trypsin (Gibco 15400-054). LX-2 human hepatic stellate cells (Millipore Sigma SCC064) were cultured in DMEM supplemented with 2% FBS (R&D Systems S12450/Atlanta Biologicals S11150) and 1% Pen-Strep (Gibco® 15140-122) and grown in Dulbecco's Modified Eagle Medium (Gibco 11965-092) 37°C with 5% CO_2. Cells were passaged when they reached 90% confluency using 0.25% Trypsin (Gibco 25200-056). For all experiments using the LX-2 cell line, cells were cultured on Matrigel (83 µg/mL) (Fisher Scientific CB-40230) for 24-hours in DMEM containing 1% Pen-Strep prior to the start of the experiment.

5.3 - Mitochondrial and glycolytic stress test

5.3.1 - XF24 Seahorse bioenergetics assay

AML12 hepatocytes (75,000 cells/well) were plated in complete medium in XF24 cell culture microplates (Agilent 100777-004) and allowed to settle overnight. The following day cells were treated for 4 hours with oxidized phospholipids (10 – 100

μg/mL) in DMEM:F12 supplemented as described. At the end of the experimental treatment, media was removed and replaced with assay appropriate medium: Mitochondrial Stress Test Medium (Corning 50-003-PB). Oxygen consumption was measured via mitochondrial stress test. The rate of pO_2 consumption was measured every ten minutes for a four-minute interval preceded by a three-minute mixing and three-minute waiting interval. Oligomycin A (Sigma-Aldrich 75351) (0.91 μM), BAM15 (Cayman Chemical Company 17811) (1.667 μM), Antimycin A (Sigma-Aldrich A8674) (7.692 μM), and Rotenone (Sigma-Aldrich R88751G) (7.692 μM) were used to interrogate basal, reserve, and maximum oxygen consumption capacity.

5.3.2 - XFe96 Seahorse bioenergetics assay

AML12 hepatocytes were plated (25,000 cells/well) in complete medium in XFe96 cell culture microplates (Agilent 101085-004) and incubated for 1 hour at room temperature before settling overnight at 37°C. The following day cells were treated for 4 hours with oxidized phospholipids (10 – 100 μg/mL) in DMEM:F12 supplemented as previously described. After treatment, media was removed and replaced with assay appropriate medium: Mitochondrial Stress Test Medium (Corning 50-003-PB) and Glycolytic Stress Test Medium (Sigma D5030) supplemented with 143 mM NaCl (Fisher S671-3) and 2 mM L-glutamine (Gibco 25030-081). Oxygen consumption was measured via mitochondrial stress test. The rate of pO_2 consumption was measured every ten minutes for a four-minute interval for thirty minutes prior to sequential challenge with (1) Oligomycin A (Sigma-Aldrich 75351) (1 μM), (2) BAM15 (Cayman Chemical Company 17811) (2

μM), and (3) Antimycin A (Sigma-Aldrich A8674) (10 μM) and Rotenone (Sigma-Aldrich R88751G) (10 μM). pO_2 consumption was measured as described previously to analyze basal, reserve, and maximum oxygen consumption capacity. Glycolytic rate was measured via extracellular acidification rate. The rate of pH change was measured every ten minutes for a four-minute interval for thirty minutes prior to sequential challenge with (1) Glucose (Sigma D9434) (20 mM), (2) Oligomycin A (Sigma-Aldrich 75351) (1 μM), and (3) 2-deoxyglucose (Sigma-Aldrich D8375) (80 mM) to interrogate basal, reserve, and stressed glycolytic rate.

5.4 - Quantitative real-time-PCR

5.4.1 - In vitro

RNA was isolated from cells lysed in RLT lysis buffer using the RNEasy Mini Kit (Qiagen 74106). Manufacturer's recommendations were followed for RNA isolation. RNA quantity and purity were analyzed by spectrometric analysis. cDNA was synthesized from 250ng of total RNA using iScript cDNA synthesis kit (Biorad 1708891) according to manufacturer's recommendations. Sensimix SYBR green (Bioline QT615-05) was used to quantify gene expression. Relative gene expression was calculated using ΔΔCq method normalized to a cyclophilin A in AML12 cells and *Hprt* in LX-2 cells.

5.4.2 - Ex vivo

Liver tissue was stored at -80°C in RNALater (Sigma-Aldrich R0901) until analysis. Liver tissue was lysed using Qiagen Tissue Lyser II (30 Hz for 15 minutes) in RLT lysis buffer. Manufacturer's recommendations were followed for RNA isolation using RNEasy Mini Kit. RNA quantity and purity were analyzed by spectrometric

analysis (260/280 - >1.8 and <2.2, 260/230 - >1.8 and <2.2). cDNA was synthesized from 250ng total RNA using iScript cDNA synthesis kit according to manufacturer's recommendations. Sensimix SYBR green was used to quantify gene expression. Relative gene expression was calculated using ΔΔCq method normalized to beta-2-microglobulin.

Primer sequences were generated using NCBI Primer Blast and span an exon-exon junction to ensure mRNA specificity and synthesized by Eurofins or Integrated DNA Technologies (table S4).

5.5 - Air oxidation of PAPC

1 mg of 1-palmitoyl-2-arachidonyl-*sn*-glycero-3-phosphocholine (PAPC) (Avanti Polar Lipids 850459C) was dried in a 13x100 borosilicate glass tube (Corning 99445-13) with nitrogen, covered loosely with aluminum foil to allow gas exchange, and oxidized by exposure to air for 7-12 days to generate the oxidized phospholipid mixture, OxPAPC. Level of oxidation was monitored by LC-MS to maintain a consistent oxidation profile.

5.6 - Copper oxidation of PLPC

10 µg of 1-palmitoyl-2-linoleoyl-*sn*-glycero-3-phosphocholine (PLPC) (Avanti Polar Lipids 850458) was transferred to a tube and dried under N_2. PLPC was resuspended in water containing CuCl (10.547 mM) and H_2O_2 (659 mM) and oxidized for 19 hours at 37°C to generate oxidized PLPC (OxPLPC). OxPLPC was extracted via liquid-liquid extraction using chloroform:methanol:water (1:1:1). Briefly, chloroform, methanol, and water were added to a glass tube. The extraction mixture was vortexed vigorously and centrifuged at 805*g* for 10 min at

20°C. After centrifugation, the organic layer was transferred to a new tube and dried under nitrogen. Oxidized PLPC was resuspended in methanol.

5.7 - Oxidized phospholipid quantification by LC-MS/MS

5.7.1 - OxPL extraction from Plasma

Plasma was collected from mice as described above and stored at -80°C in 50 µM butylated hydroxytoluene to prevent *ex vivo* oxidation. 25 µL of plasma were added to 1.975 mL of HPLC water (Tedia WS2211-001) in a 13x100 borosilicate glass tube (Corning 99445-13). 2 mL chloroform (EMD UN1888 or Fisher Scientific C607-1) and 2 mL of methanol (Sigma-Aldrich 646377-1L) containing 16.24 nM of 1-palmitoyl-2-glutaryl-*sn*-glycerol-3-phosphocholine-*d*6 (Cayman Chemical 25746) were added and vortexed vigorously. Samples were centrifuged at 805*g* (20°C) for ten minutes to accelerate phase separation. The organic phase was transferred to a new tube and 2 mL of chloroform was added to the original tube. The extraction was repeated twice more for a total of three times. Samples were dried under nitrogen and resuspended in 200 µL of methanol and vortexed vigorously. Samples were transferred to sample vials for LCMS analysis.

5.7.2 - OxPL extraction from Liver

Liver tissue was collected from mice and stored at -80°C in 50 µM in butylated hydroxytoluene to prevent *ex vivo* oxidation. Liver tissue was homogenized using a Qiagen Tissue Lyser II (30 Hz for 15 minutes) in water. Thirty-five milligrams of tissue was used for extraction as described previously (see OxPL extraction from Plasma). Samples were resuspended in 200 µL of HPLC butanol (PHARMCO-AAPER 13050-03).

5.7.3 - In silico phospholipid oxidation and method development

LPPTiger(*109*) was used to predict possible oxidation products of PAPC and PLPC. Oxidation level was set to Level 3. Maximum modification sites was set to 8, max keto was set to 8, max peroxy was set to 3, and max epoxy was set to 3. Nine hundred and eighty oxidation species were predicted for PAPC and 67 oxidation species were predicted for PLPC. Isobaric species were combined as a single analyte recording corresponding to the chemical formula. After combining isobaric species, there were 180 potential analytes for PAPC and 35 potential analytes for PLPC. Predicted analytes were validated by mass (< 5 ppm variance from predicted mass) using PAPC oxidized by air and PLPC oxidized by copper (I) chloride.

5.7.4 - Lipid Analysis

Oxidized phospholipids were measured using a ThermoFisher QExactive coupled with a Vanquish UHPLC. Samples were separated by reverse phase chromatography using a C18 Phenomenex 4.6 µm x 100 mm with 69% methanol 31% water with 10 mM ammonium acetate (Mobile Phase A) and 50% methanol 50% isopropanol with 10 mM ammonium acetate (Mobile Phase B) at a flow rate of 0.5 mL/min using the follow gradient: 0-4 min 0% B, 4-6 min 0%-17.5% B, 6-12 min 17.5% B, 12-14 min 17.5%-25% B, 14-21 min 25%% B, 21-24 min 25%-60% B, 24-33 min 60% B, 33-36 min 60%-65% B, 36-40 min 65% B, 40-43 min 65%-0% B, and 43-50 min 0% B. The QExactive was operated in positive mode using parallel reaction monitoring mode with an inclusion list and the following settings: MS^2 Resolution – 17,500; AGC target – 1e5; Maximum IT – 100 ms; Isolation

window 1.0 *m/z*; Normalized Collision Energy – 27. Analyte detection was limited to inclusion list within a specified retention window determined from *in vitro* oxidized PAPC and PLPC. Peaks corresponding to individual oxidized phospholipid species or isobaric groups were identified using Xcalibur (v4.1) QuanBrowser based on mass (<5 ppm variance from predicted mass) and validated retentions times. Peak areas were normalized to PGPC-*d*6. Biological replicates were excluded from analysis for an individual analyte if the analyte was not detected.

5.8 - Lipidomics LCMS and data analysis

The plasma lipidome was assessed using a ThermoFisher QExactive coupled with a Vanquish UHPLC. Samples were separated by reverse phase chromatography using an Thermo Scientific Acclaim™ 120 (C18 5 µm 120 Å 4.6 x 100 mm) with 50% acetonitrile, 50% water, and 0.1% formic acid with 10 mM ammonium formate (Mobile Phase A) and 88% isopropanol, 10% acetonitrile, 2% water, and 0.02% formic acid with 2 mM ammonium formate (Mobile Phase B) at a flow rate of 400 µL/min using the following gradient: 0-4 min 30-60% B, 4-10 min 60-80% B, 10-15 min 80-90% B, 15-24 min 90-100% B, 24-27 min 100% B, 27-27.1 min 100-30% B, 27.1-31 30% B. The QExactive was operated in positive mode and collected spectra using Full MS data-dependent MS^2 mode with an inclusion list containing analytes in Splash® Lipidomix® Mass Spec Standard (Avanti 330707) using the following settings: Full MS settings -- resolution – 35,000, AGC target – 1e5, Max IT – 128 ms, scan range – 200 to 1500 *m/z*; dd-MS^2 settings -- resolution – 17,500, AGC target – 2e5, Max IT – 64 ms, Loop count – 5, NCE – 40. Data were analyzed

using LipidSearch (Version 4.1.16) with the following settings: Search – Database: Q Exactive, Precursor tolerance - 5.0 ppm, Product tolerance – 8.0 ppm; Alignment – Alignment Method - Mean, Retention time tolerance - 0.25 min. Samples were normalized to the internal standard PGPC-*d*6 to control for extraction efficiency.

5.9 - *In vitro* quantification of lipid droplet

AML12 cells were fixed with 4% paraformaldehyde (diluted from 16%, Alfa Aesar 43368-9M) and stained with Hoescht Blue (Invitrogen™ 953557) and Nile Red (Invitrogen™ N1142). Two images (Zeiss Axiovert 200 with QICAM Fast 1394), one of DAPI and one of Nile Red, were taken at three locations in each well. Lipid droplet size and quantity were calculated from epifluorescent widefield micrographs using an ImageJ plugin, MRI Lipid Droplets(*149*). Lipid droplets were identified as areas larger than five pixels. MRI Lipid Droplets ImageJ plugin was used to identify nuclei in DAPI staining and count total cell number.

5.10 - *In vitro* and *ex vivo* RNA-seq

5.10.1 - In vitro

AML12 hepatocytes (100,000 cells/well) were treated with OxPAPC (100 µg/mL), truncated-OxPAPC (100 µg/m), and full-length (100 µg/mL) for four hours. RNA was isolated using RNeasy® Mini Kit (Qiagen 74106). RNA quantity and purity were analyzed by spectrometric analysis (260/280>1.8 and <2.2, 260/230>1.8 and <2.2, RIN≥8). cDNA libraries were generated using NEBNext® Ultra™ II Directional RNA library Prep Kit (New England Biosciences E7760S). cDNA library fragment size was verified using Bioanalyzer 2100. Samples were sequenced by

the UVA Genomics and Technology core with a read length of 75bp and a target depth of 10 million reads using Illumina NextSeq 500 Sequencing System.

5.10.2 - Ex vivo

After dissection, liver tissue was stored at -80°C in RNALater (Sigma-Aldrich R0901) until use. Liver tissue was lysed using Qiagen Tissue Lyser II (30 Hz for 15 minutes) in RLT Lysis buffer (Qiagen 1015762). Manufacturer's recommendations were followed for RNA isolation using RNeasy® Mini Kit (Qiagen 74106). RNA quantity and purity were analyzed by spectrometric analysis (260/280 - >1.8 and <2.2, 260/230 - >1.8 and <2.2). RNA was shipped to GeneWiz (South Plainfield, NJ). RNA was sequenced in a strand specific manner with a read length of 150 bp and a target depth of 20-30 million reads.

5.10.3 - Data Analysis

Reads were aligned using UVA Rivanna Supercluster using Spliced Transcripts Alignment to a Reference (STAR)(*150*). Reads were trimmed and aligned to the mouse reference genome (mm10) with either single- or pair-end alignment where appropriate. Aligned reads were counted and differential gene expression was calculated if reads exceeded 1 read per million using EdgeR(*151*) and RStudio. Genes were considered differentially expressed if they deviated from the control condition by 50% with a p-value less than 0.05 (*in vitro*) or 0.1 (*in vivo*). EnrichR(*117*) was used to identify pathways that were up or downregulated based on differentially regulated genes.

5.11 - MRI

Body composition analysis was performed by EchoMRI™-100H on mice prior to the start of FPC diet feeding and weekly for the duration of feeding.

5.12 - Western Blot

5.12.1 - Tissue

Tissues were lysed using Qiagen Tissue Lyser II (30 Hz for 15 minutes) in RIPA lysis buffer containing cOmplete Mini protease inhibitors (Roche 37439120) and phosphatase inhibitors (Sigma P5726 and P0044). Protein concentration was quantified via Pierce™ BCA protein Assay (Thermo Scientific 23225). 25-75 µg of total protein were separated by SDS-PAGE (8%-12%) and transferred to nitrocellulose or PVDF membranes. Membranes were blocked with Intercept Blocking Buffer (LICOR 927-70001) or 5% BSA in TBS or 5% milk powder in TBS with 0.1% Tween20 for 1 hour at room temperature. Membranes were stained with goat anti-myc [HRP] antibody (NovusBio NB600-341, 1:30000) or rabbit anti-Vinculin antibody (CST E1E9V, 1:1000) diluted in 1% milk powder in TBS with 0.1% Tween20 overnight at 4°C. Next, membranes were washed in tris-buffered saline containing 0.1% Tween20, followed by incubation 1 hour at room temperature with HRP-conjugated secondary antibodies (1:10000 dilution in 1% milk in TBS with 0.1% Tween20, CST), except for membranes incubated with the goat anti-myc [HRP] antibody. Membranes were washed in tris-buffered saline containing 0.1% Tween20 and imaged on an Odyssey Imager (LICOR Biosciences) or incubated with ECL substrate (ThermoScientific SuperSignal

34580) for 5 minutes at room temperature and imaged using the Amersham ImageQuant 800.

5.12.2 - Plasma

Plasma was diluted in loading dye (150 µL/mL) and denatured at 95°C for ten minutes. Heat denatured samples were separated by SDS-PAGE gel and transferred to nitrocellulose membranes. Membranes were blocked with PBS Blocking Buffer (LICOR Biosciences) and for 1 hour at room temperature and stained with a 1:1000 dilution of mouse anti-myc antibody (Millipore 05-724) overnight at 4°C. The blot was washed three time for 15 minutes with PBS Blocking Buffer. The blot was stained with the secondary antibody IRDye® 800CW Goat anti-Rabbit (1:10,000 in PBS) (Licor 926-32211) for 1 hour at room temperature followed by three washes with Licor PBS Blocking Buffer. The resulting blot was visualized using an Odyssey Imager (LICOR Biosciences).

5.13 - HIS/myc competitive sandwich ELISA

96-well Nunc MaxiSorp™ flat-bottom plates (ThermoFisher Scientific) were coated with rabbit anti HIS-Tag antibody (CST 2365S, 1:250 in 1x PBS) overnight at 4 °C. Coated wells were then aspirated and washed three times with 1x PBS (~1 min soaking in between). After blocking for 1 hour at room temperature with 1x ELISA/Elispot Diluent (Invitrogen, 19045636) diluted in double distilled water, wells were washed as previously described. Plasma samples were diluted 1:20 in double distilled water and added into the wells. For the HIS-competitive standard curve 2 µg HIS-protein ELISA standard (stock 50 µg/mL, Cayman Chemical, 0556338) was serially diluted in double distilled water and E06 plasma sample was added

(1:20). The E06 plasma standard curve was generated by serial dilution of plasma. An HIS-protein competitive standard curve was generated by serial dilution of HIS-tagged 4EBP1 (11.1 mg/mL). Blanks were incubated with 1x ELISA/Elispot Diluent. Plates were sealed and incubated over night at 4 °C. Following 5 washing steps, the detection antibody goat anti-c-Myc HRP-coupled (Novus P26, 1:5000 in 1x ELISA/Elispot Diluent) was added to the plates and incubated for 1 hour at room temperature. After washing seven times, 1x TMB ELISA Substrate Solution (eBioscience, Inc., E00008-1655) was pipetted into the wells and incubated for 35 minutes. Absorbance was measured using a PlateReader (BioTek) at 450 nm and 570 nm.

5.14 - Glucose and Insulin Tolerance Tests

Intraperitoneal glucose and insulin tolerance tests were performed on fasted mice at time points indicated. Mice were fasted for 6 hours, and body mass and basal blood glucose measured via tail vein nick using a glucometer (CVS Health). For GTT, 1mg/g glucose in sterile water was administered by intraperitoneal injection, and blood glucose recorded 15, 30, 45, 60, 90, and 120 minutes after injection. For ITT, Humulin R (100U/ml, Lilly) was diluted in sterile 0.9% saline, 0.75 U/kg was administered by intraperitoneal injection, and blood glucose recorded 15, 30, 45, 60, 90, and 120 minutes after injection.

5.15 - Cholesterol Assay

Hepatic cholesterol was assessed using Amplex™ Red Cholesterol Assay Kit (Invitrogen A12216). Liver tissue was weighed and lysed in 400 µL of RIPA Lysis Buffer (EMD Millipore 20-188) using Tissue Lyser II. The protein concentration of

the lysate was determined by Pierce™ BCA Protein Assay (Thermo Scientific 23225). Lysates were diluted (15 µg per reaction) and analyzed in triplicate for free, esterified, and total cholesterol according to manufacturer recommendations. Final hepatic cholesterol concentrations were reported as µg of cholesterol per mg of liver protein.

5.16 - Hydroxyproline assay

Liver tissue (20-30 mg) was lysed in 200 µL of HPLC water (Sigma-Aldrich 270733) using TissueLyser II shaking at 30 Hz for fifteen minutes. Lysates were centrifuged at 20,817*g* at 4°C for 15 minutes. Supernatants were collected and protein concentration was assessed by Pierce™ BCA protein Assay (Thermo Scientific 23225). 500 µg of protein were diluted 1:1 in 37% HCl (12.1 M) to final concentration of 1.89 mg/mL in ~6 M HCl. The lysates were incubated at 95°C for 20 hours. After 20 hours samples were cooled to room temperature and centrifuged at 13,000*g* for 10 minutes. Supernatants were collected and diluted to 4 M HCl. Hydroxyproline content was assessed using *QuickZyme* Sensitive Tissue Hydroxyproline Assay (*QuickZyme* Biosciences QZBTISHYP1) according to manufacturer recommendations.

5.17 - Statistical Analysis

Statistical analysis was performed using GraphPad Prism 9. Data are represented as the mean ± standard error of the mean. Statistical tests were applied as described in the figure legends. Statistical outliers were identified using ROUT method (Q = 2 or 5%) and excluded from analyses.

References

1. V. N. Bochkov, O. V. Oskolkova, K. G. Birukov, A.-L. Levonen, C. J. Binder, J. Stöckl, Generation and Biological Activities of Oxidized Phospholipids. *Antioxidants & Redox Signaling* **12**, 1009-1059 (2010).

2. H. Esterbauer, R. J. Schaur, H. Zollner, Chemistry and biochemistry of 4-hydroxynonenal, malonaldehyde and related aldehydes. *Free Radical Biology and Medicine* **11**, 81-128 (1991).

3. B. B. Halliwell, J. M. Gutteridge, *Free Radicals in Biology and Medicine*. (Oxford University Press, New York, ed. Second, 1985).

4. A. Reis, M. R. M. Domingues, F. M. L. Amado, A. J. Ferrer-Correia, P. Domingues, Radical peroxidation of palmitoyl-lineloyl-glycerophosphocholine liposomes: Identification of long-chain oxidised products by liquid chromatography–tandem mass spectrometry. *Journal of Chromatography B* **855**, 186-199 (2007).

5. A. D. Watson, G. Subbanagounder, D. S. Welsbie, K. F. Faull, M. Navab, M. E. Jung, A. M. Fogelman, J. A. Berliner, Structural Identification of a Novel Pro-inflammatory Epoxyisoprostane Phospholipid in Mildly Oxidized Low Density Lipoprotein. *Journal of Biological Chemistry* **274**, 24787-24798 (1999).

6. L. J. Roberts, 2nd, G. L. Milne, Isoprostanes. *J Lipid Res* **50 Suppl**, S219-223 (2009).

7. R. Radi, J. S. Beckman, K. M. Bush, B. A. Freeman, Peroxynitrite-induced membrane lipid peroxidation: The cytotoxic potential of superoxide and nitric oxide. *Archives of Biochemistry and Biophysics* **288**, 481-487 (1991).

8. S. T. Prigge, J. C. Boyington, M. Faig, K. S. Doctor, B. J. Gaffney, L. M. Amzel, Structure and mechanism of lipoxygenases. *Biochimie* **79**, 629-636 (1997).

9. H. Hock, H. Kropf, Autoxydation von Kohlenwasserstoffen und die Cumol-Phenol-Synthese. *Angewandte Chemie* **69**, 313-321 (1957).

10. M. Kobayashi, M. Yamamoto, Nrf2–Keap1 regulation of cellular defense mechanisms against electrophiles and reactive oxygen species. *Advances in Enzyme Regulation* **46**, 113-140 (2006).

11. D. Trachootham, W. Lu, M. A. Ogasawara, R. D. Nilsa, P. Huang, Redox regulation of cell survival. *Antioxid Redox Signal* **10**, 1343-1374 (2008).

12. O. A. Barski, S. M. Tipparaju, A. Bhatnagar, The aldo-keto reductase superfamily and its role in drug metabolism and detoxification. *Drug Metab Rev* **40**, 553-624 (2008).

13. J. Pizzorno, Glutathione! *Integr Med (Encinitas)* **13**, 8-12 (2014).

14. G. C. Mills, Hemoglobin catabolism: I. Glutathione peroxidase, an erythrocyte enzyme which protects hemoglobin from oxidative breakdown. *Journal of Biological Chemistry* **229**, 189-197 (1957).

15. B. O. Christophersen, Reduction of linolenic acid hydroperoxide by a glutathione peroxidase. *Biochimica et Biophysica Acta (BBA) - Lipids and Lipid Metabolism* **176**, 463-470 (1969).

16. F. Ursini, M. Maiorino, M. Valente, L. Ferri, C. Gregolin, Purification from pig liver of a protein which protects liposomes and biomembranes from peroxidative degradation and exhibits glutathione peroxidase activity on phosphatidylcholine hydroperoxides. *Biochimica et Biophysica Acta (BBA) - Lipids and Lipid Metabolism* **710**, 197-211 (1982).

17. S. J. Dixon, K. M. Lemberg, M. R. Lamprecht, R. Skouta, E. M. Zaitsev, C. E. Gleason, D. N. Patel, A. J. Bauer, A. M. Cantley, W. S. Yang, B. Morrison, 3rd, B. R. Stockwell, Ferroptosis: an iron-dependent form of nonapoptotic cell death. *Cell* **149**, 1060-1072 (2012).

18. Wan S. Yang, R. SriRamaratnam, Matthew E. Welsch, K. Shimada, R. Skouta, Vasanthi S. Viswanathan, Jaime H. Cheah, Paul A. Clemons, Alykhan F. Shamji, Clary B. Clish, Lewis M. Brown, Albert W. Girotti, Virginia W. Cornish, Stuart L. Schreiber, Brent R. Stockwell, Regulation of Ferroptotic Cancer Cell Death by GPX4. *Cell* **156**, 317-331 (2014).

19. K. Stremler, D. Stafforini, S. Prescott, T. McIntyre, Human plasma platelet-activating factor acetylhydrolase. Oxidatively fragmented phospholipids as substrates. *Journal of Biological Chemistry* **266**, 11095-11103 (1991).

20. A. Watson, M. Navab, D. Stafforini, S. Prescott, T. McIntyre, J. Berliner, A. Fogelman, in *Circulation*. (Lippincott Williams & Wilkins 530 Walnut St, Philadelphia, PA 19106-3621 USA, 1993), vol. 88, pp. 561-561.

21. N. Kono, T. Inoue, Y. Yoshida, H. Sato, T. Matsusue, H. Itabe, E. Niki, J. Aoki, H. Arai, Protection against oxidative stress-induced hepatic injury by intracellular type II platelet-activating factor acetylhydrolase by metabolism of oxidized phospholipids in vivo. *Journal of Biological Chemistry* **283**, 1628-1636 (2008).

22. X. Que, M.-Y. Hung, C. Yeang, A. Gonen, T. A. Prohaska, X. Sun, C. Diehl, A. Määttä, D. E. Gaddis, K. Bowden, J. Pattison, J. G. Macdonald, S. Ylä-Herttuala, P. L. Mellon, C. C. Hedrick, K. Ley, Y. I. Miller, C. K. Glass, K. L. Peterson, C. J. Binder, S. Tsimikas, J. L. Witztum, Oxidized phospholipids are proinflammatory and proatherogenic in hypercholesterolaemic mice. *Nature* **558**, 301-306 (2018).

23. E. Ambrogini, X. Que, S. Wang, F. Yamaguchi, R. S. Weinstein, S. Tsimikas, S. C. Manolagas, J. L. Witztum, R. L. Jilka, Oxidation-specific epitopes restrain bone formation. *Nat Commun* **9**, 2193 (2018).

24. X. Sun, J. S. Seidman, P. Zhao, T. D. Troutman, N. J. Spann, X. Que, F. Zhou, Z. Liao, M. Pasillas, X. Yang, J. A. Magida, T. Kisseleva, D. A. Brenner, M. Downes, R. M. Evans, A. R. Saltiel, S. Tsimikas, C. K. Glass, J. L. Witztum, Neutralization of Oxidized Phospholipids Ameliorates Non-alcoholic Steatohepatitis. *Cell Metab* **31**, 189-206 e188 (2020).

25. M. Palmieri, M. Almeida, I. Nookaew, H. Gomez-Acevedo, T. E. Joseph, X. Que, S. Tsimikas, X. Sun, S. C. Manolagas, J. L. Witztum, E. Ambrogini, Neutralization of oxidized phospholipids attenuates age-associated bone loss in mice. *Aging Cell* **20**, e13442 (2021).

26. S. Hörkkö, D. A. Bird, E. Miller, H. Itabe, N. Leitinger, G. Subbanagounder, J. A. Berliner, P. Friedman, E. A. Dennis, L. K. Curtiss, W. Palinski, J. L. Witztum, Monoclonal autoantibodies specific for oxidized phospholipids or oxidized phospholipid–protein adducts inhibit macrophage uptake of oxidized low-density lipoproteins. *Journal of Clinical Investigation* **103**, 117-128 (1999).

27. C. M. Upchurch, S. Yeudall, C. M. Pavelec, D. Merk, J. Greulich, M. Manjegowda, S. S. Raghavan, I. M. Bochkis, M. M. Scott, E. Perez-Reyes, N. Leitinger, Targeting oxidized phospholipids by AAV-based gene therapy in mice with established hepatic steatosis prevents progression to fibrosis. *Science Advances* **8**, eabn0050 (2022).

28. A. D. Watson, N. Leitinger, M. Navab, K. F. Faull, S. Hörkkö, J. L. Witztum, W. Palinski, D. Schwenke, R. G. Salomon, W. Sha, G. Subbanagounder, A. M. Fogelman, J. A. Berliner, Structural Identification by Mass Spectrometry of Oxidized Phospholipids in Minimally Oxidized Low Density Lipoprotein That Induce Monocyte/Endothelial Interactions

and Evidence for Their Presence in Vivo. *Journal of Biological Chemistry* **272**, 13597-13607 (1997).

29. K. G. Birukov, V. N. Bochkov, A. A. Birukova, K. Kawkitinarong, A. Rios, A. Leitner, A. D. Verin, G. M. Bokoch, N. Leitinger, J. G. Garcia, Epoxycyclopentenone-containing oxidized phospholipids restore endothelial barrier function via Cdc42 and Rac. *Circ Res* **95**, 892-901 (2004).

30. J. A. Berliner, N. Leitinger, S. Tsimikas, The role of oxidized phospholipids in atherosclerosis. *J Lipid Res* **50 Suppl**, S207-212 (2009).

31. A. Kadl, E. Galkina, N. Leitinger, Induction of CCR2-dependent macrophage accumulation by oxidized phospholipids in the air-pouch model of inflammation. *Arthritis & Rheumatism* **60**, 1362-1371 (2009).

32. A. Kadl, A. K. Meher, P. R. Sharma, M. Y. Lee, A. C. Doran, S. R. Johnstone, M. R. Elliott, F. Gruber, J. Han, W. Chen, T. Kensler, K. S. Ravichandran, B. E. Isakson, B. R. Wamhoff, N. Leitinger, Identification of a novel macrophage phenotype that develops in response to atherogenic phospholipids via Nrf2. *Circ Res* **107**, 737-746 (2010).

33. V. Serbulea, D. DeWeese, N. Leitinger, The effect of oxidized phospholipids on phenotypic polarization and function of macrophages. *Free Radic Biol Med* **111**, 156-168 (2017).

34. V. Serbulea, C. M. Upchurch, K. W. Ahern, G. Bories, P. Voigt, D. E. DeWeese, A. K. Meher, T. E. Harris, N. Leitinger, Macrophages sensing oxidized DAMPs reprogram their metabolism to support redox homeostasis and inflammation through a TLR2-Syk-ceramide dependent mechanism. *Mol Metab* **7**, 23-34 (2018).

35. V. Serbulea, C. M. Upchurch, M. S. Schappe, P. Voigt, D. E. Deweese, B. N. Desai, A. K. Meher, N. Leitinger, Macrophage phenotype and

bioenergetics are controlled by oxidized phospholipids identified in lean and obese adipose tissue. *Proceedings of the National Academy of Sciences* **115**, E6254-E6263 (2018).

36. E. A. Podrez, E. Poliakov, Z. Shen, R. Zhang, Y. Deng, M. Sun, P. J. Finton, L. Shan, M. Febbraio, D. P. Hajjar, R. L. Silverstein, H. F. Hoff, R. G. Salomon, S. L. Hazen, A novel family of atherogenic oxidized phospholipids promotes macrophage foam cell formation via the scavenger receptor CD36 and is enriched in atherosclerotic lesions. *J Biol Chem* **277**, 38517-38523 (2002).

37. E. A. Podrez, E. Poliakov, Z. Shen, R. Zhang, Y. Deng, M. Sun, P. J. Finton, L. Shan, B. Gugiu, P. L. Fox, H. F. Hoff, R. G. Salomon, S. L. Hazen, Identification of a Novel Family of Oxidized Phospholipids That Serve as Ligands for the Macrophage Scavenger Receptor CD36. *Journal of Biological Chemistry* **277**, 38503-38516 (2002).

38. E. A. Podrez, T. V. Byzova, M. Febbraio, R. G. Salomon, Y. Ma, M. Valiyaveettil, E. Poliakov, M. Sun, P. J. Finton, B. R. Curtis, J. Chen, R. Zhang, R. L. Silverstein, S. L. Hazen, Platelet CD36 links hyperlipidemia, oxidant stress and a prothrombotic phenotype. *Nature Medicine* **13**, 1086-1095 (2007).

39. V. N. Bochkov, A. Kadl, J. Huber, F. Gruber, B. R. Binder, N. Leitinger, Protective role of phospholipid oxidation products in endotoxin-induced tissue damage. *Nature* **419**, 77-81 (2002).

40. L. H. Chu, M. Indramohan, R. A. Ratsimandresey, A. Gangopadhyay, E. P. Morris, D. M. Monack, A. Dorfleutner, C. Stehlik, The oxidized phospholipid oxPAPC protects from septic shock by targeting the non-canonical inflammasome in macrophages. *Nat Commun* **9**, 996 (2018).

41. C. Erridge, S. Kennedy, C. M. Spickett, D. J. Webb, Oxidized phospholipid inhibition of toll-like receptor (TLR) signaling is restricted to TLR2 and TLR4: roles for CD14, LPS-binding protein, and MD2 as targets for specificity of inhibition. *J Biol Chem* **283**, 24748-24759 (2008).

42. V. E. Kagan, B. Gleiss, Y. Y. Tyurina, V. A. Tyurin, C. Elenström-Magnusson, S.-X. Liu, F. B. Serinkan, A. Arroyo, J. Chandra, S. Orrenius, B. Fadeel, A Role for Oxidative Stress in Apoptosis: Oxidation and Externalization of Phosphatidylserine Is Required for Macrophage Clearance of Cells Undergoing Fas-Mediated Apoptosis. *The Journal of Immunology* **169**, 487-499 (2002).

43. T. M. Grigory G Borisenko, Shang-Xi Liu, Vladimir A Tyurin, Jiang Jianfei, Fatma B Serinkan, Valerian E Kagan, Macrophage recognition of externalized phosphatidylserine and phagocytosis of apoptotic Jurkat cells-existence of a threshold. *Archives of Biochemistry and Biophysics* **413**, 12 (2003).

44. I. Zanoni, Y. Tan, M. Di Gioia, A. Broggi, J. Ruan, J. Shi, C. A. Donado, F. Shao, H. Wu, J. R. Springstead, J. C. Kagan, An endogenous caspase-11 ligand elicits interleukin-1 release from living dendritic cells. *Science* **352**, 1232-1236 (2016).

45. V. E. Kagan, G. Mao, F. Qu, J. P. Angeli, S. Doll, C. S. Croix, H. H. Dar, B. Liu, V. A. Tyurin, V. B. Ritov, A. A. Kapralov, A. A. Amoscato, J. Jiang, T. Anthonymuthu, D. Mohammadyani, Q. Yang, B. Proneth, J. Klein-Seetharaman, S. Watkins, I. Bahar, J. Greenberger, R. K. Mallampalli, B. R. Stockwell, Y. Y. Tyurina, M. Conrad, H. Bayir, Oxidized arachidonic and adrenic PEs navigate cells to ferroptosis. *Nat Chem Biol* **13**, 81-90 (2017).

46. B. Wiernicki, H. Dubois, Y. Y. Tyurina, B. Hassannia, H. Bayir, V. E. Kagan, P. Vandenabeele, A. Wullaert, T. Vanden Berghe, Excessive

phospholipid peroxidation distinguishes ferroptosis from other cell death modes including pyroptosis. *Cell Death Dis* **11**, 922 (2020).

47. C. Meisinger, J. Baumert, N. Khuseyinova, H. Loewel, W. Koenig, Plasma oxidized low-density lipoprotein, a strong predictor for acute coronary heart disease events in apparently healthy, middle-aged men from the general population. *Circulation* **112**, 651-657 (2005).

48. A. Pirillo, G. D. Norata, A. L. Catapano, LOX-1, OxLDL, and Atherosclerosis. *Mediators of Inflammation* **2013**, 152786 (2013).

49. J. A. Berliner, M. C. Territo, A. Sevanian, S. Ramin, J. A. Kim, B. Bamshad, M. Esterson, A. M. Fogelman, Minimally modified low density lipoprotein stimulates monocyte endothelial interactions. *J Clin Invest* **85**, 1260-1266 (1990).

50. E. A. Podrez, E. Poliakov, Z. Shen, R. Zhang, Y. Deng, M. Sun, P. J. Finton, L. Shan, M. Febbraio, D. P. Hajjar, R. L. Silverstein, H. F. Hoff, R. G. Salomon, S. L. Hazen, A Novel Family of Atherogenic Oxidized Phospholipids Promotes Macrophage Foam Cell Formation via the Scavenger Receptor CD36 and Is Enriched in Atherosclerotic Lesions. *Journal of Biological Chemistry* **277**, 38517-38523 (2002).

51. M. B. Boffa, M. L. Koschinsky, Oxidized phospholipids as a unifying theory for lipoprotein(a) and cardiovascular disease. *Nat Rev Cardiol* **16**, 305-318 (2019).

52. K. H. Zheng, S. Tsimikas, T. Pawade, J. Kroon, W. S. A. Jenkins, M. K. Doris, A. C. White, N. Timmers, J. Hjortnaes, M. A. Rogers, E. Aikawa, B. J. Arsenault, J. L. Witztum, D. E. Newby, M. L. Koschinsky, Z. A. Fayad, E. S. G. Stroes, S. M. Boekholdt, M. R. Dweck, Lipoprotein(a) and Oxidized Phospholipids Promote Valve Calcification in Patients With Aortic Stenosis. *J Am Coll Cardiol* **73**, 2150-2162 (2019).

53. S. Tsimikas, E. S. Brilakis, E. R. Miller, J. P. McConnell, R. J. Lennon, K. S. Kornman, J. L. Witztum, P. B. Berger, Oxidized Phospholipids, Lp(a) Lipoprotein, and Coronary Artery Disease. *New England Journal of Medicine* **353**, 46-57 (2005).

54. S. Tsimikas, S. Kiechl, J. Willeit, M. Mayr, E. R. Miller, F. Kronenberg, Q. Xu, C. Bergmark, S. Weger, F. Oberhollenzer, J. L. Witztum, Oxidized Phospholipids Predict the Presence and Progression of Carotid and Femoral Atherosclerosis and Symptomatic Cardiovascular Disease. *Journal of the American College of Cardiology* **47**, 2219-2228 (2006).

55. R. Capoulade, K. L. Chan, C. Yeang, P. Mathieu, Y. Bosse, J. G. Dumesnil, J. W. Tam, K. K. Teo, A. Mahmut, X. Yang, J. L. Witztum, B. J. Arsenault, J. P. Despres, P. Pibarot, S. Tsimikas, Oxidized Phospholipids, Lipoprotein(a), and Progression of Calcific Aortic Valve Stenosis. *J Am Coll Cardiol* **66**, 1236-1246 (2015).

56. P. R. Kamstrup, M. Y. Hung, J. L. Witztum, S. Tsimikas, B. G. Nordestgaard, Oxidized Phospholipids and Risk of Calcific Aortic Valve Disease: The Copenhagen General Population Study. *Arterioscler Thromb Vasc Biol* **37**, 1570-1578 (2017).

57. A. Weidtmann, R. Scheithe, N. Hrboticky, A. Pietsch, R. Lorenz, W. Siess, Mildly Oxidized LDL Induces Platelet Aggregation Through Activation of Phospholipase A₂. *Arteriosclerosis, Thrombosis, and Vascular Biology* **15**, 1131-1138 (1995).

58. S. M. Prescott, G. A. Zimmerman, D. M. Stafforini, T. M. McIntyre, Platelet-activating factor and related lipid mediators. *Annual review of biochemistry* **69**, 419-445 (2000).

59. B. Davis, G. Koster, L. J. Douet, M. Scigelova, G. Woffendin, J. M. Ward, A. Smith, J. Humphries, K. G. Burnand, C. H. Macphee, Electrospray

ionization mass spectrometry identifies substrates and products of lipoprotein-associated phospholipase A2 in oxidized human low density lipoprotein. *Journal of Biological Chemistry* **283**, 6428-6437 (2008).

60. S. N. Lauder, K. Allen-Redpath, D. A. Slatter, M. Aldrovandi, A. O'Connor, D. Farewell, C. L. Percy, J. E. Molhoek, S. Rannikko, V. J. Tyrrell, S. Ferla, G. L. Milne, A. W. Poole, C. P. Thomas, S. Obaji, P. R. Taylor, S. A. Jones, P. G. de Groot, R. T. Urbanus, S. Hörkkö, S. Uderhardt, J. Ackermann, P. Vince Jenkins, A. Brancale, G. Krönke, P. W. Collins, V. B. O'Donnell, Networks of enzymatically oxidized membrane lipids support calcium-dependent coagulation factor binding to maintain hemostasis. *Sci Signal* **10**, (2017).

61. N. Tavoosi, R. L. Davis-Harrison, T. V. Pogorelov, Y. Z. Ohkubo, M. J. Arcario, M. C. Clay, C. M. Rienstra, E. Tajkhorshid, J. H. Morrissey, Molecular Determinants of Phospholipid Synergy in Blood Clotting *. *Journal of Biological Chemistry* **286**, 23247-23253 (2011).

62. D. A. Slatter, C. L. Percy, K. Allen-Redpath, J. M. Gajsiewicz, N. J. Brooks, A. Clayton, V. J. Tyrrell, M. Rosas, S. N. Lauder, A. Watson, M. Dul, Y. Garcia-Diaz, M. Aldrovandi, M. Heurich, J. Hall, J. H. Morrissey, S. Lacroix-Desmazes, S. Delignat, P. V. Jenkins, P. W. Collins, V. B. O'Donnell, Enzymatically oxidized phospholipids restore thrombin generation in coagulation factor deficiencies. *JCI Insight* **3**, (2018).

63. J. B. Spinelli, H. Yoon, A. E. Ringel, S. Jeanfavre, C. B. Clish, M. C. Haigis, Metabolic recycling of ammonia via glutamate dehydrogenase supports breast cancer biomass. *Science* **358**, 941-946 (2017).

64. V. Serbulea, C. M. Upchurch, M. S. Schappe, P. Voigt, D. E. DeWeese, B. N. Desai, A. K. Meher, N. Leitinger, Macrophage phenotype and bioenergetics are controlled by oxidized phospholipids identified in lean

and obese adipose tissue. *Proc Natl Acad Sci U S A* **115**, E6254-E6263 (2018).

65. B. P. Sinder, A. R. Pettit, L. K. McCauley, Macrophages: Their Emerging Roles in Bone. *J Bone Miner Res* **30**, 2140-2149 (2015).

66. M. Almeida, E. Ambrogini, L. Han, S. C. Manolagas, R. L. Jilka, Increased Lipid Oxidation Causes Oxidative Stress, Increased Peroxisome Proliferator-activated Receptor-γ Expression, and Diminished Pro-osteogenic Wnt Signaling in the Skeleton*. *Journal of Biological Chemistry* **284**, 27438-27448 (2009).

67. L. Wang, Y. Chai, C. Li, H. Liu, W. Su, X. Liu, B. Yu, W. Lei, B. Yu, J. L. Crane, X. Cao, M. Wan, Oxidized phospholipids are ligands for LRP6. *Bone Res* **6**, 22 (2018).

68. M. Hiraoka, A. Abe, An Increase of Oxidized Phospholipids and the Role of Macrophages in Intraocular Inflammation. *Investigative Opthalmology & Visual Science* **61**, 23 (2020).

69. N. Kerur, S. Fukuda, D. Banerjee, Y. Kim, D. Fu, I. Apicella, A. Varshney, R. Yasuma, B. J. Fowler, E. Baghdasaryan, K. M. Marion, X. Huang, T. Yasuma, Y. Hirano, V. Serbulea, M. Ambati, V. L. Ambati, Y. Kajiwara, K. Ambati, S. Hirahara, A. Bastos-Carvalho, Y. Ogura, H. Terasaki, T. Oshika, K. B. Kim, D. R. Hinton, N. Leitinger, J. C. Cambier, J. D. Buxbaum, M. C. Kenney, S. M. Jazwinski, H. Nagai, I. Hara, A. P. West, K. A. Fitzgerald, S. R. Sadda, B. D. Gelfand, J. Ambati, cGAS drives noncanonical-inflammasome activation in age-related macular degeneration. *Nat Med* **24**, 50-61 (2018).

70. R. Bossardi Ramos, A. P. Adam, Molecular Mechanisms of Vascular Damage During Lung Injury. *Adv Exp Med Biol* **1304**, 95-107 (2021).

71. C. K. Probst, S. B. Montesi, B. D. Medoff, B. S. Shea, R. S. Knipe, Vascular permeability in the fibrotic lung. *European Respiratory Journal* **56**, 1900100 (2020).

72. D. De Backer, D. Orbegozo Cortes, K. Donadello, J.-L. Vincent, Pathophysiology of microcirculatory dysfunction and the pathogenesis of septic shock. *Virulence* **5**, 73-79 (2014).

73. A. Y. Meliton, F. Meng, Y. Tian, N. Sarich, G. M. Mutlu, A. A. Birukova, K. G. Birukov, Oxidized phospholipids protect against lung injury and endothelial barrier dysfunction caused by heat-inactivated Staphylococcus aureus. *American Journal of Physiology-Lung Cellular and Molecular Physiology* **308**, L550-L562 (2015).

74. S. Nonas, I. Miller, K. Kawkitinarong, S. Chatchavalvanich, I. Gorshkova, V. N. Bochkov, N. Leitinger, V. Natarajan, J. G. N. Garcia, K. G. Birukov, Oxidized Phospholipids Reduce Vascular Leak and Inflammation in Rat Model of Acute Lung Injury. *American Journal of Respiratory and Critical Care Medicine* **173**, 1130-1138 (2006).

75. K. G. Birukov, V. N. Bochkov, A. A. Birukova, K. Kawkitinarong, A. Rios, A. Leitner, A. D. Verin, G. M. Bokoch, N. Leitinger, J. G. Garcia, Epoxycyclopentenone-containing oxidized phospholipids restore endothelial barrier function via Cdc42 and Rac. *Circulation research* **95**, 892-901 (2004).

76. A. A. Birukova, E. Alekseeva, I. Cokic, C. E. Turner, K. G. Birukov, Cross talk between paxillin and Rac is critical for mediation of barrier-protective effects by oxidized phospholipids. *American Journal of Physiology-Lung Cellular and Molecular Physiology* **295**, L593-L602 (2008).

77. A. A. Birukova, I. Malyukova, A. Mikaelyan, P. Fu, K. G. Birukov, Tiam1 and βPIX mediate Rac-dependent endothelial barrier protective response

to oxidized phospholipids. *Journal of cellular physiology* **211**, 608-617 (2007).

78. A. A. Birukova, I. Malyukova, V. Poroyko, K. G. Birukov, Paxillin-β-catenin interactions are involved in Rac/Cdc42-mediated endothelial barrier-protective response to oxidized phospholipids. *American Journal of Physiology-Lung Cellular and Molecular Physiology* **293**, L199-L211 (2007).

79. A. A. Birukova, V. Starosta, X. Tian, K. Higginbotham, L. Koroniak, J. A. Berliner, K. G. Birukov, Fragmented oxidation products define barrier disruptive endothelial cell response to OxPAPC. *Transl Res* **161**, 495-504 (2013).

80. E. Dejana, F. Orsenigo, M. G. Lampugnani, The role of adherens junctions and VE-cadherin in the control of vascular permeability. *Journal of cell science* **121**, 2115-2122 (2008).

81. Y. Ke, P. Karki, J. Kim, S. Son, E. Berdyshev, V. N. Bochkov, A. A. Birukova, K. G. Birukov, Elevated truncated oxidized phospholipids as a factor exacerbating ALI in the aging lungs. *FASEB J* **33**, 3887-3900 (2019).

82. J. Huber, A. Vales, G. Mitulovic, M. Blumer, R. Schmid, J. L. Witztum, B. R. Binder, N. Leitinger, Oxidized membrane vesicles and blebs from apoptotic cells contain biologically active oxidized phospholipids that induce monocyte-endothelial interactions. *Arteriosclerosis, thrombosis, and vascular biology* **22**, 101-107 (2002).

83. M. E. Greenberg, M. Sun, R. Zhang, M. Febbraio, R. Silverstein, S. L. Hazen, Oxidized phosphatidylserine-CD36 interactions play an essential role in macrophage-dependent phagocytosis of apoptotic cells. *J Exp Med* **203**, 2613-2625 (2006).

84. S. H. Yeon, G. Yang, H. E. Lee, J. Y. Lee, Oxidized phosphatidylcholine induces the activation of NLRP3 inflammasome in macrophages. *J Leukoc Biol* **101**, 205-215 (2017).

85. Z. M. Younossi, Non-alcoholic fatty liver disease - A global public health perspective. *J Hepatol* **70**, 531-544 (2019).

86. R. Loomba, A. J. Sanyal, The global NAFLD epidemic. *Nature Reviews Gastroenterology & Hepatology* **10**, 686-690 (2013).

87. K. K. Bence, M. J. Birnbaum, Metabolic drivers of non-alcoholic fatty liver disease. *Molecular Metabolism*, 101143 (2020).

88. Z. Chen, R. Tian, Z. She, J. Cai, H. Li, Role of oxidative stress in the pathogenesis of nonalcoholic fatty liver disease. *Free Radical Biology and Medicine* **152**, 116-141 (2020).

89. D. H. Ipsen, J. Lykkesfeldt, P. Tveden-Nyborg, Molecular mechanisms of hepatic lipid accumulation in non-alcoholic fatty liver disease. *Cellular and Molecular Life Sciences* **75**, 3313-3327 (2018).

90. N. L. Gluchowski, M. Becuwe, T. C. Walther, R. V. Farese, Lipid droplets and liver disease: from basic biology to clinical implications. *Nature Reviews Gastroenterology & Hepatology* **14**, 343-355 (2017).

91. M. H. Wehmeyer, B. C. Zyriax, B. Jagemann, E. Roth, E. Windler, J. Schulze Zur Wiesch, A. W. Lohse, J. Kluwe, Nonalcoholic fatty liver disease is associated with excessive calorie intake rather than a distinctive dietary pattern. *Medicine (Baltimore)* **95**, e3887 (2016).

92. B. A. Neuschwander-Tetri, Hepatic lipotoxicity and the pathogenesis of nonalcoholic steatohepatitis: The central role of nontriglyceride fatty acid metabolites. *Hepatology* **52**, 774-788 (2010).

93. R. S. Rector, J. P. Thyfault, G. M. Uptergrove, E. M. Morris, S. P. Naples, S. J. Borengasser, C. R. Mikus, M. J. Laye, M. H. Laughlin, F. W. Booth, J. A. Ibdah, Mitochondrial dysfunction precedes insulin resistance and hepatic steatosis and contributes to the natural history of non-alcoholic fatty liver disease in an obese rodent model. *J Hepatol* **52**, 727-736 (2010).

94. Y. Wei, R. S. Rector, J. P. Thyfault, J. A. Ibdah, Nonalcoholic fatty liver disease and mitochondrial dysfunction. *World Journal of Gastroenterology* **14**, 193 (2008).

95. F. Nassir, J. Ibdah, Role of Mitochondria in Nonalcoholic Fatty Liver Disease. *International Journal of Molecular Sciences* **15**, 8713-8742 (2014).

96. S. Schuster, D. Cabrera, M. Arrese, A. E. Feldstein, Triggering and resolution of inflammation in NASH. *Nature Reviews Gastroenterology & Hepatology* **15**, 349-364 (2018).

97. T. Kisseleva, D. Brenner, Molecular and cellular mechanisms of liver fibrosis and its regression. *Nature Reviews Gastroenterology & Hepatology*, (2020).

98. S. Caldwell, Y. Ikura, D. Dias, K. Isomoto, A. Yabu, C. Moskaluk, P. Pramoonjago, W. Simmons, H. Scruggs, N. Rosenbaum, T. Wilkinson, P. Toms, C. K. Argo, A. M. S. Al-Osaimi, J. A. Redick, Hepatocellular ballooning in NASH. *Journal of Hepatology* **53**, 719-723 (2010).

99. T. Tsuchida, S. L. Friedman, Mechanisms of hepatic stellate cell activation. *Nat Rev Gastroenterol Hepatol* **14**, 397-411 (2017).

100. K. Kazankov, S. M. D. Jørgensen, K. L. Thomsen, H. J. Møller, H. Vilstrup, J. George, D. Schuppan, H. Grønbæk, The role of macrophages in

nonalcoholic fatty liver disease and nonalcoholic steatohepatitis. *Nature Reviews Gastroenterology & Hepatology* **16**, 145-159 (2019).

101. Y. Takahashi, T. Fukusato, Histopathology of nonalcoholic fatty liver disease/nonalcoholic steatohepatitis. *World J Gastroenterol* **20**, 15539-15548 (2014).

102. V. A. Piazzolla, A. Mangia, Noninvasive Diagnosis of NAFLD and NASH. *Cells* **9**, 1005 (2020).

103. A. Kadl, P. R. Sharma, W. Chen, R. Agrawal, A. K. Meher, S. Rudraiah, N. Grubbs, R. Sharma, N. Leitinger, Oxidized phospholipid-induced inflammation is mediated by Toll-like receptor 2. *Free Radic Biol Med* **51**, 1903-1909 (2011).

104. K. G. Birukov, P. Karki, Injured lung endothelium: mechanisms of self-repair and agonist-assisted recovery (2017 Grover Conference Series). *Pulm Circ* **8**, 2045893217752660 (2018).

105. P. Karki, A. Meliton, A. Shah, Y. Tian, T. Ohmura, N. Sarich, A. A. Birukova, K. G. Birukov, Role of truncated oxidized phospholipids in acute endothelial barrier dysfunction caused by particulate matter. *PLoS One* **13**, e0206251 (2018).

106. E. Ambrogini, X. Que, S. Wang, F. Yamaguchi, R. S. Weinstein, S. Tsimikas, S. C. Manolagas, J. L. Witztum, R. L. Jilka, Oxidation-specific epitopes restrain bone formation. *Nature Communications* **9**, (2018).

107. Y. Imai, K. Kuba, G. G. Neely, R. Yaghubian-Malhami, T. Perkmann, G. Van Loo, M. Ermolaeva, R. Veldhuizen, Y. H. C. Leung, H. Wang, H. Liu, Y. Sun, M. Pasparakis, M. Kopf, C. Mech, S. Bavari, J. S. M. Peiris, A. S. Slutsky, S. Akira, M. Hultqvist, R. Holmdahl, J. Nicholls, C. Jiang, C. J. Binder, J. M. Penninger, Identification of Oxidative Stress and Toll-like

Receptor 4 Signaling as a Key Pathway of Acute Lung Injury. *Cell* **133**, 235-249 (2008).

108. X. Wang, Z. Zheng, J. M. Caviglia, K. E. Corey, T. M. Herfel, B. Cai, R. Masia, R. T. Chung, J. H. Lefkowitch, R. F. Schwabe, I. Tabas, Hepatocyte TAZ/WWTR1 Promotes Inflammation and Fibrosis in Nonalcoholic Steatohepatitis. *Cell Metab* **24**, 848-862 (2016).

109. Z. Ni, G. Angelidou, R. Hoffmann, M. Fedorova, LPPtiger software for lipidome-specific prediction and identification of oxidized phospholipids from LC-MS datasets. *Sci Rep* **7**, 15138 (2017).

110. Z. Ahmed, A. Ravandi, G. F. Maguire, A. Emili, D. Draganov, B. N. La Du, A. Kuksis, P. W. Connelly, Multiple substrates for paraoxonase-1 during oxidation of phosphatidylcholine by peroxynitrite. *Biochem Biophys Res Commun* **290**, 391-396 (2002).

111. K. Sabatini, J. P. Mattila, F. M. Megli, P. K. Kinnunen, Characterization of two oxidatively modified phospholipids in mixed monolayers with DPPC. *Biophys J* **90**, 4488-4499 (2006).

112. J.-P. Mattila, K. Sabatini, P. K. J. Kinnunen, Interaction of Cytochrome c with 1-Palmitoyl-2-azelaoyl-sn-glycero-3-phosphocholine: Evidence for Acyl Chain Reversal. *Langmuir* **24**, 4157-4160 (2008).

113. C. P. Thomas, L. T. Morgan, B. H. Maskrey, R. C. Murphy, H. Kühn, S. L. Hazen, A. H. Goodall, H. A. Hamali, P. W. Collins, V. B. O'Donnell, Phospholipid-esterified Eicosanoids Are Generated in Agonist-activated Human Platelets and Enhance Tissue Factor-dependent Thrombin Generation. *Journal of Biological Chemistry* **285**, 6891-6903 (2010).

114. K. Kayganich-Harrison, D. Rose, R. Murphy, J. Morrow, L. Roberts, Collision-induced dissociation of F2-isoprostane-containing phospholipids. *Journal of Lipid Research* **34**, 1229-1235 (1993).

115. V. Bochkov, B. Gesslbauer, C. Mauerhofer, M. Philippova, P. Erne, O. V. Oskolkova, Pleiotropic effects of oxidized phospholipids. *Free Radic Biol Med* **111**, 6-24 (2017).

116. M. V. Kuleshov, M. R. Jones, A. D. Rouillard, N. F. Fernandez, Q. Duan, Z. Wang, S. Koplev, S. L. Jenkins, K. M. Jagodnik, A. Lachmann, M. G. McDermott, C. D. Monteiro, G. W. Gundersen, A. Ma'ayan, Enrichr: a comprehensive gene set enrichment analysis web server 2016 update. *Nucleic Acids Res* **44**, W90-97 (2016).

117. E. Y. Chen, C. M. Tan, Y. Kou, Q. Duan, Z. Wang, G. Meirelles, N. R. Clark, A. Ma'Ayan, Enrichr: interactive and collaborative HTML5 gene list enrichment analysis tool. *BMC Bioinformatics* **14**, 128 (2013).

118. H. K. Min, A. Kapoor, M. Fuchs, F. Mirshahi, H. Zhou, J. Maher, J. Kellum, R. Warnick, M. J. Contos, A. J. Sanyal, Increased hepatic synthesis and dysregulation of cholesterol metabolism is associated with the severity of nonalcoholic fatty liver disease. *Cell Metab* **15**, 665-674 (2012).

119. W. Xue, J. Wang, W. Jiang, C. Shi, X. Wang, Y. Huang, C. Hu, Caveolin-1 alleviates lipid accumulation in NAFLD associated with promoting autophagy by inhibiting the Akt/mTOR pathway. *Eur J Pharmacol* **871**, 172910 (2020).

120. M. Li, D. Chen, H. Huang, J. Wang, X. Wan, C. Xu, C. Li, H. Ma, C. Yu, Y. Li, Caveolin1 protects against diet induced hepatic lipid accumulation in mice. *PLoS One* **12**, e0178748 (2017).

121. M. Han, W. Pioronska, S. Wang, Z. C. Nwosu, C. Sticht, S. Wang, Y. Gao, M. P. Ebert, S. Dooley, C. Meyer, Hepatocyte caveolin-1 modulates metabolic gene profiles and functions in non-alcoholic fatty liver disease. *Cell Death Dis* **11**, 104 (2020).

122. M. Tan, R. Mosaoa, G. T. Graham, A. Kasprzyk-Pawelec, S. Gadre, E. Parasido, O. Catalina-Rodriguez, P. Foley, G. Giaccone, A. Cheema, B. Kallakury, C. Albanese, C. Yi, M. L. Avantaggiati, Inhibition of the mitochondrial citrate carrier, Slc25a1, reverts steatosis, glucose intolerance, and inflammation in preclinical models of NAFLD/NASH. *Cell Death Differ* **27**, 2143-2157 (2020).

123. M. Pérez-Carreras, P. Del Hoyo, M. A. Martín, J. C. Rubio, A. Martín, G. Castellano, F. Colina, J. Arenas, J. A. Solis-Herruzo, Defective hepatic mitochondrial respiratory chain in patients with nonalcoholic steatohepatitis. *Hepatology* **38**, 999-1007 (2003).

124. P. Greenspan, E. P. Mayer, S. D. Fowler, Nile red: a selective fluorescent stain for intracellular lipid droplets. *The Journal of Cell Biology* **100**, 965-973 (1985).

125. B. H. Maskrey, A. Bermúdez-Fajardo, A. H. Morgan, E. Stewart-Jones, V. Dioszeghy, G. W. Taylor, P. R. S. Baker, B. Coles, M. J. Coffey, H. Kühn, V. B. O'Donnell, Activated Platelets and Monocytes Generate Four Hydroxyphosphatidylethanolamines via Lipoxygenase. *Journal of Biological Chemistry* **282**, 20151-20163 (2007).

126. P. Trivedi, S. Wang, S. L. Friedman, The Power of Plasticity-Metabolic Regulation of Hepatic Stellate Cells. *Cell Metab*, (2020).

127. T. Tsuchida, S. L. Friedman, Mechanisms of hepatic stellate cell activation. *Nature Reviews Gastroenterology & Hepatology* **14**, 397-411 (2017).

128. X. Liu, S. B. Rosenthal, N. Meshgin, J. Baglieri, S. G. Musallam, K. Diggle, K. Lam, R. Wu, S. Q. Pan, Y. Chen, K. Dorko, S. Presnell, C. Benner, M. Hosseini, H. Tsukamoto, D. Brenner, T. Kisseleva, Primary Alcohol-Activated Human and Mouse Hepatic Stellate Cells Share Similarities in

Gene-Expression Profiles. *Hepatology Communications* **4**, 606-626 (2020).

129. P. X. Shaw, S. Hörkkö, M.-K. Chang, L. K. Curtiss, W. Palinski, G. J. Silverman, J. L. Witztum, Natural antibodies with the T15 idiotype may act in atherosclerosis, apoptotic clearance, and protective immunity. *Journal of Clinical Investigation* **105**, 1731-1740 (2000).

130. G. N. Ioannou, The Role of Cholesterol in the Pathogenesis of NASH. *Trends Endocrinol Metab* **27**, 84-95 (2016).

131. P. Friedman, S. Horkko, D. Steinberg, J. L. Witztum, E. A. Dennis, Correlation of antiphospholipid antibody recognition with the structure of synthetic oxidized phospholipids. Importance of Schiff base formation and aldol condensation. *J Biol Chem* **277**, 7010-7020 (2002).

132. K. L. Gillotte, S. Hörkkö, J. L. Witztum, D. Steinberg, Oxidized phospholipids, linked to apolipoprotein B of oxidized LDL, are ligands for macrophage scavenger receptors. *Journal of Lipid Research* **41**, 824-833 (2000).

133. E. M. Bulger, R. V. Maier, Antioxidants in Critical Illness. *Archives of Surgery* **136**, 1201-1207 (2001).

134. J. M. Gutteridge, J. Mitchell, Redox imbalance in the critically ill. *British Medical Bulletin* **55**, 49-75 (1999).

135. M. J. Cummings, H. A. Mattill, The Auto-Oxidation of Fats with Reference to Their Destructive Effect on Vitamin E. *The Journal of Nutrition* **3**, 421-432 (1931).

136. J. Flieger, W. Flieger, J. Baj, R. Maciejewski, Antioxidants: Classification, Natural Sources, Activity/Capacity Measurements, and Usefulness for the Synthesis of Nanoparticles. *Materials (Basel)* **14**, (2021).

137. R. M. Bannerman, S. T. Callender, D. L. Williams, Effect of Desferrioxamine and D.T.P.A. in Iron Overload. *Br Med J* **2**, 1573-1577 (1962).

138. K. Takeda, Y. Shimada, M. Amano, T. Sakai, T. Okada, I. Yoshiya, Plasma lipid peroxides and alpha-tocopherol in critically ill patients. *Crit Care Med* **12**, 957-959 (1984).

139. J. Abilés, A. P. de la Cruz, J. Castaño, M. Rodríguez-Elvira, E. Aguayo, R. Moreno-Torres, J. Llopis, P. Aranda, S. Argüelles, A. Ayala, A. M. de la Quintana, E. M. Planells, Oxidative stress is increased in critically ill patients according to antioxidant vitamins intake, independent of severity: a cohort study. *Critical Care* **10**, R146 (2006).

140. Y. L. Jiang, H. Y. Liu, M. M. Tang, J. Y. Cheng, H. Zhao, L. Fu, Serum Level of 4-Hydroxynonenal in Community-Acquired Pneumonia: A Potential Biomarker for Severity and Prognosis. *Front Med (Lausanne)* **9**, 798343 (2022).

141. P. Risé, S. Eligini, S. Ghezzi, S. Colli, C. Galli, Fatty acid composition of plasma, blood cells and whole blood: Relevance for the assessment of the fatty acid status in humans. *Prostaglandins, Leukotrienes and Essential Fatty Acids* **76**, 363-369 (2007).

142. D. W. Ma, B. M. Arendt, L. M. Hillyer, S. K. Fung, I. McGilvray, M. Guindi, J. P. Allard, Plasma phospholipids and fatty acid composition differ between liver biopsy-proven nonalcoholic fatty liver disease and healthy subjects. *Nutr Diabetes* **6**, e220 (2016).

143. M. Waskom, seaborn: statistical data visualization. *Journal of Open Source Software* **6**, (2021).

144. U. Matt, O. Sharif, R. Martins, T. Furtner, L. Langeberg, R. Gawish, I. Elbau, A. Zivkovic, K. Lakovits, O. Oskolkova, B. Doninger, A. Vychytil, T.

Perkmann, G. Schabbauer, C. J. Binder, V. N. Bochkov, J. D. Scott, S. Knapp, WAVE1 mediates suppression of phagocytosis by phospholipid-derived DAMPs. *The Journal of Clinical Investigation* **123**, 4540-4540 (2013).

145. C. N. Serhan, Pro-resolving lipid mediators are leads for resolution physiology. *Nature* **510**, 92-101 (2014).

146. P. Pletka, R. B. Hickler, Blood prostaglandin A (PGA) levels in normal human subjects. *Prostaglandins* **7**, 107-115 (1974).

147. S. L. Friedman, Hepatic stellate cells: protean, multifunctional, and enigmatic cells of the liver. *Physiol Rev* **88**, 125-172 (2008).

148. C. A. Schneider, W. S. Rasband, K. W. Eliceiri, NIH Image to ImageJ: 25 years of image analysis. *Nature Methods* **9**, 671-675 (2012).

149. V. Bäcker, ImageJ macro tool sets of biological image analysis. *Proceedings of the ImageJ User and Developer Conference, Luxembourg* **24**, (2012).

150. A. Dobin, C. A. Davis, F. Schlesinger, J. Drenkow, C. Zaleski, S. Jha, P. Batut, M. Chaisson, T. R. Gingeras, STAR: ultrafast universal RNA-seq aligner. *Bioinformatics* **29**, 15-21 (2013).

151. M. D. Robinson, D. J. Mccarthy, G. K. Smyth, edgeR: a Bioconductor package for differential expression analysis of digital gene expression data. *Bioinformatics* **26**, 139-140 (2010).

Appendix

LPPTiger Nomenclature (previously identified species)	Parent Lipid	*m/z*	Formula	LPPTiger Predicted Structure(s)
1. PAPC	---	782	$C_{44}H_{80}NO_8P$	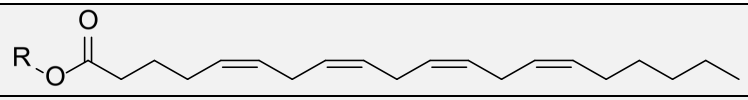
2. PLPC	---	758	$C_{42}H_{80}NO_8P$	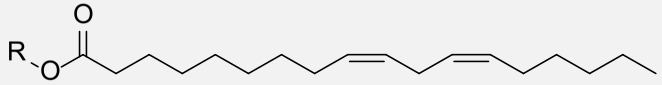
3. 16:0 LysoPC	---	496	$C_{24}H_{50}NO_7P$	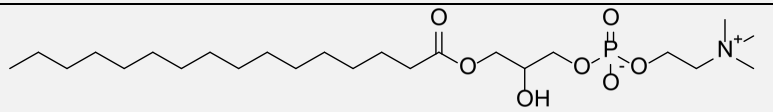
4. 18:1 LysoPC	---	522	$C_{26}H_{52}NO_7P$	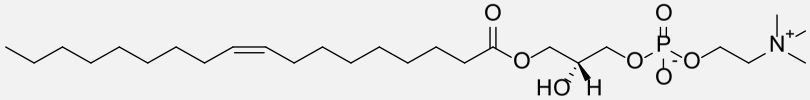
5. 18:2 LysoPC	---	520	$C_{26}H_{54}NO_7P$	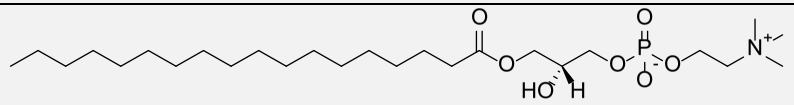
6. 18:0 LysoPC	---	524	$C_{26}H_{54}NO_7P$	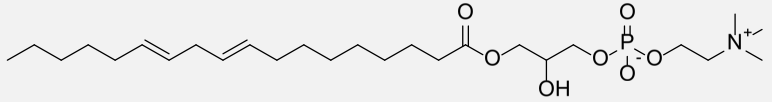
7. 16:0/12:1[CHO]	PLPC	690	$C_{36}H_{68}NO_9P$	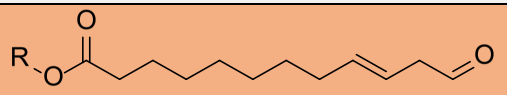
8. POBPC	PAPC	580	$C_{28}H_{54}NO_9P$	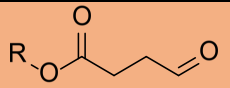
9. C35H62NO11P	PAPC	704	$C_{35}H_{62}NO_{11}P$	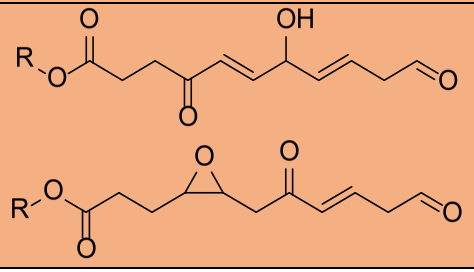

				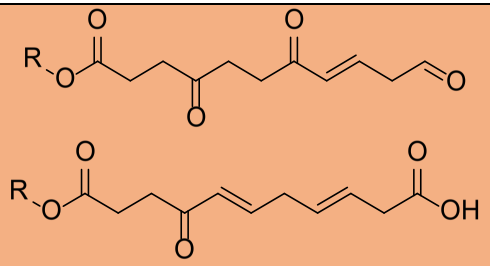
10. 16:0/7:0[1xOH,CHO]	PAPC	638	$C_{31}H_{60}NO_{10}P$	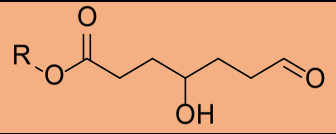
11. PONPC	PLPC	650	$C_{33}H_{64}NO_9P$	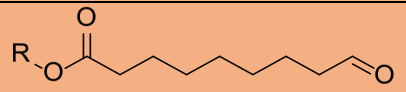
12. C35H64NO10P	PAPC	690	$C_{35}H_{64}NO_{10}P$	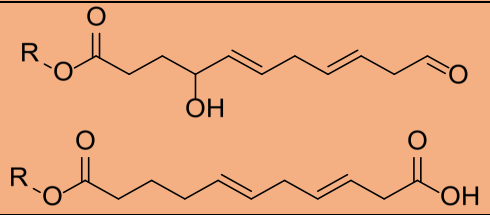
13. 16:0/11:1[CHO]	PLPC	676	$C_{35}H_{66}NO_9P$	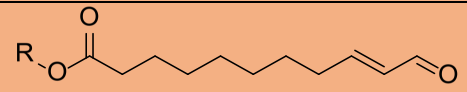
14. 16:0/8:0[CHO] (POOPC)	PLPC	636	$C_{32}H_{62}NO_9P$	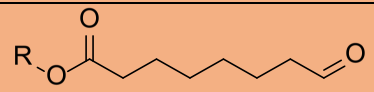
15. C35H64NO12P	PAPC	722	$C_{35}H_{64}NO_{12}P$	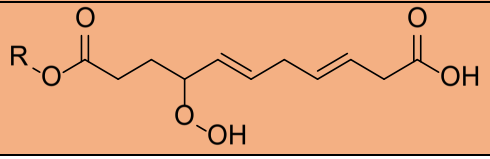

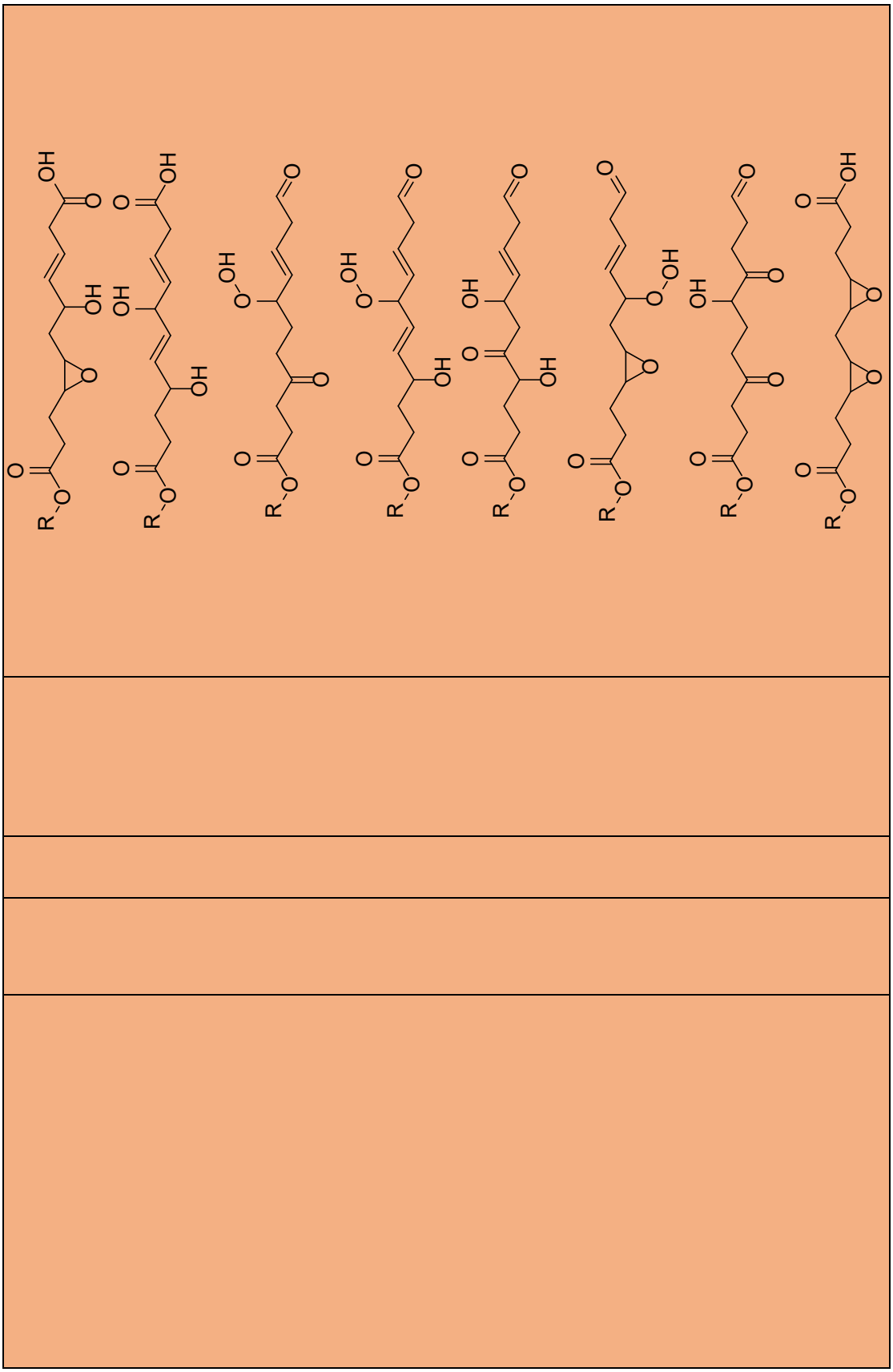

				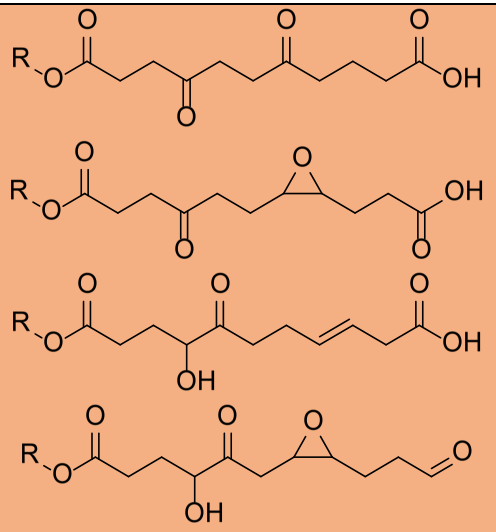
16. C32H60NO10P	PAPC	650	$C_{32}H_{60}NO_{10}P$	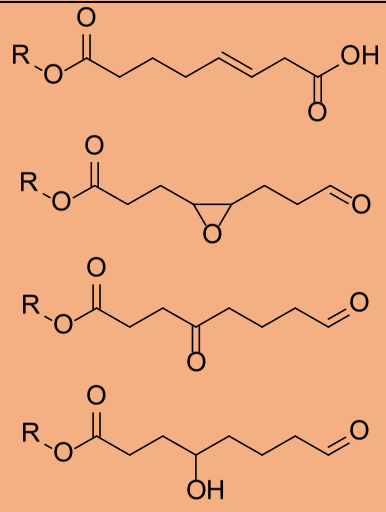

17. 16:0/10:2[CHO]	PAPC	660	$C_{34}H_{62}NO_9P$	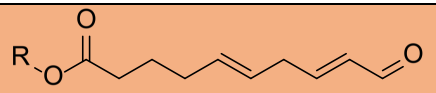
18. POVPC	PAPC	594	$C_{29}H56NO_9P$	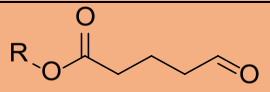
19. C34H62NO11P	PAPC	692	$C_{34}H_{62}NO_{11}P$	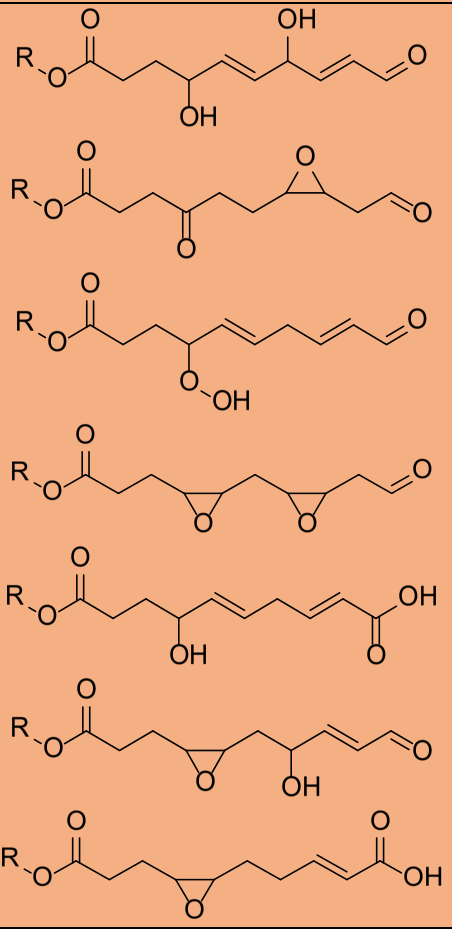

				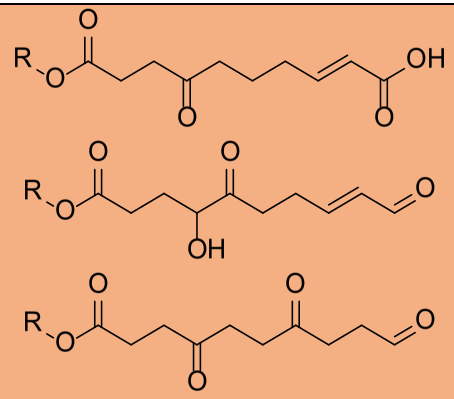
20. 16:0/7:1[CHO]	PAPC	620	$C_{31}H_{58}NO_9P$	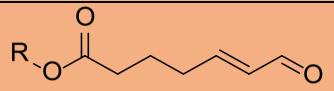
21. PazPC	PLPC	666	$C_{33}H_{64}NO_{10}P$	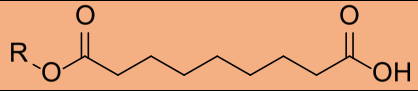
22. C42H80NO11P (HPODE-PC)	PLPC	806	$C_{42}H_{80}NO_{11}P$	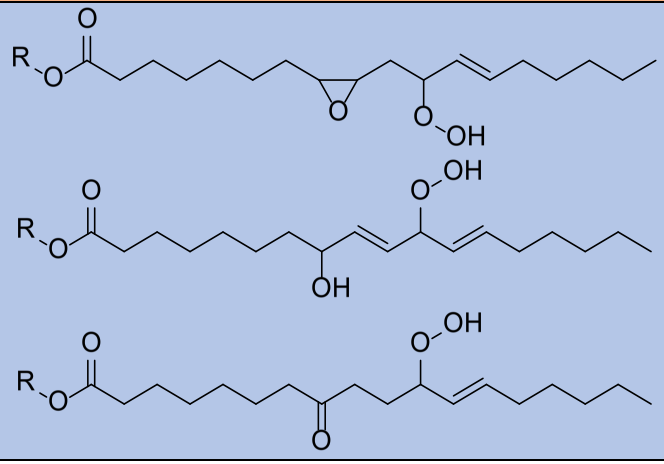

23. 16:0/18:2[2xOOH]	PLPC	822	$C_{42}H_{80}NO_{12}P$	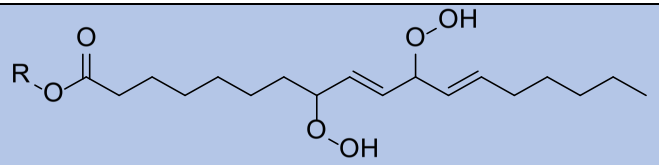
24. C42H78NO10P	PLPC	788	$C_{42}H_{78}NO_{10}P$	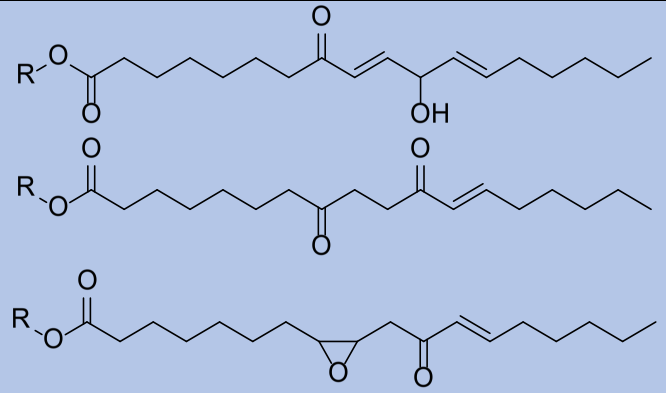
25. C44H80NO9P (HETE-PC)	PAPC	798	$C_{44}H_{80}NO_9P$	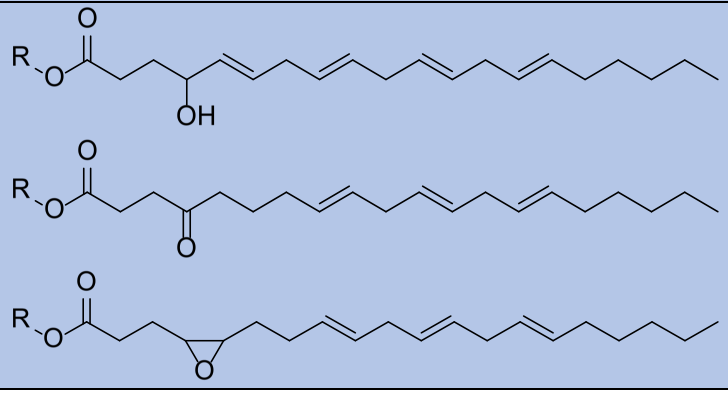

26. C44H80NO11P (Isoprostane-PC, Isoketal-PC)	PAPC	830	$C_{44}H_{80}NO_{11}P$	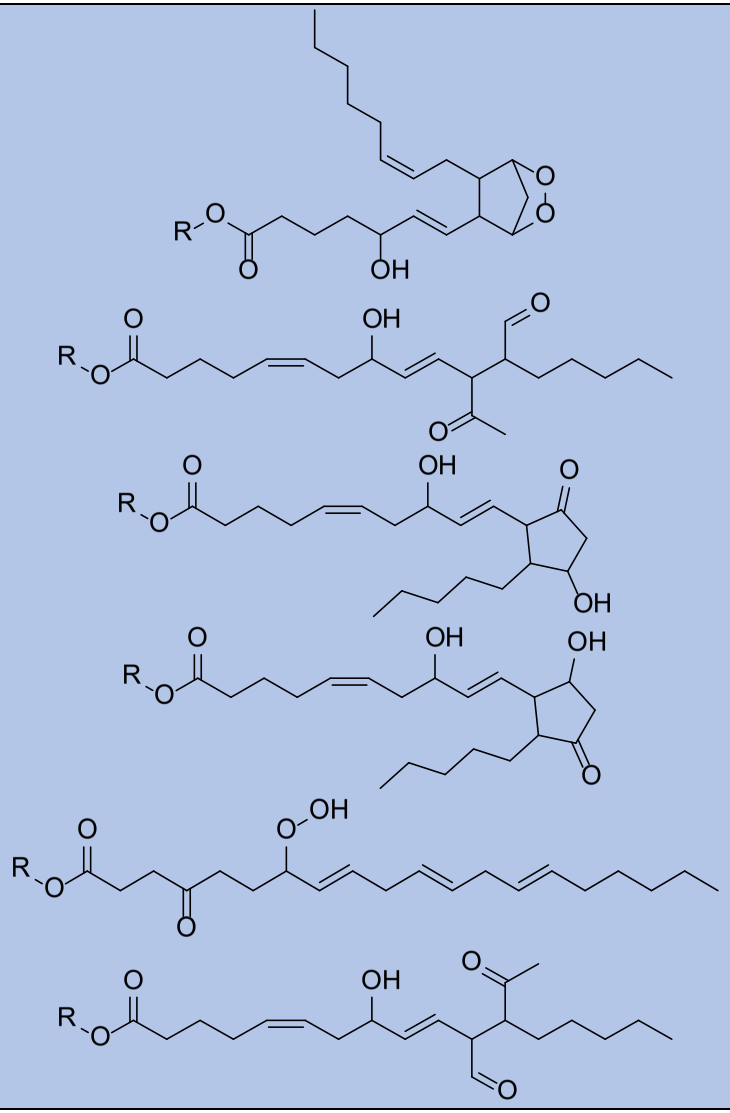

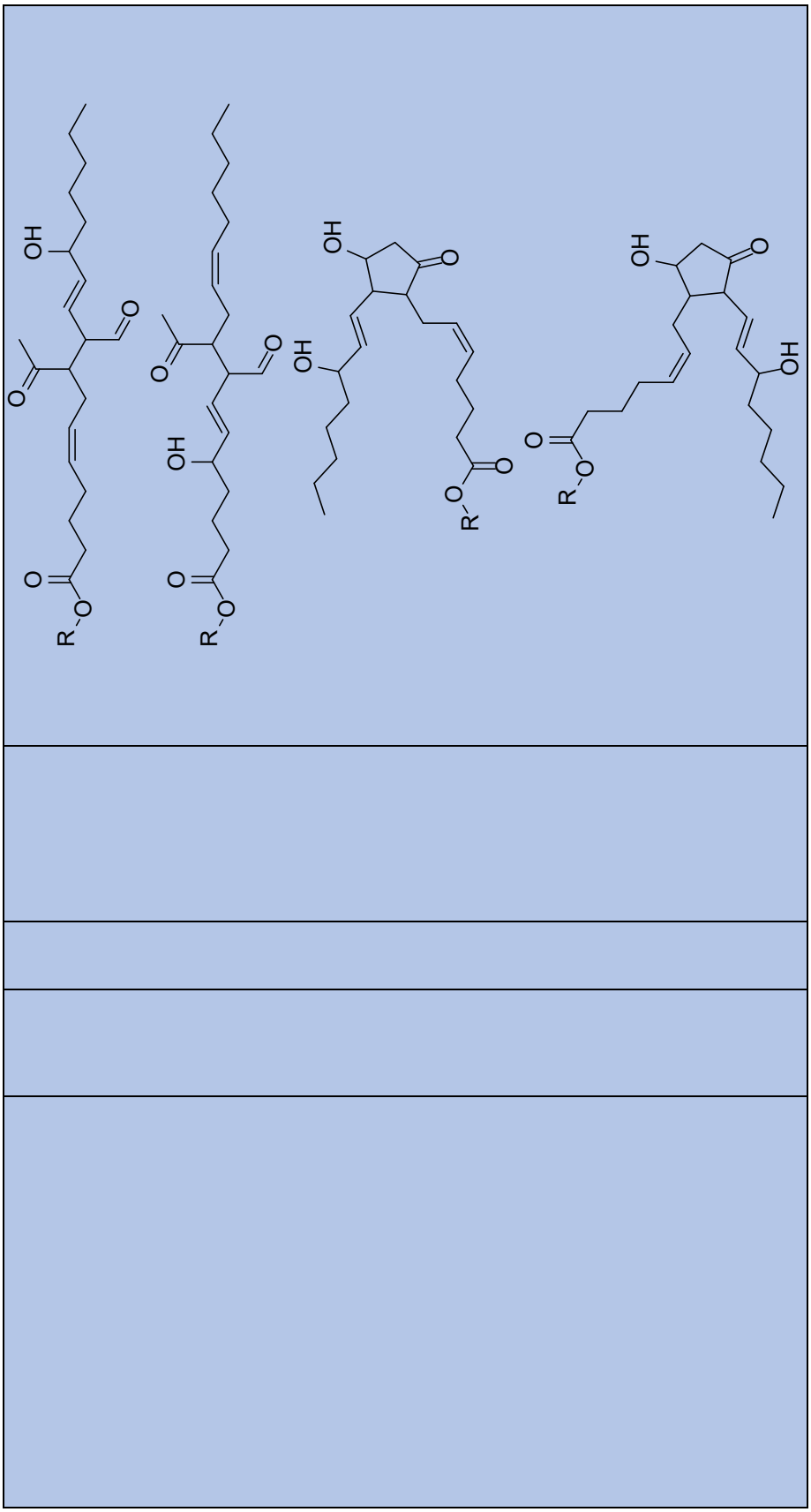
OH
O
O
O
R
O
OH
O
O
O
R
O
OH
O
O
O
R
O
OH
O
OH

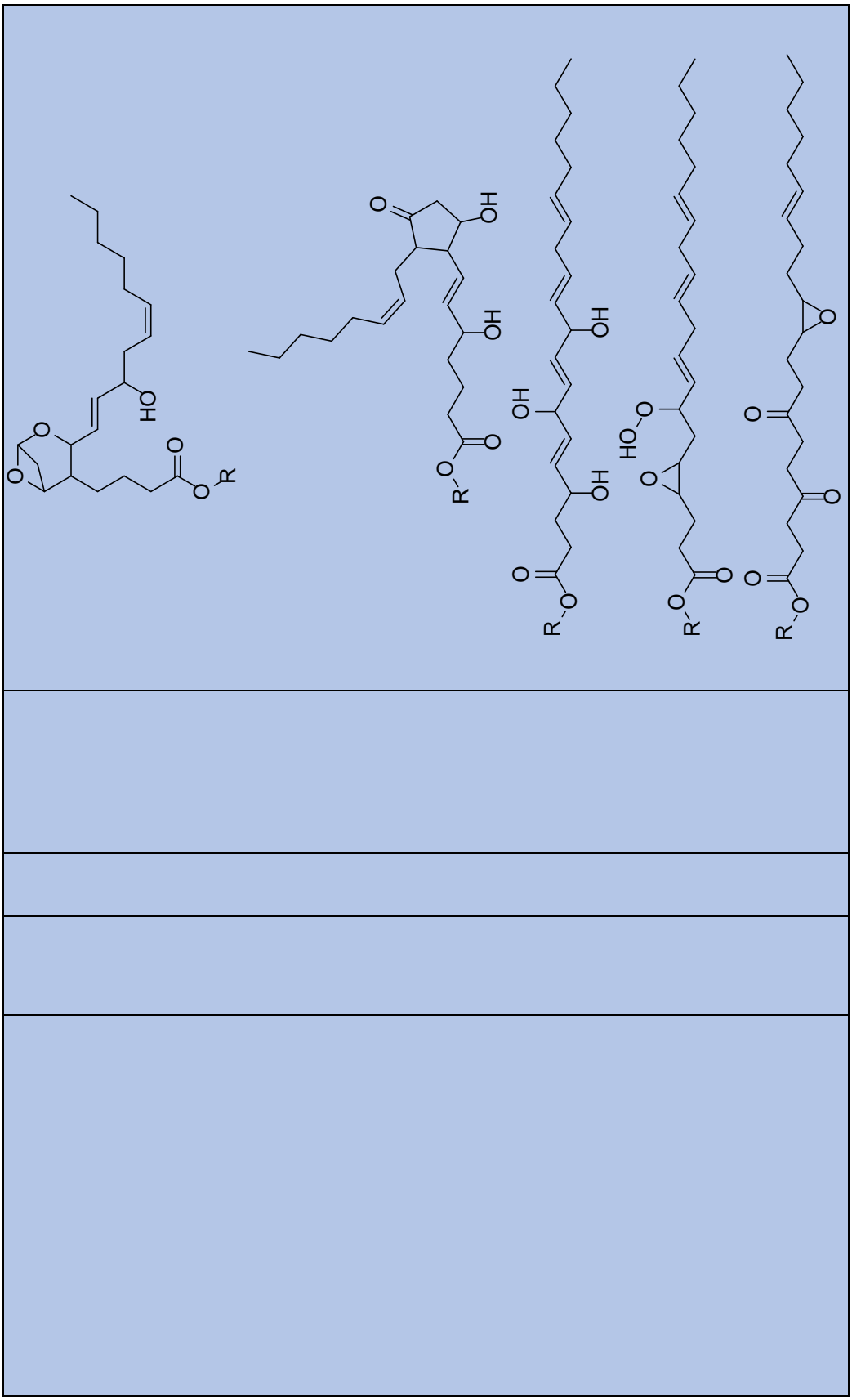
HO
O
O
O
R
O
OH
OH
O
R
OH
OH
O
R
HO
O
O
R
O
O
O
R

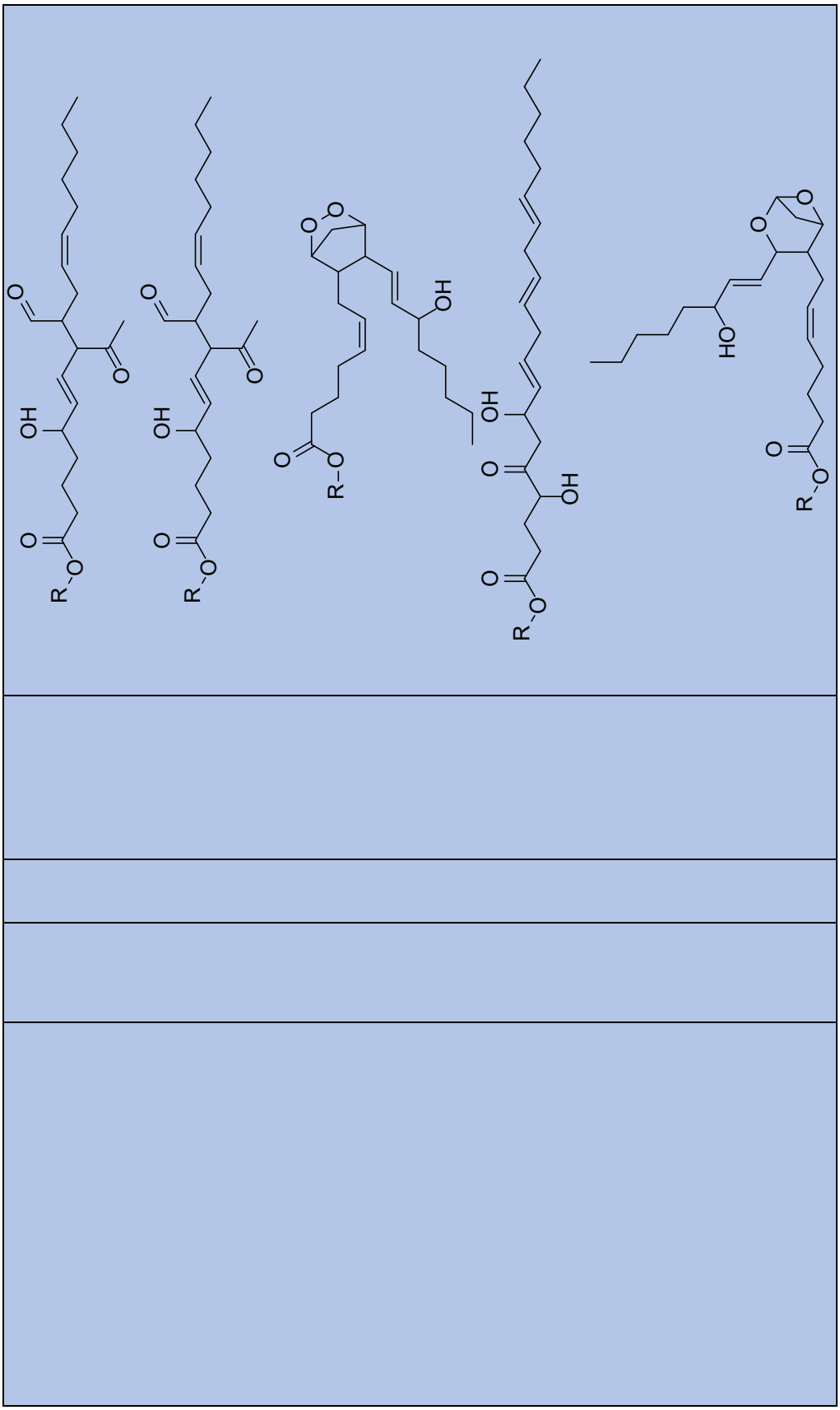
O
OH
O
O
R
O
O
O
OH
O
O
R
O
O
O
O
OH
O
R
O
OH
O
O
R
O
HO
O
O
O
R
O

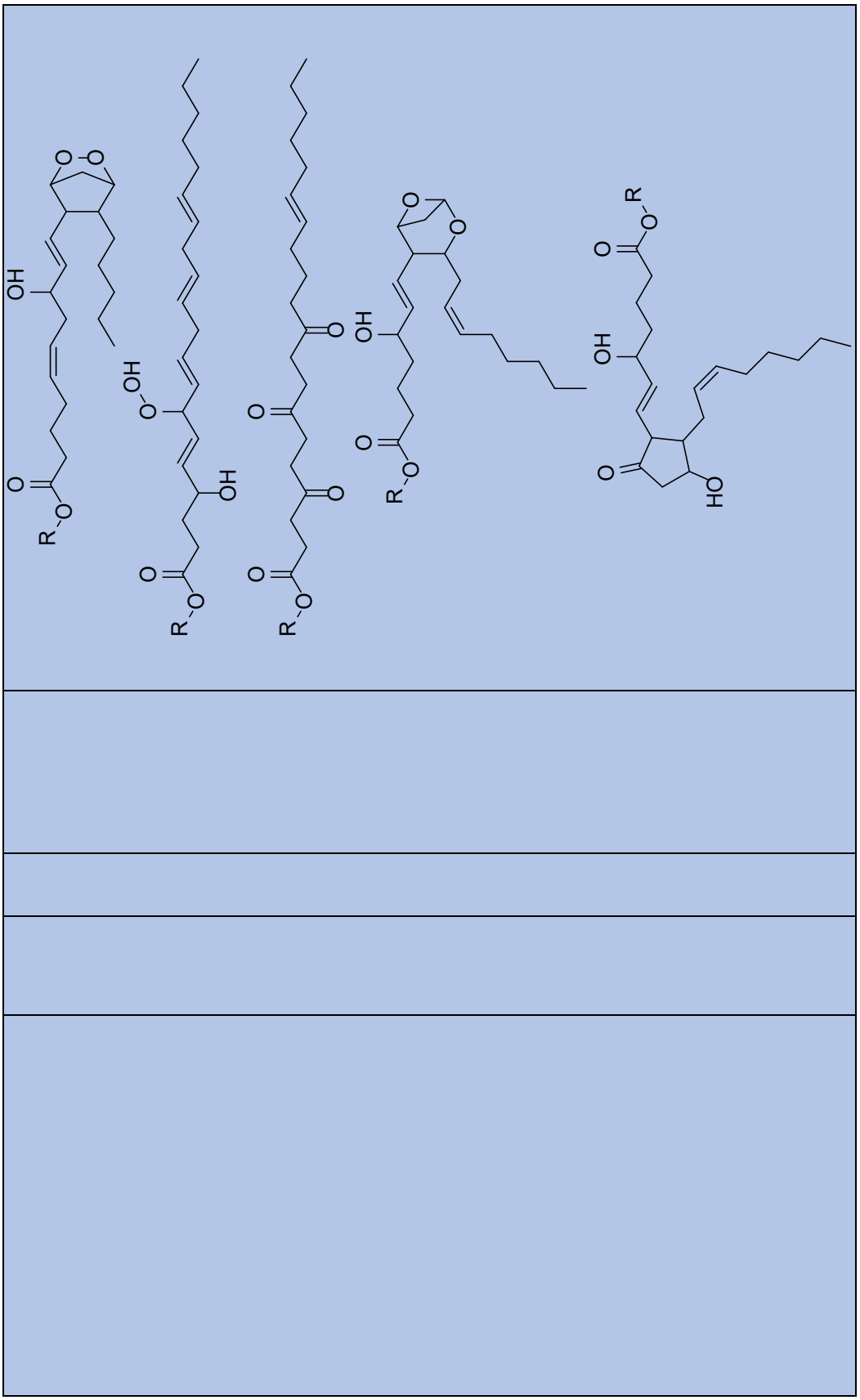
OH
O
O
R
O
O
OH
O
OH
O
R
O
O
O
O
R
O
OH
O
O
R
O
O
OH
O
R
HO

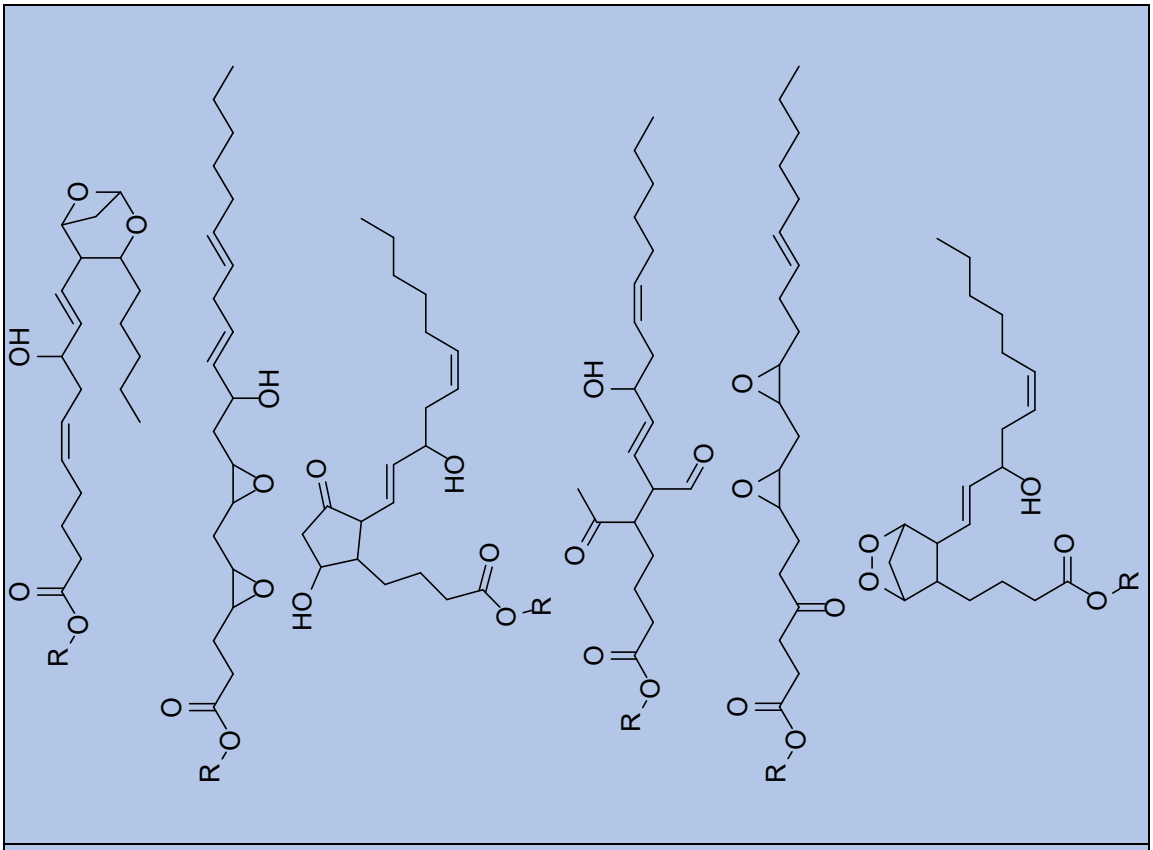
OH
O
O
O
R
O
OH
O
O
O
R
O
HO
HO
O
O
R
O
OH
O
O
R
O
O
O
O
O
R
O
HO
O
O
O
R

				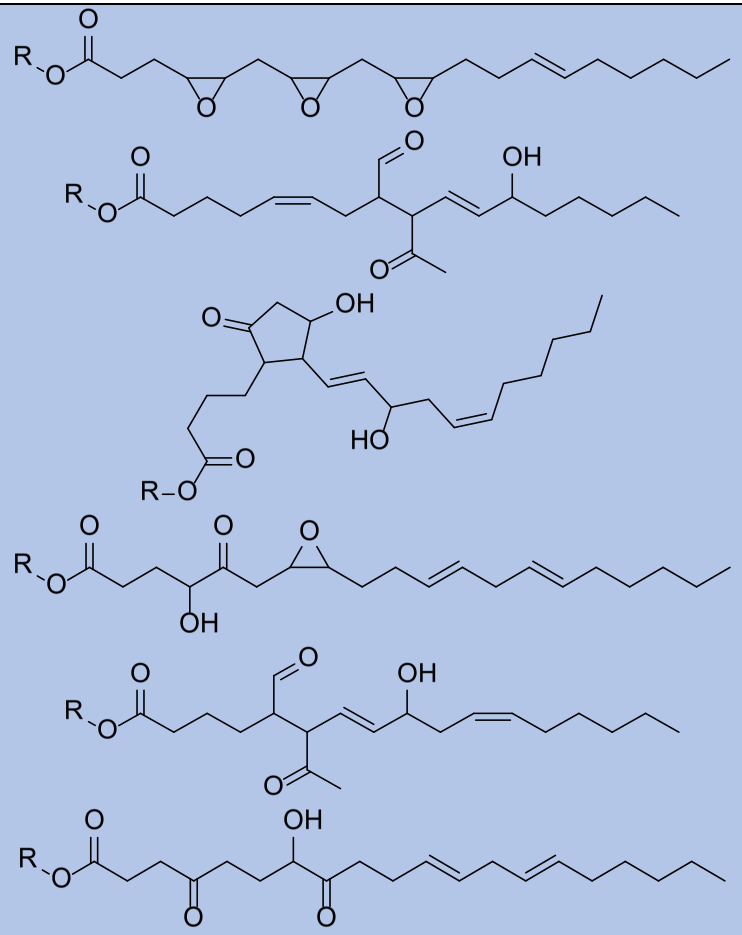
27. C42H80NO9P (HODE-PC)	PLPC	774	$C_{42}H_{80}NO_9P$	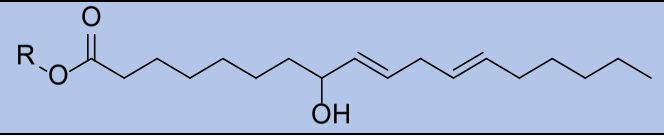

				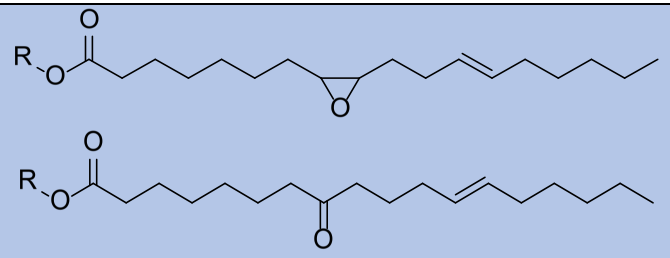
28. 16:0/18:2[2xDB,1xKETO] (KODE-PC)	PLPC	772	$C_{42}H_{78}NO_9P$	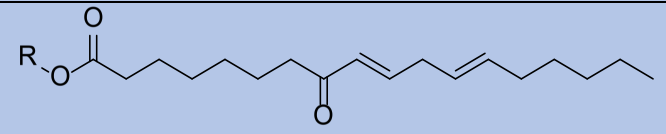
29. 16:0/18:1[1xDB,1xOH] (HOME-PC)	PLPC	776	$C_{42}H_{82}NO_9P$	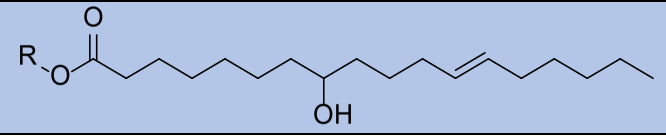

Supplemental Table 2. Gene expression of AML12 hepatocytes treated with truncated OxPAPC, full-length OxPAPC, and OxPAPC. Gene expression represented as log_2 of the fold change compared to vehicle. Genes regulated single treatment are highlighted in orange (truncated OxPAPC), blue (full-length OxPAPC), and purple (OxPAPC).

Gene Symbol	Truncated	Full length	OxPAPC
1110002E22Rik	---	---	-1.06
1700011H14Rik	---	---	-0.83
1700066M21Rik	---	---	-0.74
1810011O10Rik	-1.11	---	---
2010111I01Rik	0.86	---	---
2310007B03Rik	---	---	-1.15
2310022B05Rik	---	---	-0.68
2410131K14Rik	0.77	---	0.86
2810417H13Rik	-0.77	---	-1.13
3010026O09Rik	---	---	-1.62
3110002H16Rik	---	---	0.72
3110043O21Rik	0.78	---	1.14
4921536K21Rik	---	---	1.63
4930427A07Rik	---	---	-0.82
4930430F08Rik	0.79	---	---
5031439G07Rik	---	---	0.75
5730508B09Rik	---	---	-0.97
9230110C19Rik	1.26	---	---
9330159F19Rik	---	---	0.97
9930012K11Rik	---	---	-0.95
AA415398	---	---	0.82
Aasdhppt	---	---	-0.75
Abca8b	2.5	1.43	2.74
Abcb6	2.03	1.35	1.77
Abcc1	1.9	1.58	2.02
Abcc2	3.72	2.81	4.08
Abcc4	1.53	1.37	1.71
Abcc5	1.03	---	1.04
Abcd4	---	---	0.87
Abhd4	1.36	1.03	1.64
Abhd5	---	---	0.92
Ablim1	-0.8	---	-0.77
Abr	1.05	---	1.2
Abtb1	1.24	---	1.02
Acan	-0.91	---	---
Acot2	1.01	---	1.38
Acox2	1.12	---	1.72
Acrbp	---	---	0.92
Actb	---	---	-0.67
Actg1	-0.72	---	-0.95
Actn1	-0.78	---	-0.72
Adamts1	-1.17	-1.36	---
Adamts6	-1.5	-1.58	-1.5
Adamts9	-1.73	-1.22	-1.73
Adap2	---	---	-1.26
Adgra2	-1.03	---	-0.81
Adgrg1	---	---	1.14
Adh7	2.75	1.86	1.86
Adprm	1.08	---	1.31
Adra1a	2.56	1.79	2.5
Adrm1	0.81	---	1.13
Afap1	---	---	0.85
Ahnak2	1.14	0.81	1.16
Ahr	-1.54	-0.92	-1.52
Ahsa1	0.79	---	0.84
Ahsa2	1.42	0.77	1.39
AI846148	---	---	0.88
Ajuba	---	---	-0.96
Akap1	---	---	-0.96
Akap12	-0.86	---	-0.99
Akap8l	0.79	---	1.05
Akr1c13	0.8	---	---
Akr1c14	2.3	1.37	1.73
Akr1c19	3.31	2.39	3.16
Akt1s1	---	---	0.78
Alas1	0.91	0.81	0.96
Aldh18a1	---	---	0.67
Aldh1a1	2.27	1.5	1.7
Aldh1l2	---	---	1.06
Aldh2	---	---	0.71
Aldh3a2	0.83	---	0.92
Aldoa	---	---	0.85
Alg6	---	---	-0.96
Als2	0.75	---	0.79

Amacr	---	---	-0.88
Ammecr1	---	---	-0.75
Amotl2	-0.86	---	-1.58
Ampd3	3.35	3.12	3.67
Anapc16	---	---	0.79
Angptl4	-0.97	---	-1.4
Angptl6	---	---	1.34
Ankle1	---	---	-1.24
Ankrd1	-2.23	-0.98	-2.75
Ankrd11	---	---	0.91
Ankrd12	---	---	1.05
Ankrd40	---	---	-0.63
Ankrd49	---	---	-0.8
Anln	-0.73	---	-0.91
Antxr2	-0.79	---	---
Anxa7	---	---	0.75
Aox1	2.67	2.07	2.79
Ap1ar	---	---	-0.76
Ap1s3	---	---	-0.84
Apba3	---	---	0.78
Apobr	2.59	1.14	3.37
Aqp9	1.84	---	2.08
Areg	---	---	1.37
Arhgap18	---	---	-0.82
Arhgap19	---	---	-1.35
Arhgap27	---	---	0.72
Arhgap8	-1.23	---	-1.22
Arhgef39	---	---	-1.01
Arid4b	---	---	0.7
Arid5a	---	---	1.36
Arih2	---	---	0.8
Arl4a	---	---	0.79
Arl4c	-1.13	-0.85	-1.65
Arl4d	1.19	---	---
Arl5b	---	---	0.93
Arl8a	---	---	0.95
Armcx3	---	---	0.96
Arrdc2	1.08	---	0.91
Arrdc3	0.66	---	---
Asns	0.69	---	0.78
Aspm	---	---	-1.38
Atad5	---	---	-1.02
Atf3	1.39	---	4.41
Atf4	---	---	1.11
Atf5	1.01	---	1.15

Atg12	---	---	0.65
Atg14	0.97	---	1.17
Atp10a	-1.01	---	---
Atp5sl	0.85	---	0.87
Atp6v0a1	---	---	1.09
Atp7a	---	---	0.79
Atxn1	---	---	-0.81
Atxn7l2	---	---	0.77
Aurkb	-0.73	---	-1.09
Avl9	---	---	0.82
B2m	---	---	0.73
B4galt7	---	---	0.75
B4gat1	---	---	-0.78
Bach1	1.63	1.01	1.98
Bag3	1.62	1.42	2.57
Bahcc1	-0.99	---	-1.36
Bahd1	---	---	0.65
Bbc3	---	---	0.86
Bbs12	---	---	-0.98
BC005537	0.71	---	0.92
BC025446	-0.88	---	-0.77
BC055324	---	---	-0.65
Bcar1	-1.31	---	-1.47
Bcl3	-0.86	---	---
Blcap	---	---	1.03
Blvrb	3.83	3.03	3.95
Bmf	---	---	-0.94
Bnip3	0.97	---	0.91
Bok	---	---	-1.16
Bora	-0.97	---	-1.31
Borcs5	---	---	-0.81
Brd2	---	---	0.89
Bsdc1	0.79	---	1.13
Btc	---	---	1.01
Bub1b	---	---	-0.88
C2cd4c	1.04	---	---
C2cd5	---	---	-0.8
Cachd1	2.24	1.67	2.61
Cacna1h	---	-1.03	-0.95
Cacnb2	-1.06	---	---
Cacybp	---	---	0.85
Cad	---	---	-0.83
Calcoco1	1.15	---	1.11
Calr3	2.88	2.24	2.91
Camkk1	---	---	-1.43

Camkk2	-0.89	---	-1.16
Camkmt	---	---	0.9
Capn5	-0.92	---	-0.74
Car15	---	---	1.41
Card10	-0.75	---	-1.45
Casc4	-0.97	---	---
Casp8ap2	---	---	-0.89
Cat	1.64	1.36	1.62
Cav1	-0.79	---	-0.76
Cav2	-0.88	---	-1.12
Cbr1	1.6	0.89	1.32
Cbx4	---	---	-0.81
Cbx6	---	---	-1
Cc2d2a	---	---	-0.86
Ccbe1	-1.42	---	-1.21
Ccdc117	0.83	---	0.75
Ccdc186	---	---	0.8
Ccdc28a	---	---	0.75
Ccdc71l	---	---	0.74
Ccdc88a	1.06	0.99	1.43
Ccdc92	---	---	0.79
Ccl2	-1.21	-1.12	-1.78
Ccna2	---	---	-0.99
Ccnb1	---	---	-1.05
Ccnb2	---	---	-0.84
Ccnd1	-0.96	---	-1.21
Ccnd3	-0.73	---	-0.93
Ccne1	-1.99	---	-2.41
Ccne2	-1.25	---	-1.64
Ccnf	---	---	-0.85
Ccng2	0.96	---	1.31
Ccsap	---	---	-1.36
Cd3eap	---	---	-1.11
Cd44	-0.88	---	---
Cd59a	0.94	---	1.06
Cd9	---	---	0.7
Cdc20	---	---	-0.87
Cdc25b	---	---	-0.74
Cdc25c	---	---	-0.91
Cdc42ep2	1.79	1.56	1.69
Cdc42ep5	---	---	0.93
Cdc6	-1.13	---	-1.35
Cdc7	-0.74	---	-0.99
Cdca2	---	---	-0.65
Cdca7	-1.22	---	-1.77
Cdca7l	---	---	-1.16
Cdk2	-0.75	---	-0.72
Cdk6	-0.84	---	-0.86
Cdkn1a	---	---	0.74
Cdkn2aipnl	---	---	-0.88
Cdkn2b	1.75	1.24	2.02
Cdkn2c	---	---	-0.79
Cdkn2d	---	---	-1.62
Cdr2l	---	---	0.95
Cds2	0.97	---	0.87
Cdt1	-0.87	---	-0.67
Cebpa	1.59	---	1.67
Cebpb	---	---	1.27
Cenpa	---	---	-1.1
Cenpf	---	---	-0.74
Cenpl	---	---	-0.78
Cep55	---	---	-0.85
Cep78	---	---	-0.71
Cep85l	---	---	1.61
Cep89	---	---	-0.69
Cfap43	-0.72	---	---
Cgn	---	---	-1.52
Cgnl1	1.48	1.15	1.53
Chac1	---	---	2.38
Chaf1b	-0.74	---	---
Chchd10	---	---	1.33
Chd2	---	---	1.12
Chka	-0.99	-0.76	-0.7
Chmp1b	---	---	0.73
Chn2	-0.86	---	---
Chordc1	0.97	0.82	1.06
Chpf2	2.13	1.39	2.03
Chrnb2	1.29	---	1.39
Chst15	---	---	-0.7
Cish	---	---	1.01
Ckap2	-0.77	---	-0.87
Clcf1	---	---	0.84
Clcn2	---	---	0.88
Clcn6	---	---	0.9
Cldn2	-0.8	---	-0.89
Clic4	---	---	0.93
Clip2	---	---	0.81
Clk1	---	---	0.82
Clk3	---	---	0.67
Clk4	---	---	0.8

Clmn	---	---	-0.79
Clspn	---	---	-0.73
Cnn2	-0.95	---	-1.18
Cnnm2	0.86	---	---
Cnot6	---	---	-0.68
Cnppd1	0.98	---	1.14
Cobl	---	---	0.93
Coil	---	---	-0.9
Col11a2	1.41	---	1.46
Col4a5	---	---	-0.8
Coro2a	---	---	1.01
Cotl1	---	---	-0.72
Cpeb2	---	---	1.13
Cpt1a	0.92	---	0.83
Cpt1b	---	---	0.87
Crb2	---	---	-1.19
Crebrf	---	---	0.9
Creg1	2.32	2	2.58
Creld1	0.9	---	---
Crem	0.84	---	1.41
Crim1	-0.72	---	-0.82
Crlf1	---	0.97	1.24
Crocc	---	---	-0.88
Crocc2	---	---	-1.12
Crtc1	1.05	0.94	1.34
Cryab	---	---	1.15
Csf1	---	---	0.73
Csnk1e	---	---	0.76
Csrnp2	0.72	---	0.8
Cstb	---	---	0.72
Ctdsp2	---	---	-0.67
Ctdspl	---	---	-0.9
Ctgf	-3.76	-2.09	-4.45
Cth	1.17	---	1.35
Ctns	---	---	0.97
Ctps	---	---	-1.04
Ctsb	---	---	0.65
Ctsd	0.92	---	1.07
Cxcl1	-1.26	---	---
Cxcl5	-1.53	-1.17	-2.39
Cyb5a	1.76	1.63	1.97
Cyb5r1	---	---	0.97
Cyld	---	---	-1.08
Cyp1a1	2.61	1.97	---
Cyp2j6	0.85	---	1
Cyp3a13	---	---	0.94
Cyp51	2.25	---	2.51
Cyr61	-1.36	---	-1.75
Cys1	---	---	1.17
D630003M21Rik	---	---	-1.42
D930048N14Rik	---	---	-1.1
Dact2	1.33	---	0.88
Dbt	---	---	-0.87
Dck	---	---	-0.84
Dcun1d3	---	---	1.01
Ddit3	1.6	---	2.82
Ddit4	0.98	---	2.1
Ddx11	---	---	-1.01
Ddx20	---	---	-0.88
Ddx41	---	---	-0.81
Ddx51	---	---	-0.72
Dedd2	2.46	1.48	2.77
Dennd4a	---	---	1.07
Depdc1a	---	---	-1.04
Depdc7	1.05	---	1.49
Deptor	1.06	---	0.91
Dgat2	---	---	1.09
Dhcr24	0.67	---	---
Dhodh	---	---	-0.86
Dhrs13	---	---	-1.09
Dhrs3	-1.34	-1.18	-1.91
Dhrs9	-1.26	---	---
Dimt1	-0.78	---	-1.08
Dip2b	---	---	0.81
Dkc1	-0.74	---	-0.8
Dlg5	---	---	0.99
Dlgap4	---	---	0.98
Dlk2	-1.04	---	-1.98
Dna2	-1.13	---	-1.22
Dnaja1	1.2	0.88	1.63
Dnaja4	1.51	0.99	2.74
Dnajb1	1.38	0.99	2.96
Dnajb2	1.47	0.84	1.41
Dnajb4	1.96	1.6	2.23
Dnajb9	---	---	1.48
Dnajc27	-1.16	---	-1.15
Dnase2a	1.46	1.19	1.4
Dnhd1	---	---	1.14
Dnph1	---	---	-1
Dock5	---	---	0.84

Dpp7	---	---	0.9
Dpy19l1	---	---	-0.97
Dsel	---	---	-0.79
Dtl	-1.29	---	-1.29
Dtx2	---	---	0.78
Dusp1	2.31	2.06	4.15
Dusp10	-0.79	---	-0.66
Dusp14	-1.07	---	-1.03
Dusp18	1.46	1.08	1.44
Dusp4	1.36	0.8	1.86
Dusp5	-1.21	---	---
Dusp6	---	---	0.98
Dusp7	-1.22	---	-0.84
Dut	---	---	-0.86
Dync1h1	---	---	0.77
Dync1li1	---	---	0.67
Dyrk1b	1.12	---	1.44
Dzip1l	---	---	-0.76
E2f6	0.96	0.89	1.08
E2f7	-0.88	---	-0.95
E2f8	-1.51	---	-1.61
E330009J07Rik	1.11	---	1.19
Eaf1	---	---	0.89
Ecm1	---	---	0.74
Ect2	-0.76	---	-1.03
Edn1	---	---	-1.95
Eea1	---	---	0.83
Eef2kmt	---	---	-0.71
Eepd1	-0.83	---	-1.18
Efcab8	---	---	0.95
Efnb1	1	---	1.22
Efnb2	-1.42	-0.68	-1.13
Egfr	-0.96	---	---
Egr1	-3.62	-2.38	---
Eid3	1.97	1.82	2.33
Eif2s2	---	---	0.83
Eif4ebp1	0.83	---	1.16
Elf1	---	---	1.01
Elmo1	---	---	0.97
Eml4	-0.86	---	-0.83
Emp1	-0.89	---	-0.8
Enc1	-1.22	---	-1.05
Endod1	---	---	-0.66
Engase	---	---	-1.29
Enpp1	-0.88	-0.84	-0.86
Enpp4	---	---	-0.83
Entpd5	1.52	1.07	1.46
Epb41	---	---	0.86
Epha7	---	---	-1.04
Ephx1	1.63	1.29	1.82
Eprs	---	---	0.73
Ercc6l	---	---	-0.8
Ereg	---	---	0.81
Eri1	---	---	-0.7
Eri2	---	---	-0.79
Ern1	---	---	1
Ero1l	---	---	0.77
Ero1lb	1.15	0.86	1.12
Errfi1	-1.2	-0.89	---
Esd	1.61	1.4	1.54
Espl1	---	---	-1.03
Esyt1	---	---	0.72
Etaa1	---	---	-0.97
Ets1	-0.84	---	-0.83
Exo1	-0.74	---	-1.01
Ext1	-0.78	---	-0.79
Eya2	---	---	1.14
Ezr	---	---	0.71
F2rl1	-1.35	---	-1.29
F3	-2.17	-0.89	-2.19
Faap100	-0.84	---	-0.98
Faap24	---	---	-0.84
Fadd	---	---	-0.83
Fads1	---	---	0.89
Fads2	0.99	---	1.23
Fam102a	---	---	1.09
Fam102b	-1.32	-0.87	-1.06
Fam118a	---	---	-0.78
Fam126a	---	---	0.74
Fam13a	2.35	1.44	2.43
Fam21	0.91	---	1.07
Fam214b	1.04	---	1.17
Fam219a	1.98	1.44	2.02
Fam63a	---	---	0.72
Fam64a	---	---	-1.08
Fam65b	-1.92	-1.29	-2.88
Fam73b	---	---	-0.76
Fam83d	---	---	-1.1
Fam83g	---	---	1.29
Fam83h	---	---	0.87

Fam84b	---	-0.83	---
Fanca	---	---	-0.8
Fancb	---	---	-0.92
Fancd2	---	---	-0.68
Fbxl20	0.77	---	0.76
Fbxo11	---	---	0.72
Fbxo30	1.01	---	1.11
Fbxo31	0.98	---	1.03
Fbxo32	1.06	---	0.89
Fbxo48	---	---	-1.23
Fbxo5	-1.08	---	-1.55
Fbxo9	1.06	0.82	0.82
Fchsd1	0.97	---	---
Fchsd2	-1.08	---	-1.09
Fdft1	1.32	---	1.44
Fech	---	0.79	0.8
Fen1	---	---	-0.93
Fermt1	-1	-0.75	-1.14
Fermt2	-0.73	---	-0.87
Fermt3	---	---	1.73
Fgd3	1.18	0.93	---
Fgf1	2.37	1.98	2.17
Fgfrl1	---	---	0.77
Fhdc1	---	---	1.1
Fhl2	-0.96	---	-1.22
Fhl3	-0.79	---	---
Fignl1	-0.71	---	-1.34
Fip1l1	---	---	0.74
Fjx1	---	---	-0.8
Flcn	---	---	0.77
Flrt2	-2.03	---	-1.72
Flrt3	---	---	0.91
Flywch1	1.13	---	1
Fndc4	---	---	-0.94
Fopnl	1.14	1	0.98
Fosl2	---	---	0.91
Foxj1	---	---	-1.1
Foxn3	---	---	1.02
Foxo3	---	---	0.88
Foxq1	1.74	1.46	1.45
Fpgt	0.78	---	---
Frmd4a	-0.85	---	---
Frmd6	-1.32	-0.8	-1.24
Fth1	1.66	1.64	2.14
Ftl1	1.37	0.89	1.52
Fxyd5	---	---	1
Fzd4	---	---	-0.9
Fzd7	1.09	0.75	1.06
G0s2	---	---	-1.12
G6pdx	0.79	---	1.23
Gaa	0.72	---	0.93
Gabarapl1	2.43	1.61	2.64
Gabpb2	---	---	-0.76
Gadd45a	1.68	---	2.29
Gadd45b	---	---	-1.32
Gart	---	---	-0.81
Gas2l3	---	---	-0.88
Gata3	---	---	1.52
Gba	---	---	0.73
Gbe1	1.44	0.91	1.6
Gch1	1.32	---	1.6
Gclc	3.72	3.31	4.12
Gclm	2.61	2.26	2.72
Gcnt2	---	---	0.76
Gcnt3	---	---	-0.91
Gdf11	---	---	0.89
Gdf15	1.93	1.48	4.41
Gemin4	---	---	-0.95
Gemin8	-1.11	---	-0.99
Ggta1	-0.71	---	-0.75
Ghdc	---	---	0.8
Ghitm	---	---	0.66
Gimd1	---	---	-0.79
Gjb1	1.21	1.18	1.59
Gjb3	-0.89	---	-1.55
Gla	0.95	---	1.11
Glis2	---	---	-0.92
Glmp	---	---	0.77
Glul	1.12	0.77	1.28
Glyat	2.5	2.01	2.81
Gm10073	---	---	1.23
Gm21949	---	---	-1.15
Gm21972	---	---	0.93
Gm42878	---	---	0.72
Gm42906	---	---	-1.22
Gm43518	---	---	-0.86
Gm43552	1.15	0.82	1.1
Gm45208	---	---	0.69
Gm7694	1.05	---	1.08
Gm8797	---	---	1.26

Gm9938	---	---	-0.94
Gmnn	---	---	-0.9
Gnal	---	---	0.77
Gpam	-0.77	---	-1.19
Gpcpd1	1.72	1.12	1.93
Gpd1l	---	---	-0.7
Gpi1	---	---	0.76
Gpr137b	0.81	0.88	1.12
Gpr180	---	---	-0.98
Gprc5a	-1.34	---	---
Gpt2	---	---	0.88
Gpx1	0.82	---	---
Gramd1a	---	---	0.79
Gramd3	---	---	0.96
Gramd4	-0.91	-0.71	-0.88
Grasp	---	---	0.8
Grik5	---	---	1.01
Grina	---	---	0.72
Grk6	---	---	-0.81
Grn	0.78	---	0.82
Gsg2	-0.99	---	-1.51
Gsr	1.36	1.26	1.48
Gss	2.37	1.6	2.38
Gsta1	7.09	6.46	6.79
Gsta3	3.11	2.35	2.96
Gsta4	5.13	4.49	4.69
Gstm1	1.91	1.55	2.28
Gsto1	---	---	0.77
Gstp1	2.35	1.63	1.76
Gtf2ird1	---	---	0.99
Gxylt2	-1.18	---	-1.13
H1f0	-1.11	---	-1.51
H2-DMa	1.39	---	1.4
Hap1	---	---	-0.9
Haus5	---	---	-1.07
Havcr1	-1.5	-0.92	-1.54
Hax1	---	---	0.87
Hbegf	-1.1	---	-0.9
Hbp1	0.97	---	1.24
Hdac4	---	---	0.74
Heatr3	---	---	-0.68
Heca	---	---	0.95
Hells	-1.38	---	-1.41
Herpud1	---	---	1.16
Hes1	-0.97	---	-1.41
Hfe	2.39	1.88	2.22
Hgs	---	---	0.87
Hhipl1	---	---	1.31
Hid1	---	---	1.39
Hist1h1c	1.16	---	1.05
Hist3h2a	0.96	---	0.81
Hivep2	-1.05	---	---
Hk2	-1.17	---	---
Hmga2	-0.84	---	---
Hmgcr	1.29	---	1.48
Hmgcs1	1.37	---	1.35
Hmmr	---	---	-0.87
Hmox1	6.6	6.03	7.55
Hnf1b	-1.02	---	---
Hnrnpr	---	---	-0.75
Homer3	0.97	0.71	1.13
Hook1	---	---	-0.76
Hpdl	---	---	-1.05
Hr	---	---	1.12
Hs3st3b1	1.17	---	---
Hsd17b7	---	---	0.87
Hsf2	---	---	0.81
Hsp90aa1	1.19	0.86	1.71
Hsp90ab1	0.81	---	1.21
Hspa1a	5.39	4.26	6.42
Hspa1b	5.38	4.36	6.45
Hspa2	---	---	0.8
Hspa4l	1.17	---	1.12
Hspa8	1.14	1	1.61
Hspb1	2.25	1.58	3.3
Hspb8	1.84	1.47	2.11
Hsph1	2.12	1.46	2.65
Htatip2	2	1.05	1.66
Htr1b	-1.25	---	-1.37
Hyal1	1.03	---	1.15
Hyal3	1.09	0.83	1.37
Icam1	-1.15	---	-0.85
Ick	1.64	1.52	2.04
Id2	-1	---	-1.45
Idh1	2.64	1.48	2.54
Idi1	1.27	---	0.98
Ier3	---	---	0.67
Iffo2	-0.72	---	-0.74
Ifi202b	0.85	---	1.47
Ifi203	---	---	1.03

Ifi47	---	---	-1.2
Ifit2	---	---	-1.44
Ifngr1	---	---	-0.74
Ifnlr1	---	---	-1.01
Igfbp3	-0.86	---	-0.67
Igip	---	---	-1.15
Igsf9	-0.9	---	-1.16
Igtp	1.52	1.24	1.33
Ikbkg	1.45	1.06	1.06
Ikzf2	---	---	-1.38
Il11	---	---	1.26
Il18rap	---	---	-1.01
Il1r1	---	---	-1.17
Il24	-2.11	---	-1.7
Il33	---	---	0.72
Il4ra	0.96	0.91	1.15
Il5ra	-2.91	-2	-3.48
Il7	---	---	0.99
Impact	1.41	1	1.75
Inhba	-1.43	---	-0.87
Inhbb	-1.15	---	-2.33
Inpp4b	-1.81	---	-1.21
Inpp5j	0.91	---	1.25
Insig1	2.28	---	3.06
Ipp	---	---	-0.93
Iqck	---	---	0.89
Iqgap3	-0.77	---	-0.89
Irs2	1.09	1.03	0.75
Itga3	-0.81	---	---
Itga6	---	---	-0.64
Itga7	1.33	1.09	1.84
Itgb6	-1.59	-1.04	-2.88
Itpripl1	---	---	-0.75
Itsn1	---	---	0.7
Jade2	-1.78	-1.07	-2.28
Jade3	0.85	---	1.07
Jag1	-1.18	-0.78	-1.12
Jmjd6	---	---	0.75
Jrk	---	---	-0.82
Jun	---	---	2.46
Junb	-1.18	---	-0.97
Jup	---	---	0.74
Kank3	---	---	-1.4
Kbtbd8	---	---	-1.19
Kcmf1	---	---	0.91

Kcnab1	---	---	-0.71
Kcnk5	---	---	-0.84
Kctd18	0.92	---	---
Kdm2a	---	---	0.83
Kdm3a	---	---	0.83
Kdm4a	0.83	---	0.89
Keap1	0.97	---	0.95
Kif11	---	---	-0.82
Kif14	---	---	-1.21
Kif15	---	---	-0.82
Kif18a	-0.81	---	-1.04
Kif1b	0.76	---	0.91
Kif20a	---	---	-0.63
Kif20b	---	---	-0.7
Kif21a	0.94	---	1.32
Kif23	---	---	-0.68
Kif24	---	---	-0.99
Kif2a	1.03	0.94	1.4
Kif2c	---	---	-0.71
Kif3c	0.83	---	1.1
Kif7	---	---	-1.21
Kifc3	---	---	-0.9
Kitl	1.07	0.83	0.85
Klc4	0.91	---	0.78
Klf11	0.89	---	1.17
Klf15	---	---	-1.62
Klf16	-0.95	---	-0.89
Klf4	---	---	1.43
Klf5	---	---	0.81
Klf6	---	---	0.69
Klf7	-0.99	---	-1
Klf9	---	---	1.02
Klhl15	---	---	0.73
Klhl21	---	---	0.74
Klhl24	1.46	---	1.58
Klhl26	---	---	0.79
Klhl5	---	---	-0.7
Krt7	---	---	-0.88
Krt80	-1.04	---	-1.83
Ksr1	1.26	0.97	1.19
L2hgdh	---	---	-0.68
L3mbtl2	---	---	-0.86
Lancl2	---	---	-0.63
Lancl3	1.28	1.24	1.13
Lasp1	---	---	-0.71

Layn	1.25	1.05	1.71
Lcmt2	---	---	-0.83
Ldlr	1.51	---	1.72
Lfng	---	---	-1.02
Lgals8	0.77	---	1.26
Lgalsl	---	---	-0.99
Lgr6	-1.36	---	-1.73
Lhfpl2	---	---	0.76
Lif	-1.2	---	-1.04
Lig1	-0.8	---	-0.87
Lin37	---	---	0.85
Lipe	0.95	---	1.03
Lmbr1l	---	---	0.72
Lmcd1	-1.96	-1.15	-2.26
Lmln	---	---	-1.45
Lmnb2	---	---	-0.86
Lonrf3	---	---	0.83
Lpar2	0.69	---	---
Lpcat1	-0.91	---	-1.37
Lpcat4	-0.84	---	-0.74
Lpin1	1.99	---	2.41
Lpin2	1.31	---	1.61
Lrig1	-0.76	---	-0.64
Lrp8	1.38	1.28	1.66
Lrr1	---	---	-1.2
Lrrc49	---	---	0.73
Lrrc8c	-1.21	---	---
Lrrc8d	---	---	0.97
Lrrfip2	---	---	0.94
Lrtm2	1.44	---	---
Lss	1.09	---	0.93
Lurap1l	---	---	-0.8
Ly75	---	---	-0.79
Ly96	---	---	1.27
Lyar	-0.76	---	---
Maff	---	---	1.07
Mafg	1.19	0.8	1.39
Mafk	---	---	0.96
Maml2	-0.96	---	---
Man2a1	---	---	0.68
Maoa	1.08	---	0.9
Map1b	---	---	1.44
Map1lc3b	1.13	---	1.34
Map2k6	-1.55	-0.95	-1.38
Map3k4	---	---	-0.69
Map4k4	---	---	0.78
Mapk9	0.78	---	0.96
Mapkapk5	---	---	0.72
Mars2	---	---	-1.09
Masp1	-0.92	---	-1.08
Mat2a	---	---	-0.97
Mb21d2	---	---	0.91
Mccc2	---	---	-0.9
Mcm2	-0.9	---	-0.87
Mcm3	-0.88	---	-0.91
Mcm4	-0.91	---	-0.9
Mcm6	---	---	-0.69
Mcoln1	---	---	0.73
Mdfic	---	---	0.65
Mdm1	---	---	-1
Mdm2	---	---	0.96
Mecom	-1.52	-1.07	-1.55
Mef2d	---	---	0.9
Melk	---	---	-0.79
Mettl21a	---	---	-0.83
Mettl7a1	1.85	1.46	1.76
Mettl7b	1.15	1.18	1.34
Mfsd6	0.9	---	1.25
Mgat3	---	---	-1.35
Mgea5	0.69	---	0.85
Mgst1	1.79	1.33	1.62
Mgst2	1.57	1.41	1.33
Mia3	---	---	0.68
Mib2	---	---	0.82
Mical2	-0.99	---	-0.81
Micall2	---	---	-0.85
Mid1ip1	---	---	-0.93
Mipol1	---	---	-0.7
Mkx	---	---	-1.02
Mlkl	0.85	0.8	1.14
Mllt11	1.13	1.31	2.2
Mlycd	---	---	-0.89
Mmachc	-1.16	---	-1.29
Mmp11	0.82	---	---
Mmp13	---	---	1.14
Mms22l	---	---	-0.83
Mndal	---	---	0.88
Mns1	---	---	-0.89
Mocos	2.53	1.75	2.86
Mocs1	1.11	---	1.23

Mogs	---	---	-1.09
Mplkip	---	---	-0.83
Mpp4	1.14	1.06	1.38
Mpzl3	---	---	0.83
Mras	---	---	0.91
Mrc1	-1.77	-1.04	-1.76
Mre11a	---	---	-0.68
Mrpl14	1.03	---	0.88
Mrps6	0.96	---	1.02
Msantd3	1.15	1.05	1.3
Msantd4	0.73	---	---
Msh6	-1.09	---	-1.53
Msmo1	1.54	---	1.51
Msrb3	---	---	-0.76
Mtcl1	-0.81	---	---
mt-Co1	---	---	1.06
Mthfd1	---	---	-0.71
Mthfr	1.19	---	1.31
Mtmr10	-1.72	-0.75	-1.7
Mtmr3	---	---	0.71
Mttp	---	---	0.88
Mturn	1.45	---	1.32
Mvd	0.92	---	---
Mxd1	---	---	0.95
Mxd3	-1.39	---	-1.89
Mxd4	0.73	---	---
Myc	-0.75	---	-0.63
Myo5c	0.75	---	0.72
N4bp3	---	---	-0.84
Naif1	---	---	0.82
Nampt	1.07	---	1.49
Nanos1	-1.19	---	-1.01
Napa	---	---	0.68
Napb	1.1	---	1.16
Napepld	---	---	-1.02
Narf	0.89	---	0.72
Nars	---	---	0.73
Nat6	1.05	---	1.29
Nbeal2	-0.78	---	-1.01
Ncaph	-0.68	---	-0.8
Ncbp2	---	---	-0.77
Ndel1	---	---	0.75
Ndrg1	1.6	0.85	2.41
Neil3	---	---	-0.81
Nek6	-0.84	---	-0.78
Net1	-0.95	---	-0.7
Neurl1b	---	---	-1.01
Neurl3	---	-1.06	---
Nfatc4	1.18	---	---
Nfe2l1	---	---	0.83
Nfkb2	-0.83	---	---
Nfkbia	-1	-0.77	---
Nfkbie	---	---	-0.75
Nfkbiz	-0.85	---	-1.05
Ngf	1.47	1.5	2.29
Nid1	0.95	1.26	1.36
Nif3l1	1.06	---	1.41
Noa1	---	---	-1.06
Nolc1	-0.73	---	---
Notch2	---	---	0.77
Npc1	---	---	0.91
Npcd	---	---	-0.99
Nploc4	---	---	0.94
Npnt	-0.93	---	-0.89
Nr1h4	-1.15	---	-1.29
Nr4a1	-1.21	---	---
Nrarp	---	---	-1.35
Nrep	0.98	---	---
Nrg1	-0.9	---	---
Nsdhl	1.29	---	1.28
Nsfl1c	---	---	0.69
Nuak1	---	---	-0.8
Nuak2	---	---	-1.44
Nub1	0.78	---	0.82
Nucks1	---	---	-0.67
Nudt12	0.95	---	---
Nuf2	-0.75	---	-1.03
Numbl	2.19	1.74	2.31
Nup107	---	---	-0.73
Nup210l	---	---	0.69
Nup37	---	---	-0.97
Nup85	---	---	-0.83
Nupl2	---	---	-1.1
Nupr1	1.55	---	2.14
Nusap1	---	---	-0.93
Nxt1	---	---	-0.83
Nyap1	---	---	1.09
Obfc1	-0.66	---	---
Oip5	---	---	-0.76
Olfr56	---	---	-1.19

Onecut1	---	---	-1.64
Osbpl9	---	---	0.69
Oser1	---	---	1.4
Osgin1	2.1	1.87	2.75
Otud4	-0.93	---	-0.79
P2ry1	---	---	-1.01
P4ha1	1.35	0.79	1.66
P4ha2	---	---	0.74
Pacsin2	---	---	0.72
Padi2	-0.81	---	-1.1
Pafah2	0.91	---	0.68
Pag1	-1.2	---	-1.35
Palld	-1.09	---	-0.85
Palmd	-0.96	---	-1.1
Pank1	---	---	-0.83
Papd5	---	---	0.74
Papd7	---	---	-0.66
Papss2	1.73	---	1.98
Parp1	---	---	-0.66
Parp8	-1	---	---
Parpbp	-0.79	---	-1.01
Pax3	---	---	0.97
Pbk	---	---	-1.19
Pcdh1	-0.79	---	---
Pcdh7	-1.6	-0.98	-1.41
Pcdh9	---	---	1.55
Pcsk9	1.5	---	1.35
Pcx	1.54	---	1.31
Pcyt2	0.84	---	0.74
Pdcd4	0.8	---	---
Pddc1	---	---	-0.83
Pde4b	---	1.38	1.09
Pdgfb	-1.72	-1.09	-2.37
Pdk4	1.35	---	1.12
Pdlim7	---	---	1.04
Pdss1	-0.77	---	-0.73
Pdxk	-1.02	-1.03	-1.36
Pex13	1.09	---	1.12
Pfas	---	---	-0.87
Pgd	2.41	1.99	2.39
Pgm2l1	0.91	---	0.77
Phf1	0.99	---	1.19
Phf10	---	---	1.04
Phf19	-1.62	-0.9	-2.02
Phlda1	---	0.84	1.67

Pif1	-0.91	---	-1.59
Pik3ap1	0.92	---	0.74
Pilra	-0.73	---	---
Pilrb1	-0.94	---	---
Pim3	---	---	-0.81
Pla2g4a	1.13	0.91	0.86
Plat	---	---	0.71
Plau	-1.47	---	-1.3
Plaur	---	---	0.85
Pld3	---	---	0.73
Plek2	-1.03	---	-0.8
Plekha2	---	---	-0.75
Plekha7	-0.98	---	-1
Plekho1	---	---	0.74
Plekho2	-0.73	---	---
Plk1	-0.72	---	-1.08
Plk3	1.5	1.29	3.27
Plk4	---	---	-0.72
Plod1	---	---	0.68
Plod2	1.32	0.82	1.84
Plscr2	---	---	-1.01
Plxnd1	-0.78	---	---
Pmaip1	---	---	0.77
Pmvk	1.37	---	1.17
Pnpla8	---	---	0.71
Pnrc1	1.07	---	1.81
Pold1	---	---	-0.83
Pole2	-1.01	---	-0.98
Polh	-0.81	---	-1.08
Por	---	---	0.74
Pou6f1	1.04	---	1.22
Ppard	1.09	1.02	1.73
Ppat	-0.76	---	-0.94
Ppl	-0.71	---	-0.96
Ppp1r13b	---	---	0.91
Ppp1r13l	---	---	-0.89
Ppp1r15a	1.17	---	2.72
Ppp1r3e	---	---	-0.87
Ppp3ca	---	---	0.89
Pqlc2	1.22	0.82	1.34
Prc1	---	---	-0.85
Prdm2	---	---	0.9
Prdx1	0.93	---	0.92
Prdx6	2.18	1.58	2.28
Prex2	---	---	-0.88

Prim1	---	---	-0.63
Prim2	-0.81	---	---
Prkci	-0.69	---	-0.84
Prob1	1.01	---	0.84
Procr	3.31	2.74	4.38
Prodh	---	---	-0.99
Prorsd1	---	---	-1
Proser2	1.75	1.65	2.02
Prox1	---	---	1.03
Prr13	1.16	1.05	1.67
Prss23	-1.24	-0.9	-2.03
Prx	---	---	0.83
Psap	0.84	---	0.79
Psmb3	---	---	1
Psmc6	---	---	0.74
Psmd11	0.9	0.78	1.12
Psmd4	---	---	0.79
Psmd5	0.9	0.72	0.84
Psme4	0.74	---	0.83
Psph	1.01	---	1.06
Ptger4	---	---	1.26
Ptgr1	1.42	---	1.11
Ptgs2	2.08	2.1	3.18
Ptprb	-0.9	---	-1.36
Ptrh2	---	---	-0.89
Purb	---	---	-0.71
Pvr	---	---	1.27
Pxmp2	-1.35	---	-1.31
Pxylp1	---	---	-1.24
Pycr1	---	---	0.73
Rab17	---	---	-1.05
Racgap1	---	---	-0.71
Rad18	---	---	-0.73
Rad23b	---	---	0.76
Rad51ap1	-0.73	---	-0.99
Radil	2.05	1.86	2.3
Raf1	---	---	0.76
Ralgps2	-0.84	---	-0.73
Ranbp6	---	---	-0.75
Rap2b	---	---	0.91
Raph1	---	---	1.32
Rasgrf2	-0.92	---	---
Rasgrp3	---	-0.86	-1.53
Rasl12	---	---	-0.84
Rassf6	1.37	1.18	1.5
Rassf8	0.78	---	0.69
Rbbp6	---	---	0.78
Rbm33	---	---	0.76
Rbpms2	---	---	0.8
Rccd1	---	---	-0.8
Rcl1	---	---	-0.66
Rdh10	---	---	-1.16
Recql	---	---	-0.91
Reep6	---	---	1.48
Relb	-1.21	-1.21	-1.04
Rem2	-1.2	---	-1.17
Reps1	---	---	0.9
Rfc3	-0.88	---	-0.71
Rfc5	-0.73	---	-0.92
Rgs17	---	---	0.83
Rgs20	-0.85	---	---
Rhbdd1	---	---	1.06
Rhbdf2	---	---	1.06
Rhob	---	---	0.89
Rhobtb3	---	---	-0.74
Rhpn2	1.1	0.86	1.14
Riok3	0.73	---	0.84
Rit1	1.46	0.9	1.48
Rmi2	-1.11	---	-1.08
Rnd1	-1.25	---	-0.75
Rnd2	1.09	---	1.04
Rnf115	---	---	0.95
Rnf145	-1.5	-0.76	-1.86
Rnf183	3.14	2.69	3.72
Rnf19b	---	---	1.05
Rnf39	-1.08	---	-1.42
Rnf41	---	---	0.68
Rock2	---	---	0.79
Ror1	-1.36	---	-1.39
Rora	1.38	---	2.18
Rorb	---	---	0.93
RP23- 145I16.3	0.94	---	0.99
Rragd	1.36	---	1.28
Rrm1	---	---	-0.64
Rrm2	-0.75	---	-0.82
Rrp12	---	---	-0.93
Rrp1b	-1.06	---	-1.09
Rsrp1	---	---	0.75
Rtkn2	---	---	-1.1
Runx2	-1.1	---	-1.19

Rusc2	---	0.77	1.14
Rybp	---	---	0.95
Ryr3	---	---	1.78
S1pr2	-1.07	---	-1.12
Saraf	0.98	---	0.93
Sars	---	---	0.78
Sat1	---	---	1.13
Sbds	---	---	1.17
Sc5d	---	---	0.89
Scamp5	---	---	-1
Scarb1	0.85	---	0.89
Scd2	1.36	---	0.68
Schip1	---	---	-1.15
Scpep1	0.77	---	0.85
Sdpr	-0.84	---	-1.41
Sec24d	---	---	1.29
Sel1l3	0.92	---	1.28
Sema6c	1.06	---	---
10-Sep	---	---	-0.73
Sepw1	1.19	---	---
Serinc3	---	---	0.86
Serpinb9	1.48	1.16	1.52
Serpinb9b	1.13	1.06	1.33
Serpind1	-1.63	---	-1.39
Serpinh1	---	---	0.74
Sertad2	---	---	0.8
Sertad3	0.91	---	0.97
Sertad4	-1.77	-1.21	-2.08
Sesn2	---	---	1.38
Sesn3	1.3	0.91	1.39
Sf1	---	---	0.71
Sfxn4	---	---	0.78
Sgk1	1.09	1.13	1.1
Sgk3	---	---	0.82
Sgtb	1.15	---	1.7
Sh3bgrl2	---	---	0.86
Sh3bp1	-1.07	---	-0.9
Sh3bp2	2.1	1.54	2.65
Sh3bp5	-0.72	---	-0.95
Sh3tc1	0.92	---	0.77
Shank2	---	---	-0.93
Shcbp1	---	---	-0.8
Shmt1	-0.89	---	-0.94
Siglecg	---	---	-0.98
Sim2	---	---	0.74

Six4	1.4	1.3	1.29
Six5	---	---	-1.03
Ska1	---	---	-0.84
Ska3	---	---	-0.84
Skp2	---	---	-0.83
Slbp	---	---	-0.8
Slc12a2	---	---	-0.78
Slc16a10	---	---	1.58
Slc16a13	1.05	---	0.82
Slc16a6	1.11	---	1.17
Slc19a2	---	---	0.77
Slc1a4	3.01	2	3.54
Slc20a1	---	---	1.09
Slc22a23	1.51	1.27	1.74
Slc22a4	1.91	1.51	2.07
Slc25a1	0.77	---	0.96
Slc25a12	---	---	-0.66
Slc25a15	---	---	-0.99
Slc25a27	---	---	1.04
Slc25a33	0.93	---	1.25
Slc25a45	---	---	1
Slc25a48	-1.01	---	-1.63
Slc27a6	-1.31	---	-1.13
Slc29a2	-1.45	---	-1.24
Slc2a1	0.97	0.77	1.72
Slc2a2	---	---	-1.47
Slc30a1	---	---	-1.05
Slc35b2	-0.97	---	-1.15
Slc35d1	---	---	0.95
Slc35e2	---	---	0.81
Slc35e4	---	---	0.96
Slc35g1	---	---	-0.71
Slc36a4	---	---	-0.77
Slc38a2	---	---	0.97
Sfxn4	---	---	0.78
Sgk1	1.09	1.13	1.1
Sgk3	---	---	0.82
Sgtb	1.15	---	1.7
Sh3bgrl2	---	---	0.86
Sh3bp1	-1.07	---	-0.9
Sh3bp2	2.1	1.54	2.65
Sh3bp5	-0.72	---	-0.95
Sh3tc1	0.92	---	0.77
Shank2	---	---	-0.93
Shcbp1	---	---	-0.8

Shmt1	-0.89	---	-0.94
Siglecg	---	---	-0.98
Sim2	---	---	0.74
Six4	1.4	1.3	1.29
Six5	---	---	-1.03
Ska1	---	---	-0.84
Ska3	---	---	-0.84
Skp2	---	---	-0.83
Slbp	---	---	-0.8
Slc12a2	---	---	-0.78
Slc16a10	---	---	1.58
Slc16a13	1.05	---	0.82
Slc16a6	1.11	---	1.17
Slc19a2	---	---	0.77
Slc1a4	3.01	2	3.54
Slc20a1	---	---	1.09
Slc22a23	1.51	1.27	1.74
Slc22a4	1.91	1.51	2.07
Slc25a1	0.77	---	0.96
Slc25a12	---	---	-0.66
Slc25a15	---	---	-0.99
Slc25a27	---	---	1.04
Slc25a33	0.93	---	1.25
Slc25a45	---	---	1
Slc25a48	-1.01	---	-1.63
Slc27a6	-1.31	---	-1.13
Slc29a2	-1.45	---	-1.24
Slc2a1	0.97	0.77	1.72
Slc2a2	---	---	-1.47
Slc30a1	---	---	-1.05
Slc35b2	-0.97	---	-1.15
Slc35d1	---	---	0.95
Slc35e2	---	---	0.81
Slc35e4	---	---	0.96
Slc35g1	---	---	-0.71
Slc36a4	---	---	-0.77
Slc38a2	---	---	0.97
Sprr1a	-1.57	---	---
Spry1	---	---	-0.78
Spry2	-0.85	---	-0.95
Spry4	---	---	0.95
Spsb4	-1.12	---	-1.82
Sqle	1.63	---	1.61
Sqrdl	2.25	1.72	2.06
Sqstm1	2.77	1.85	3.27

Srd5a1	-0.89	---	-0.99
Srebf2	---	---	0.78
Srf	-1.01	---	-1.17
Srgap3	-1.87	-1.39	-1.77
Srm	-0.86	---	-0.87
Srr	---	---	1.2
Srrm4	---	---	0.86
Srsf10	---	---	-0.73
Srxn1	4.29	3.51	4.9
Ss18l1	---	---	0.83
Ssbp2	-0.92	---	-0.77
St13	---	---	0.89
Stambpl1	-1.09	---	-0.73
Stard13	-0.82	---	-1.2
Stard4	1.19	---	0.91
Stard9	---	---	0.98
Stat1	---	---	-0.94
Stat2	0.86	---	0.79
Stip1	---	---	1
Stk10	0.75	---	1.26
Stk40	---	---	0.68
Stx3	---	---	0.78
Stxbp1	---	---	1.04
Stxbp6	---	---	-0.86
Styk1	0.86	---	0.85
Suv39h2	---	---	-0.75
Swap70	---	---	0.67
Swt1	---	---	0.99
Syvn1	---	---	0.73
Tacc2	1.23	0.72	1.39
Tada1	---	---	-0.75
Tada2a	-0.72	---	-0.72
Taf7	1.46	1.23	2.04
Taldo1	0.91	---	0.87
Tapbpl	0.85	---	0.78
Tbc1d1	-0.77	---	---
Tbc1d9	---	---	0.97
Tbce	---	---	0.67
Tbcel	1.05	0.81	1.15
Tbl2	---	---	-1.04
Tcf19	-1.23	---	-1.44
Tcp11l2	1	---	1.26
Tdrp	1.14	---	1.06
Tef	0.86	---	---
Tex9	-1.04	---	-0.92

Tfap2a	1.03	---	1.58
Tfe3	---	---	1.21
Tfrc	-1.9	-1.12	-1.62
Tgif2	---	---	-1.17
Tgoln1	---	---	0.69
Thbs1	-2.6	-1.32	-3.45
Them4	---	---	1.04
Thnsl1	---	---	-0.78
Thrb	1.79	1.67	2.08
Tiam2	-0.74	---	-0.69
Ticam1	---	---	1
Ticrr	---	---	-0.98
Tigit	-0.9	---	---
Timeless	-0.79	---	-1.03
Tipin	-1.02	---	-1.31
Tk1	-1.21	---	-1.93
Tkt	0.71	---	0.91
Tlk2	---	---	0.76
Tm4sf4	---	---	-1.4
Tmco4	---	---	1.04
Tmem117	2.23	1.53	2.38
Tmem171	-1.6	---	-1.1
Tmem18	---	---	-0.92
Tmem194b	---	---	-1.03
Tmem2	---	---	-0.73
Tmem216	---	---	-0.76
Tmem37	1.19	1.34	1.25
Tmem38a	---	---	0.93
Tmem41b	0.85	---	1.19
Tmem55a	0.87	---	0.91
Tmem57	---	---	0.76
Tmem63b	---	---	0.71
Tmie	1.62	1.23	1.19
Tmpo	---	---	-0.87
Tmppe	0.75	---	0.69
Tnc	-0.99	-0.78	---
Tnfaip2	-0.83	---	---
Tnfaip3	-2.24	-1.44	-2.86
Tnfrsf1a	---	---	0.84
Tnfsf9	---	---	1.15
Tnnc1	1.41	---	1.85
Tns1	---	---	-1.11
Tob1	---	---	1.12
Tob2	0.67	---	0.97
Tollip	---	---	0.85

Tom1	---	---	1.16
Tom1l1	---	---	0.75
Top2a	-0.69	---	-0.99
Tor1aip2	---	---	0.75
Tor4a	---	---	-0.68
Tox	---	---	0.85
Tpx2	---	---	-0.68
Trdmt1	---	---	-0.79
Trib1	-0.86	---	-0.79
Trib3	2.39	---	3.31
Trim16	---	0.88	1.35
Trim17	0.97	---	0.86
Trim36	---	---	1.4
Trim46	---	---	1.12
Trim59	---	---	-0.76
Trim6	0.92	---	1.08
Trio	---	---	0.88
Trip10	---	---	0.92
Trmt1l	---	---	0.85
Trmt2a	---	---	-0.78
Trnt1	---	---	-0.67
Trp53bp2	---	---	0.7
Trp53inp1	1.51	---	2.05
Trp53inp2	---	---	0.91
Tsc22d1	---	---	-0.78
Tsc22d2	---	---	0.94
Tsc22d3	0.97	---	1.16
Tsfm	---	---	-0.91
Tshz1	1.12	1.12	1.48
Tsku	1.61	1.83	1.6
Tspan8	---	---	-1.01
Tspyl2	0.99	---	1.38
Ttc26	---	---	-0.79
Ttc30b	---	---	-0.79
Ttc7	-0.82	---	-0.74
Ttk	---	---	-0.71
Tuba1a	---	---	1.22
Tuba4a	0.81	0.92	1.19
Tubb2a	1.64	1.09	2.01
Tubb2b	---	---	0.78
Tubb6	-0.87	---	-0.78
Txnrd1	1.9	1.71	2
Ubap1	0.87	---	1.36
Ubash3b	-1.14	---	-1.02
Ubb	1.21	1.1	2.2

Ubc	1.72	1.34	3.52
Ube2h	---	---	0.75
Ube2j1	---	---	0.69
Ube2o	1.02	---	1.22
Ube4b	---	---	0.79
Ubl3	0.8	0.78	0.8
Ubqln1	---	---	0.81
Ubr4	---	---	0.87
Ubr7	---	---	-1.13
Ubtd1	---	---	0.96
Ubxn4	1.17	0.95	1.39
Ubxn8	---	---	0.65
Ugdh	1.48	1.17	1.52
Ugt1a1	1.16	0.87	0.94
Ugt1a10	1.1	0.88	0.97
Ugt1a2	1.16	0.87	0.94
Ugt1a5	1.16	0.87	0.95
Ugt1a6a	1.1	0.85	0.93
Ugt1a6b	1.09	0.87	0.96
Ugt1a7c	1.1	0.88	0.97
Ugt1a8	1.1	0.88	0.97
Ugt1a9	1.1	0.88	0.97
Ugt2b34	4.29	3.39	4.22
Uhrf1	-1.04	---	-1.17
Ulk1	0.73	---	0.95
Ung	-3.05	-0.9	-3.56
Usp1	---	---	-0.82
Usp14	---	---	0.67
Usp20	0.91	---	---
Usp22	---	---	0.96
Usp35	1.27	---	1.24
Usp43	-1.03	---	-0.89
Uspl1	---	---	0.69
Uts2b	---	---	-1.56
Vamp1	1.04	---	1.04
Vash2	---	---	0.88
Vasn	1.03	0.77	1.36
Vcam1	-1.86	-1.42	-1.96
Vegfa	2.39	1.74	3.57
Vegfc	-0.99	-0.96	-0.82
Vgll3	-0.96	---	-1.14
Vil1	-1.09	---	-1.31
Vipas39	---	---	0.78
Vldlr	1.07	---	1.16
Vnn1	1.03	---	---

Vps18	1.08	---	1.08
Vps37b	0.85	---	1.63
Vstm5	-1.17	---	-0.92
Wbp2	---	---	0.7
Wbscr27	1.4	---	0.96
Wdhd1	-0.84	---	-1.13
Wdr35	---	---	-0.78
Wdr5b	---	---	-1.27
Wdr6	-0.77	---	-1.5
Wdr76	-0.8	---	-1.14
Wdr77	---	---	-0.7
Wdr81	1.15	---	0.99
Wee1	---	---	-0.92
Whamm	0.97	---	1.12
Wipi2	---	---	0.66
Wnt10a	-0.95	---	-1.22
Wnt4	1.5	1.15	1.33
Wnt7b	-1.42	-0.75	-1.41
Wrb	---	---	-0.99
Xkr9	2.05	1.3	2.05
Xpo1	---	---	0.72
Xpot	---	---	0.65
Xrcc2	---	---	-1.06
Xrcc6	---	---	-0.69
Xrcc6bp1	---	---	-0.92
Xxylt1	---	---	-0.86
Ypel2	---	---	1.1
Ypel5	2.39	1.44	2.61
Ywhag	0.94	---	1.27
Zadh2	0.82	0.69	0.7
Zbtb10	---	---	1.14
Zbtb12	---	---	-0.96
Zbtb2	---	---	1.09
Zbtb21	---	---	1.01
Zbtb37	---	---	-0.94
Zbtb45	---	---	-0.73
Zbtb7b	---	---	0.9
Zc2hc1c	1.16	---	0.92
Zdhhc18	1.52	1.28	1.65
Zeb2	---	---	0.98
Zfand2a	1.9	1.22	3.27
Zfand5	1.43	0.89	1.68
Zfp142	---	---	1.21
Zfp185	---	---	1.14
Zfp324	---	---	-1.46

Zfp36	---	---	1.91
Zfp365	1.19	---	1.23
Zfp367	-0.88	---	-1.06
Zfp385a	---	---	0.74
Zfp39	---	---	-1.02
Zfp395	---	---	-0.86
Zfp41	---	---	-0.82
Zfp418	---	---	0.99
Zfp516	---	---	0.91
Zfp617	---	---	0.72
Zfp651	---	---	-0.89
Zfp703	---	---	0.79
Zfp867	---	---	-0.93
Zfp874a	1	---	0.83
Zfp874b	1.04	---	1.36

Zfp945	---	---	0.96
Zfp958	---	---	-0.88
Zfp961	---	---	-0.76
Zfpm1	---	---	1.12
Zfpm2	-1.2	---	---
Zfyve1	0.84	---	1.06
Zgrf1	---	---	-1.07
Zhx3	-0.93	---	-1.09
Zik1	---	---	-1.24
Zmynd19	---	---	-0.74
Zrsr1	2.11	1.61	2.54
Zswim4	---	---	1.01
Zswim6	---	---	1.12
Zwint	0.94	0.82	1.15
Zyx	-1.14	---	---

Supplemental Table 3. Oxidized phospholipids detected after development of hepatic fibrosis. *In silico* predicted structures of oxidized phospholipids derived from PAPC or PLPC detected in mouse plasma after twenty weeks on FPC diet. CHO – aldehyde, COOH – carboxylic acid, OH – hydroxy, OOH – hydroperoxy, KETO – ketone, EPOXY – epoxide.

LPPTiger Nomenclature (previously known species)	Parent Lipid	*m/z*	Formula	LPPTigr Predicted Structure(s)
1. PAPC	---	782	$C_{44}H_{80}NO_8P$	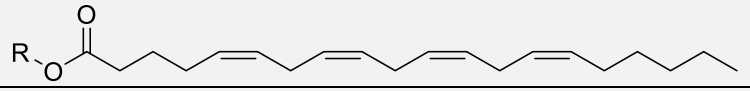
2. PLPC	---	758	$C_{42}H_{80}NO_8P$	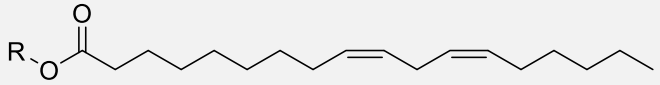
3. 16:0 LysoPC	---	496	$C_{24}H_{50}NO_7P$	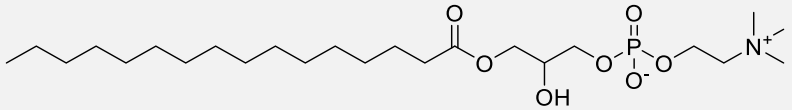
4. 18:0 LysoPC	---	524	$C_{26}H_{54}NO_7P$	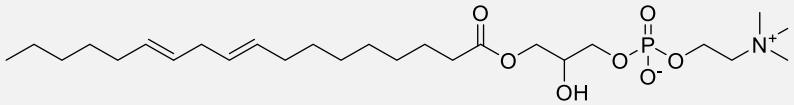
5. 18:1 LysoPC	---	522	$C_{26}H_{52}NO_7P$	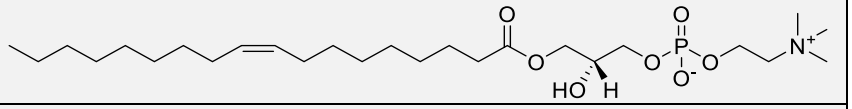
6. 18:2 LysoPC	---	520	$C_{26}H_{54}NO_7P$	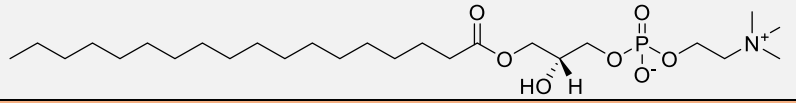
7. C37H66NO11P	PAPC	732	$C_{37}H_{66}NO_{11}P$	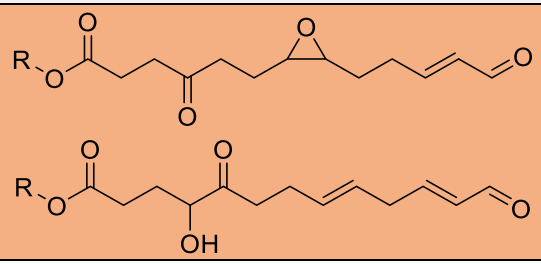

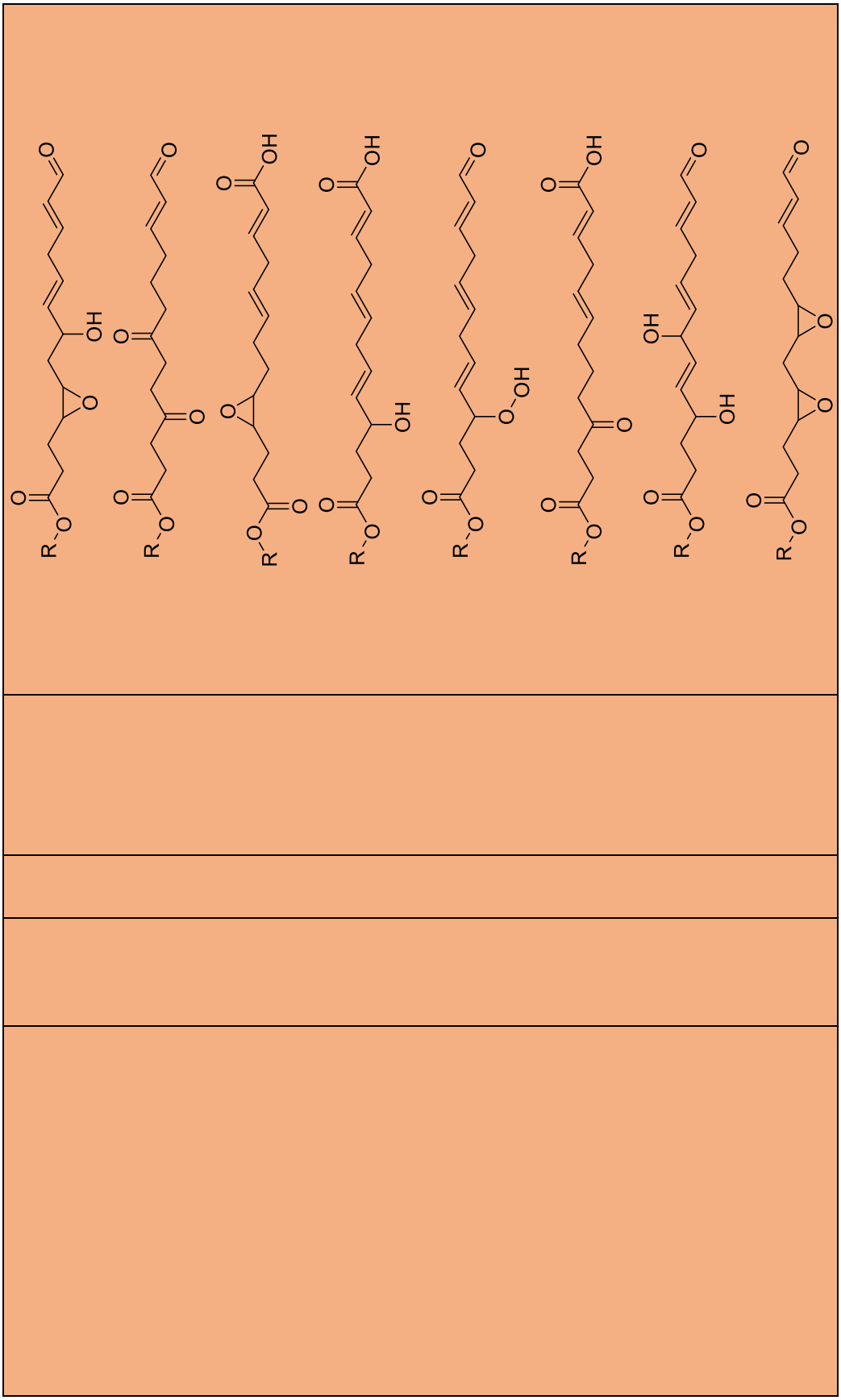

8. 16:0/7:0[1xOH,CHO]	PAPC	638	$C_{31}H_{60}NO_{10}P$	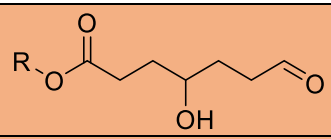
9. PONPC	PLPC	650	$C_{33}H_{64}NO_9P$	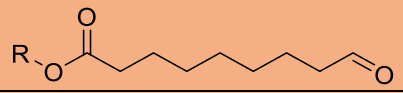
10. 16:0/12:1[CHO]	PLPC	690	$C_{36}H_{68}NO_9P$	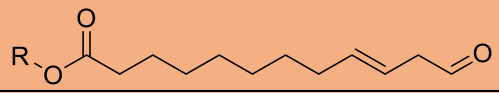
11. C34H62NO11P	PAPC	692	$C_{34}H_{62}NO_{11}P$	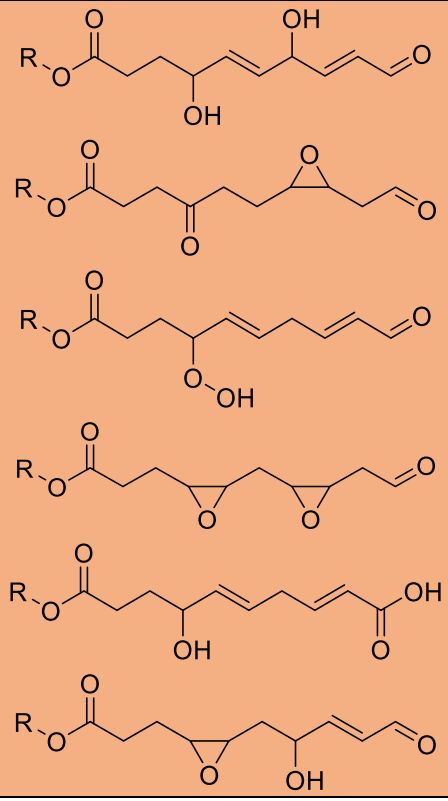

				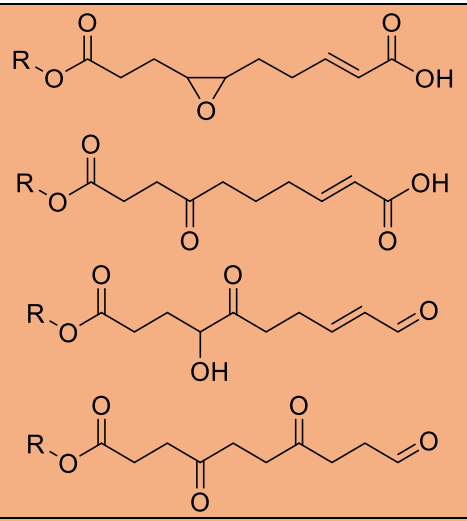
12. 16:0/11:1[CHO]	PLPC	676	$C_{35}H_{66}NO_9P$	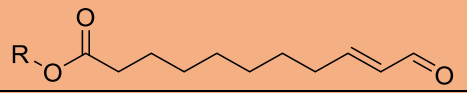
13. POBPC	PAPC	580	$C_{28}H_{54}NO_9P$	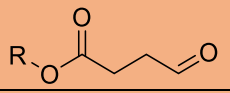
14. 16:0/8:0[CHO] (POOPC)	PLPC	636	$C_{32}H_{62}NO_9P$	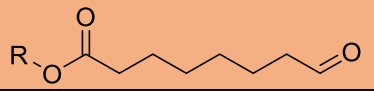
15. C35H64NO12P	PAPC	722	$C_{35}H_{64}NO_{12}P$	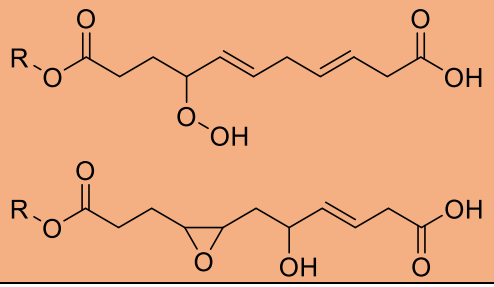

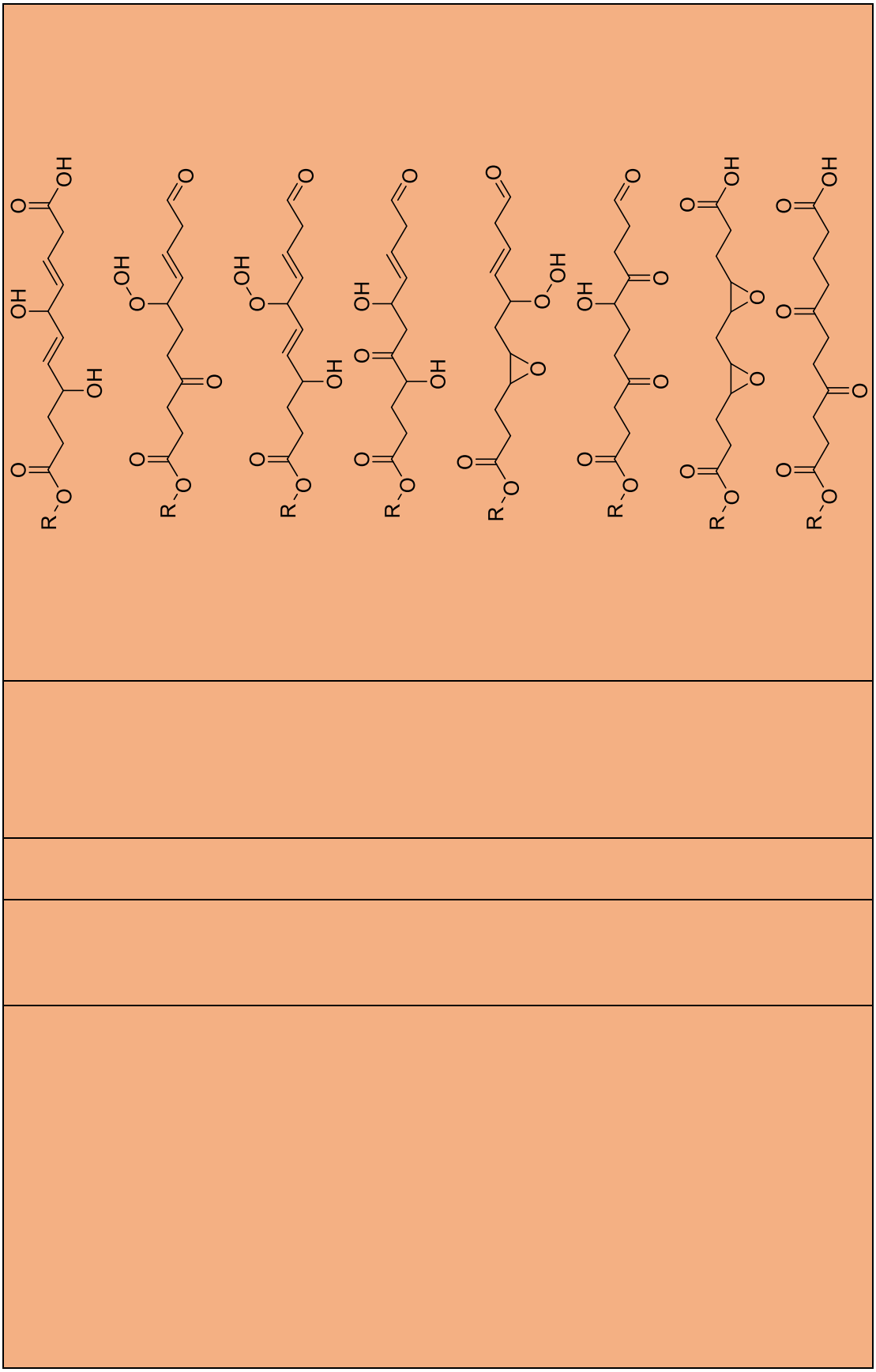

				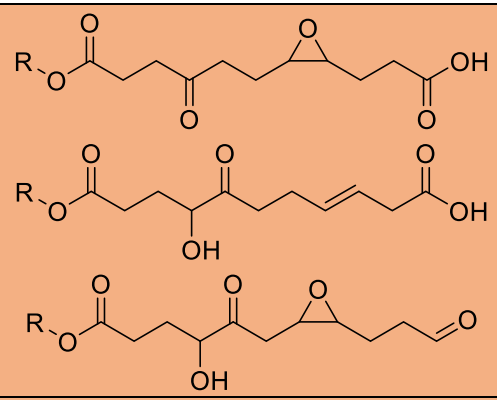
16. C35H64NO10P	PAPC	690	$C_{35}H_{64}NO_{10}P$	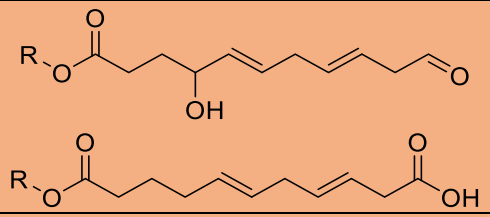
17. C35H62NO11P	PAPC	704	$C_{35}H_{62}NO_{11}P$	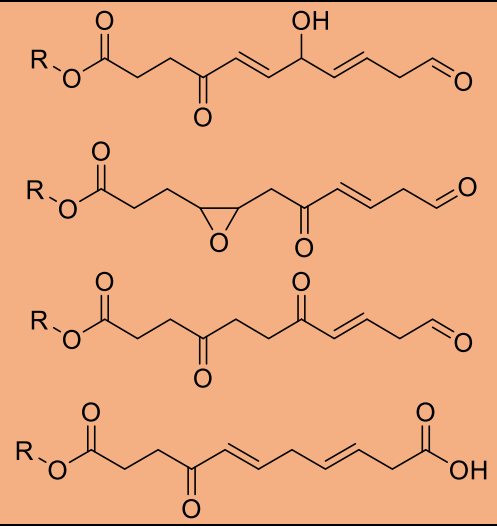

18. POVPC	PAPC	594	$C_{29}H_{56}NO_9P$	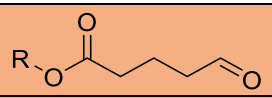
19. 16:0/10:2[CHO]	PAPC	660	$C_{34}H_{62}NO_9P$	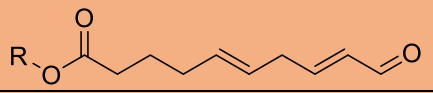
20. C36H68NO10P (HODA-PC)	PLPC	706	$C_{36}H_{68}NO_{10}P$	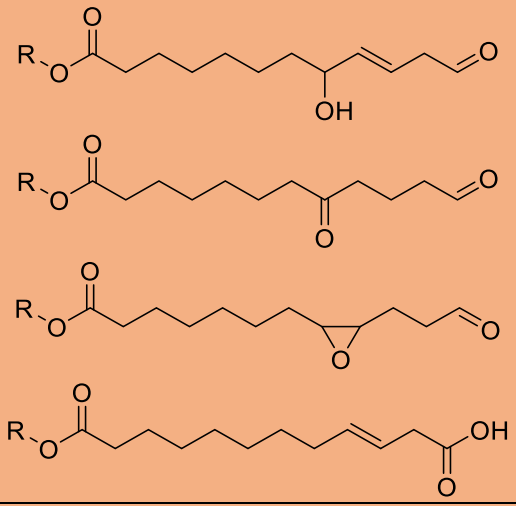
21. 16:0/7:1[CHO]	PAPC	620	$C_{31}H_{58}NO_9P$	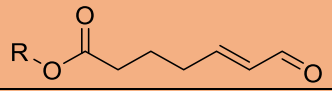
22. KOOA-PC	PAPC	648	$C_{32}H_{58}NO_{10}P$	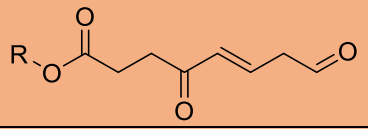
23. C32H60NO11P (HOdiA-PC)	PAPC	666	$C_{32}H_{60}NO_{11}P$	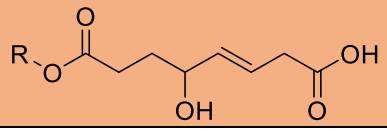

				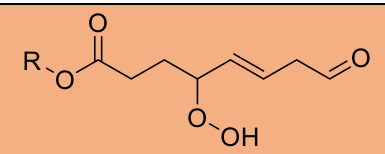 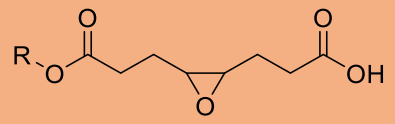 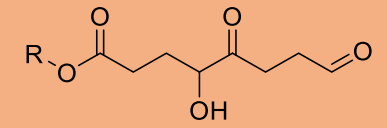 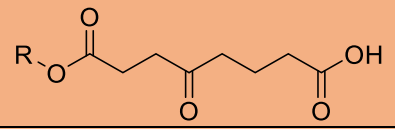
24. 16:0/10:2[1xKETO,CHO]	PAPC	674	$C_{34}H_{60}NO_{10}P$	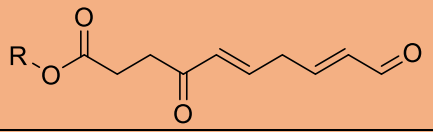
25. PazPC	PLPC	666	$C_{33}H_{64}NO_{10}P$	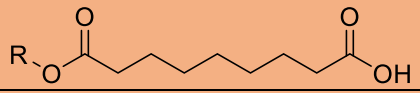
26. C32H60NO10P (HOOA-PC)	PAPC	650	$C_{32}H_{60}NO_{10}P$	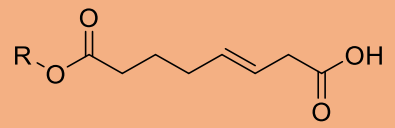 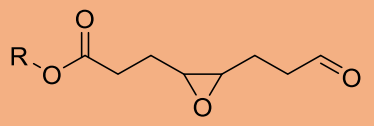 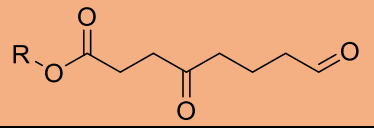

				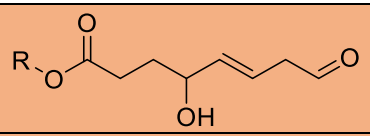
27. PGPC	PAPC	610	$C_{29}H_{56}NO_{10}P$	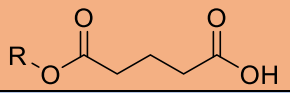
28. C42H78NO10P	PLPC	788	$C_{42}H_{78}NO_{10}P$	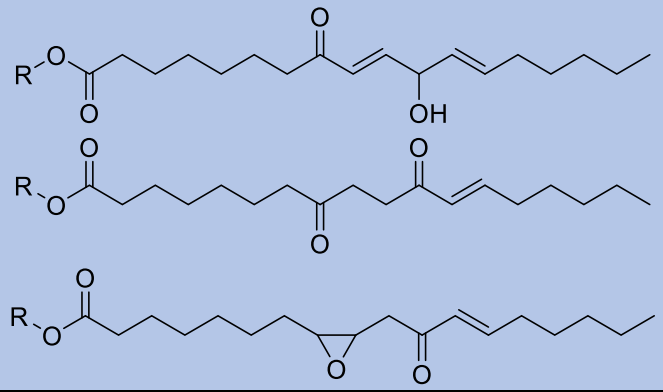
29. C42H80NO9P (HODE-PC)	PLPC	774	$C_{42}H_{80}NO_9P$	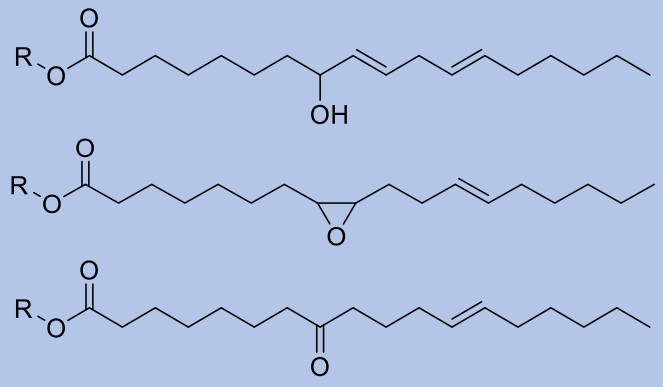

30. 16:0/20:4[2xKETO]	PAPC	810	$C_{44}H_{76}NO_{10}P$	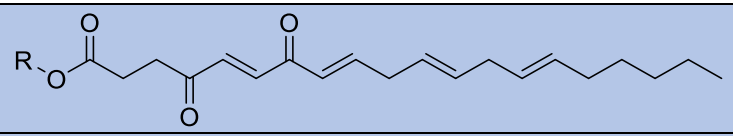
31. C44H80NO11P	PAPC	830	$C_{44}H_{80}NO_{11}P$	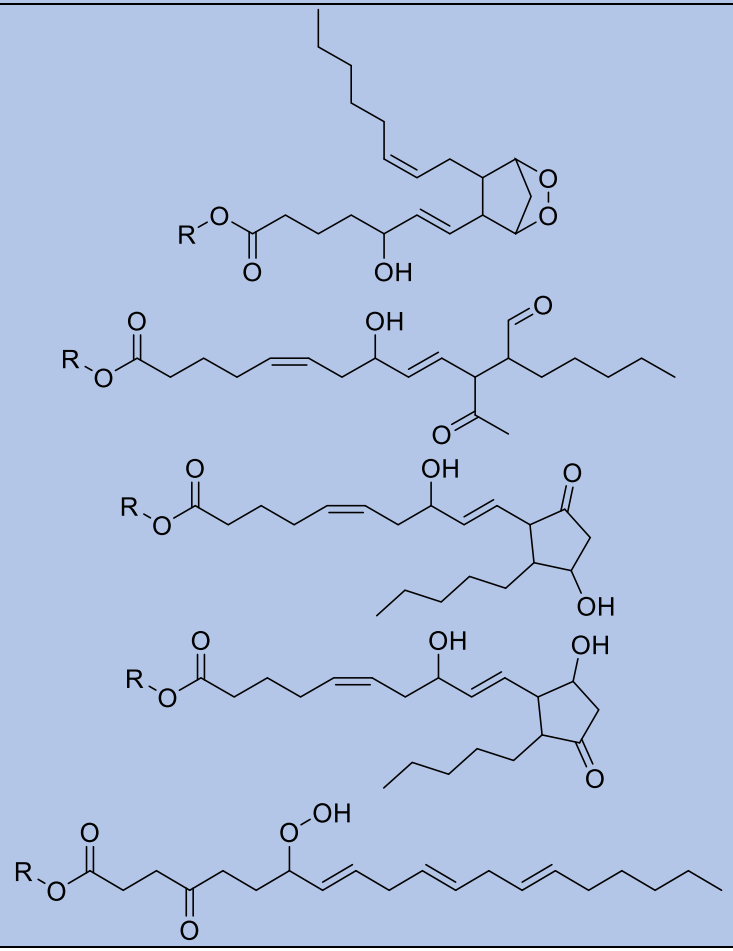

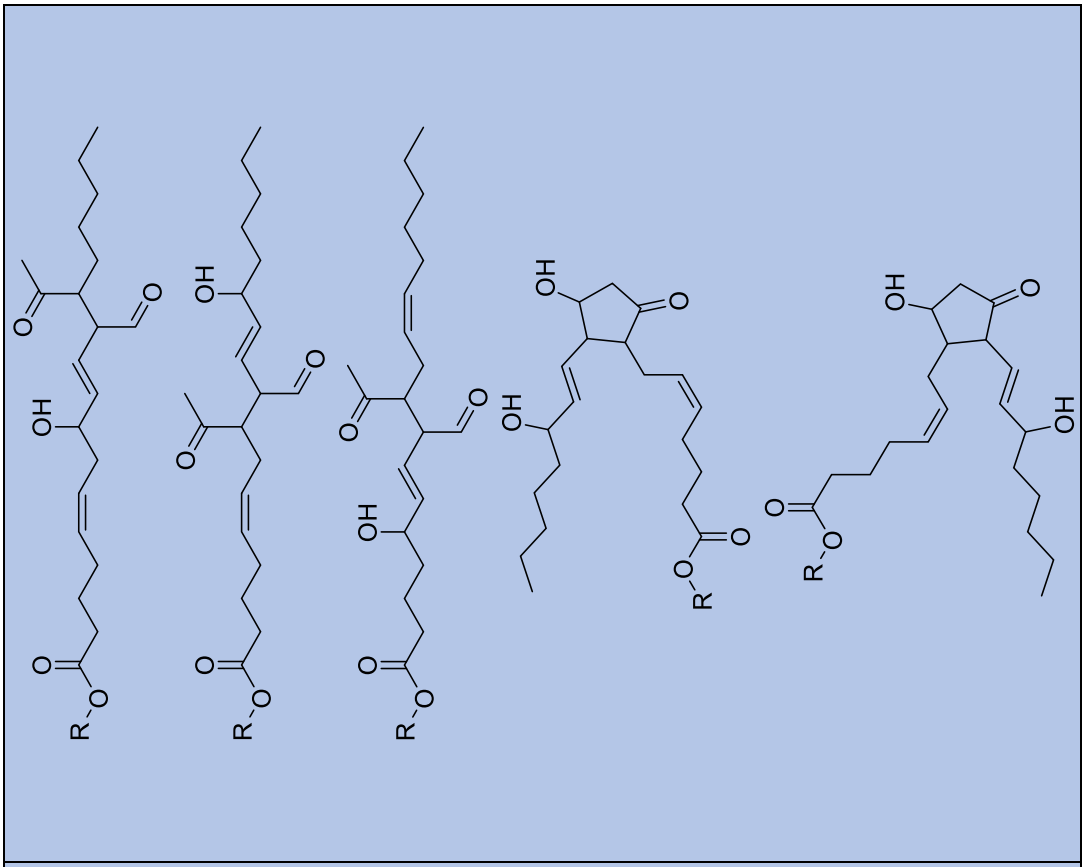
O
OH
O
O
R
O
O
OH
O
O
R
O
O
OH
O
O
R
O
OH
O
O
R
O
OH
O
OH

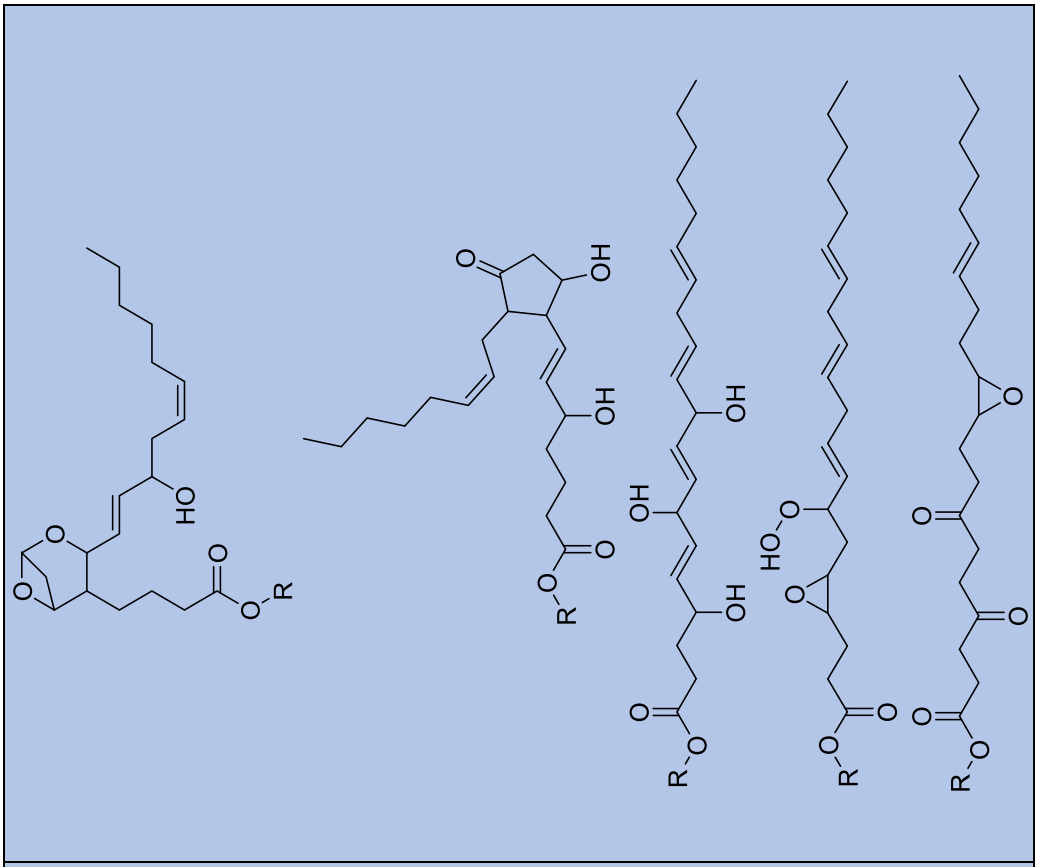
HO
O
O
O
R
O
OH
O
OH
O
R
OH
OH
OH
O
R
HO
O
O
R
O
O
O
R

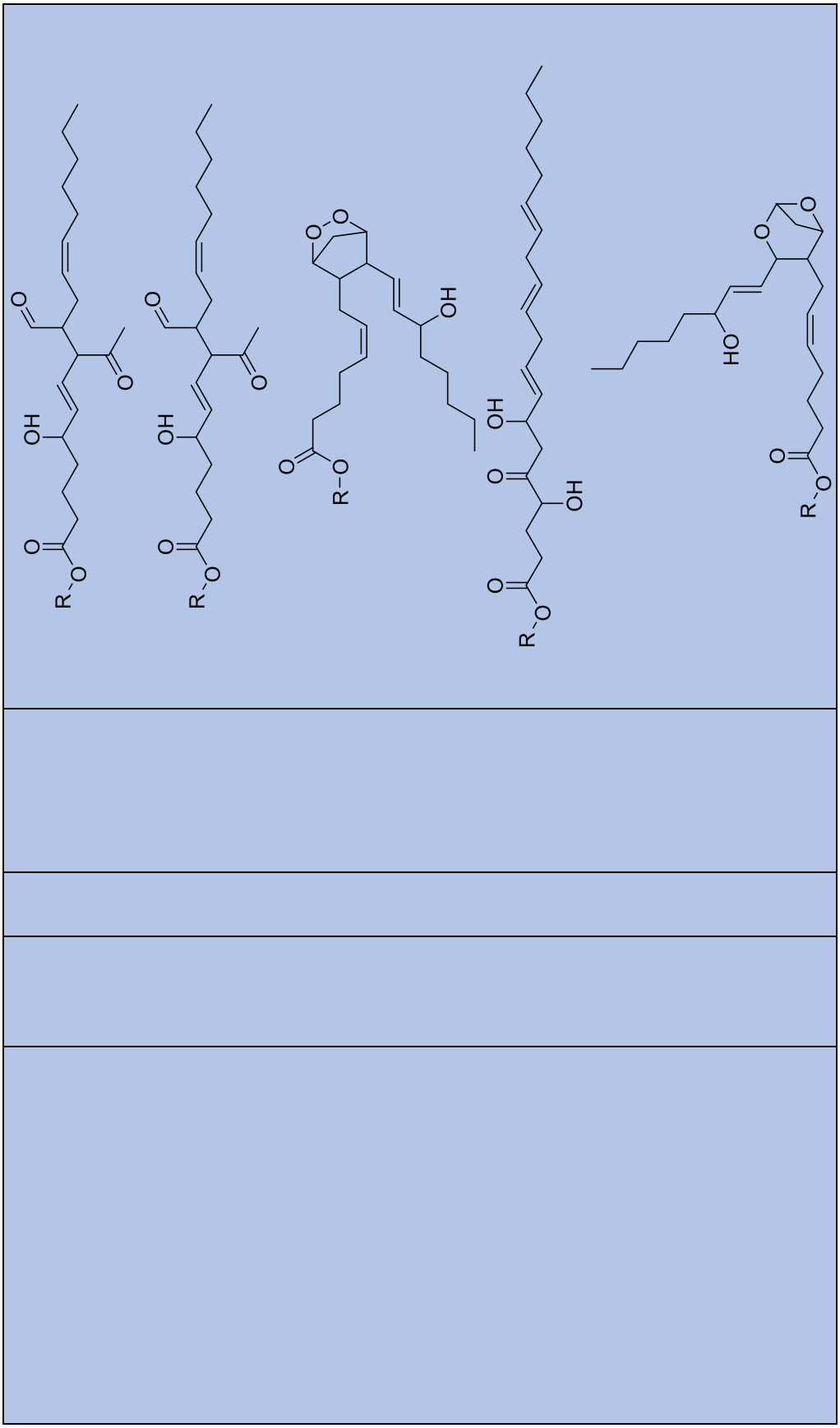
O
OH
O
O
R
O
O
OH
O
O
R
O
O
O
O
OH
O
R
O
OH
O
OH
O
R
O
HO
O
O
O
R
O

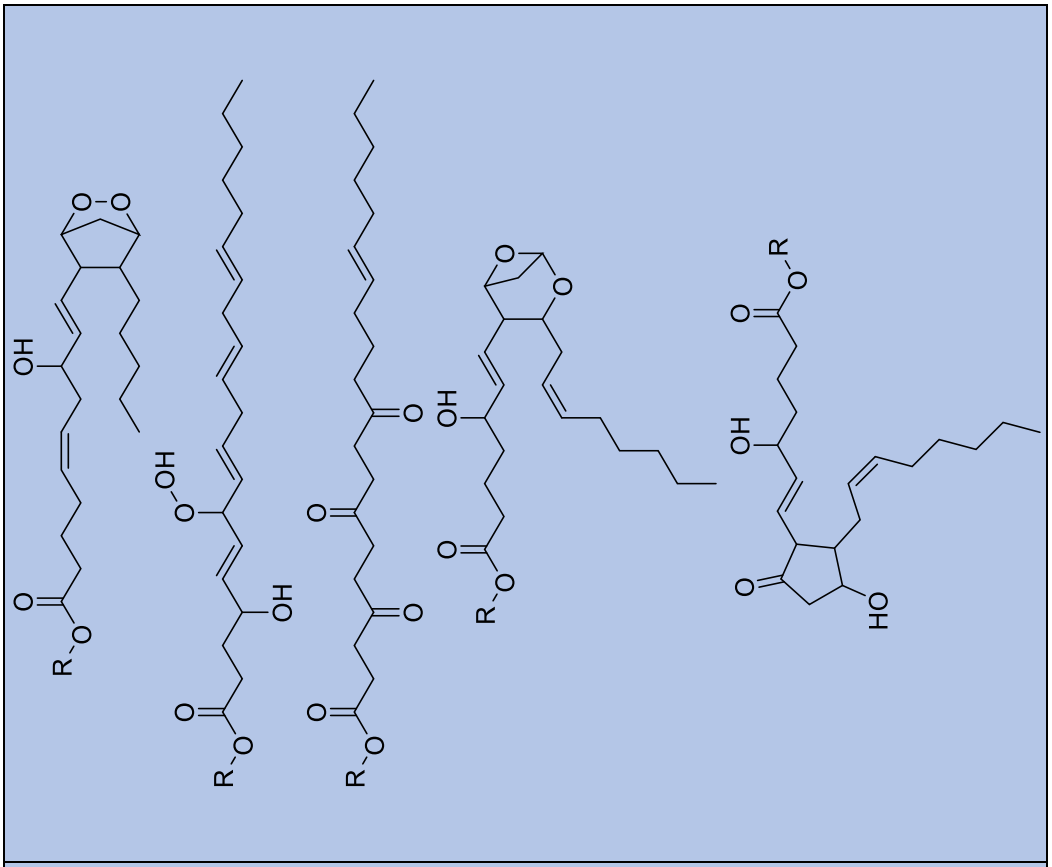
OH
O
O
R
O
O
O
OH
O
OH
O
O
R
O
O
O
O
O
O
O
R
O
OH
O
O
R
O
O
OH
HO

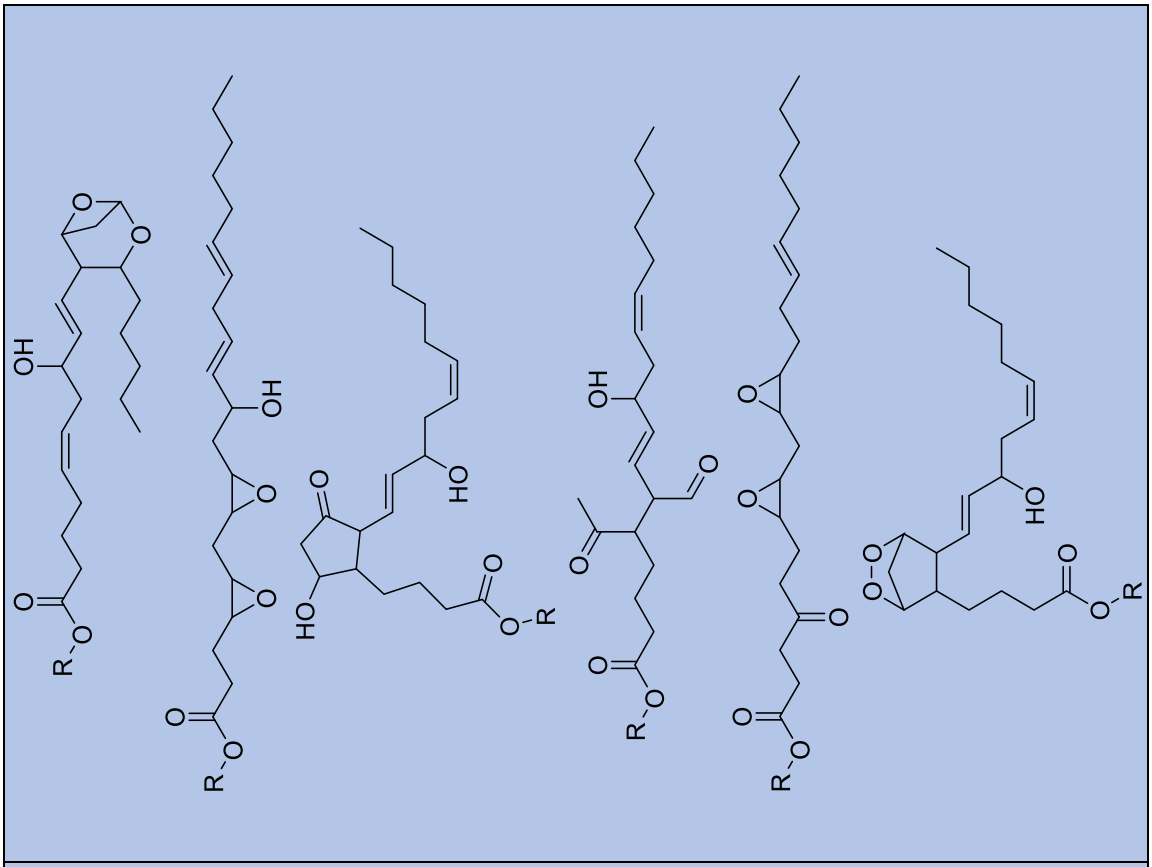
OH
O
O
O
R
O
OH
O
O
O
R
O
HO
O
HO
O
R
O
OH
O
O
O
R
O
O
O
O
O
R
O
HO
O
O
O
R

				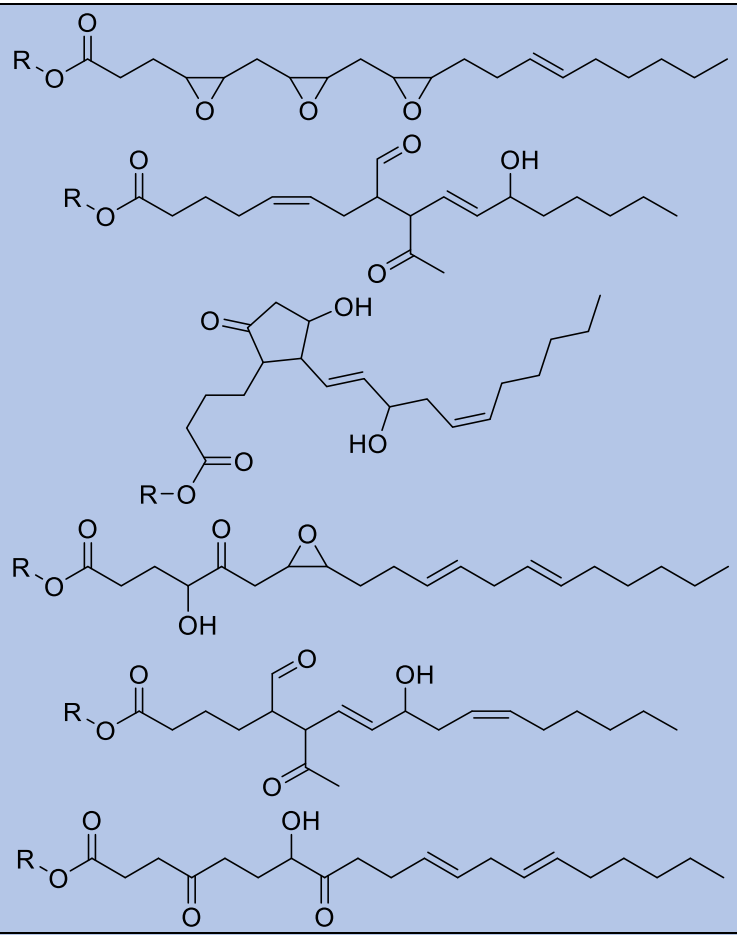
32. C44H80NO9P (HETE-PC)	PAPC	798	$C_{44}H_{80}NO_9P$	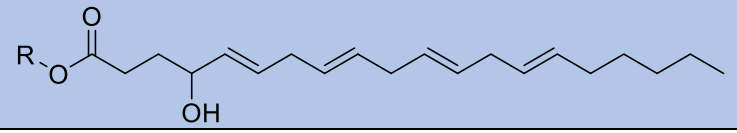

				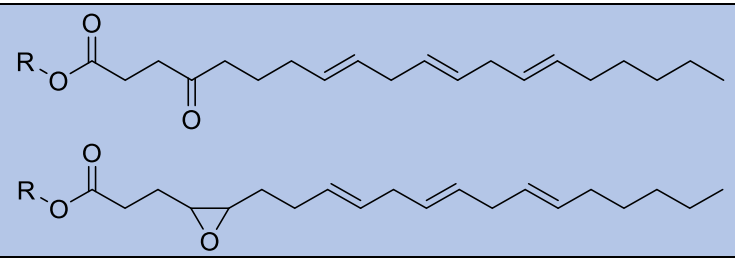
33. C42H80NO11P	PLPC	806	$C_{42}H_{80}NO_{11}P$	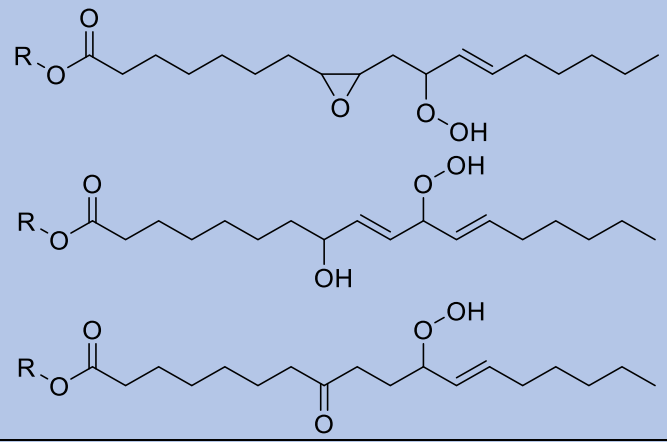
34. 16:0/18:2[1xKETO] (KODE-PC)	PLPC	772	$C_{42}H_{78}NO_9P$	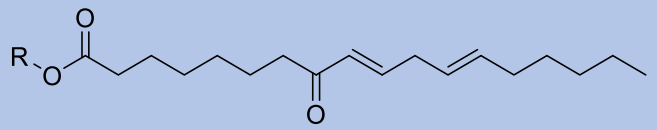
35. 16:0/18:1[1xOH] (HOME-PC)	PLPC	776	$C_{42}H_{82}NO_9P$	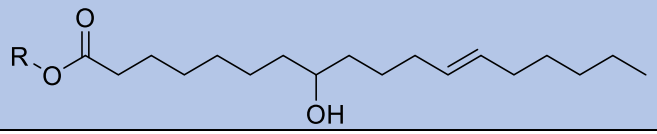

Supplemental Table 4. Forward and reserve primer sequences for cDNA and genomic DNA amplification.

Gene	Species	Primer orientation	Sequence
Hmox1	*Mus musculus*	Forward	ACAGCCCCACCAAGTTCAAA
		Reserve	TCTGCAGGGGCAGTATCTTG
Gclm	*Mus musculus*	Forward	TGGAGCAGCTGTATCAGTGG
		Reserve	AGAGCAGTTCTTTCGGGTCA
Pgd	*Mus musculus*	Forward	CTCCTCGACTCTGCTTCGTC
		Reserve	CGGCATCTTCTTGTCGTGTC
Acly	*Mus musculus*	Forward	TGATGGGAGAAGTTGGGAAG
		Reserve	ATCAGCTCGGGACTCAGAAA
Hmgcoas	*Mus musculus*	Forward	ACAAGCCTGACATGCTCTCC
		Reserve	TTCAGGAACATCCGAGCTAGA
Hmgcoar	*Mus musculus*	Forward	TCTTGTGGAATGCTCTGTGA
		Reserve	AAGCTCTAGGACCAGCGACA
Adamtsl2	*Mus musculus*	Forward	ATGTGAGCCCATTGGCTGTG
		Reserve	TCGGTACTTGACCACTGTGC
Timp2	*Mus musculus*	Forward	ATGGCAACCCCATCAAGAGG
		Reserve	TGGGACAGCGAGTGATCTTG
Timp1	*Mus musculus*	Forward	TCGGACCTGGTCATAAGGC
		Reserve	GTACGCCAGGGAACCAAGAA
Mmp2	*Mus musculus*	Forward	GTGTTCTTCGCAGGGAATGAG
		Reserve	GATGCTTCCAAACTTCACGCT
Itga8	*Mus musculus*	Forward	ACACGTTCCTCAAGAGAAAGAA
		Reserve	GGAGTGGCCCAAATAACCGA
Col15a1	*Mus musculus*	Forward	CTGTCCACTTTCCGAGCCTTT
		Reserve	AAAGCACTTGGCCCTTGAGA
Col8a1	*Mus musculus*	Forward	GGCAAAGAGTACCCACACCTACC
		Reserve	GACCTTGTTCTCCGCGCAAACTG
Col4a2	*Mus musculus*	Forward	TCGTTCAGCCAGGTTGCATT
		Reserve	AAAGCCCTTGAGCCCTTGTT
Col5a2	*Mus musculus*	Forward	TGGGGACTGATGGTACACCT
		Reserve	GGATCACCCGATTGTCCTCG
Adam8	*Mus musculus*	Forward	TGAACAAGCAGCGTCTACGA
		Reserve	CTGGGAGTGGTGAACTGGAC
Fgfr1	*Mus musculus*	Forward	TCCCTGTGGAAGTGGAGTCT
		Reserve	GCTACAGGCCTACGGTTTGG
Tgfbr1	*Mus musculus*	Forward	GGCGAAGGCATTACAGTGTT
		Reserve	TGGTGAATGACAGTGCGGTT
Itga9	*Mus musculus*	Forward	GCTCTCGCTGTAGCCCATC
		Reserve	ACCCACGAGGACCCAGC
Col6a1	*Mus musculus*	Forward	AGGGCTACAAGGAACCATGC
		Reserve	TTTCCTCGCTCCCCCTCATA

Tgfbr2	*Mus musculus*	Forward	CCAAGTCGGATGTGGAAATGG
		Reserve	TGTCGCAAGTGGACAGTCTC
Col14a1	*Mus musculus*	Forward	TGAAGCACCCACAGCCATAG
		Reserve	TCCAGGCACCATAACCACTTC
Itga1	*Mus musculus*	Forward	TCAGTGGAGAGCAGATCGGA
		Reserve	CCCACAGGGCTCATTCTTGT
Adam9	*Mus musculus*	Forward	GGGCCGACGTATAATGCAAAG
		Reserve	CAGGTGGCGGTCTGGAG
CypA	*Mus musculus*	Forward	CGATGACGAGCCCTTGG
		Reserve	TCTGCTGTCTTTGGAACTTTGTC
B2m	*Mus musculus*	Forward	ATTCACCCCCACTGAGACTG
		Reserve	TGCTATTTCTTTCTGCGTGC
Hmox1	*Homo sapiens*	Forward	AAGACTGCGTTCCTGCTCAAC
		Reserve	AAAGCCCTACAGCAACTGTCG
Gclm	*Homo sapiens*	Forward	GCGAGGAGCTTCATGATTGT
		Reserve	TGTGCAACTCCAAGGACTGA
Hprt	*Homo sapiens*	Forward	AGGCGAACCTCTCGGCTTTC
		Reserve	CAAGACGTTCAGTCCTGTCCATA
scFv-E06	*N/A*	Forward	GTACTGCTGCTCTGGGTTCC
		Reserve	CACTGGCCGTGCAACTAATG